Hydrogel-Based Immune-Isolating Capsules Protect Human Ovarian Tissue and Promote Restoration of Ovarian Endocrine Function in Ovariectomized Mice

by

Margaret A. Brunette

A dissertation submitted in partial fulfillment
of the requirements for the degree of
Doctor of Philosophy
(Biomedical Engineering)
in the University of Michigan
2024

Doctoral Committee:

Associate Professor Ariella Shikanov, Chair
Professor Marilia Cascalho
Professor Vasantha Padmanabhan
Professor Jan Stegemann
Assistant Professor Min Xu

Margaret A. Brunette

mabrunet@umich.edu

ORCID iD: 0000-0003-0712-4121

© Margaret A. Brunette 2024

Dedication

To all those who have supported me throughout my education, and to Milo and Luna for sticking with me through it all.

Acknowledgements

This work would not have been able to be completed without a large group of support. I would like to start by thanking my advisor, Dr. Ariella Shikanov. I really appreciate the experience of working in your lab. I started out not knowing anything about ovarian biology or animal handling, and since then I have learned so much about how to be a scientist, how to effectively communicate my research, and how to be not so critical of my work. The change I see in myself from where I started six years ago in your lab is remarkable, and I know it will serve me well in the future. I would also like to thank my committee members Dr. Marilia Cascalho, Dr. Jan Stegemann, Dr. Vasantha Padmanabhan, and Dr. Min Xu. I have appreciated your support and guidance through this process, particularly during the COVID years.

I would also like to thank my previous research advisors, Dr. Rupak Rajachar and Dr. Ramille Shah. When I began college at Michigan Tech, I was unaware that research was a path I could take for a career. I am eternally grateful to you both for giving me the opportunity to work in your labs, and for your continuing mentorship.

This work would not have been possible without my lab mates. You have been there for me when experiments didn't work and when I needed a shoulder to cry on. You have been there when my world blew up and I was trying not to go stir crazy during COVID. You took me to Kroger so I could change my car oil and then jumped my car because it was actually a dead battery. You have helped me move countless times (well,

five times actually) and been the people that come walk my dogs so I can be in lab longer. You have driven an hour round trip to jump my car so I wouldn't be late for cytology and have been there for heart-to-hearts in the surgery room. You have also taught me all the hip new slang the kids are using these days and delt with my usually very caffeinated self. I could go on and on, but you have all truly had a massive impact on my life.

Finally, I could not have done this without my family. Grad school is intense, and I am forever grateful for my dogs Milo and Luna bringing levity to my day-to-day. Mom and Dad, thank you for always supporting me on this journey. It has been a long road with many turns, but you are always in my corner supporting me through it all – I can't wait to see where the road goes next.

Table of Contents

Dedication ii

Acknowledgements iii

List of Tables vii

List of Figures viii

List of Appendices xii

Abstract xiii

Chapter 1 Introduction 1

1.1 Endocrine complications are a result of anticancer treatments in adolescence. .. 1

1.2 Folliculogenesis is disrupted after gonadotoxic treatment. 2

1.3 Hormone replacement therapy has limitations that could be addressed with encapsulated ovarian allografts. 4

1.4 Evaluating the efficacy of immune-isolation technology in ovarian allograft transplantation. 6

1.5 Translating the immune-isolating dual capsule for human ovarian allografts. 8

Chapter 2 Human Ovarian Follicles Xenografted in Immunoisolating Capsules Survive Long Term Implantation in Mice 12

2.1 Introduction 12

2.2 Materials and Methods 14

2.3 Results 23

2.4 Discussion 31

Chapter 3 Human Ovarian Tissue Encapsulated in an Immune-Isolating Hydrogel Restores Ovarian Endocrine Function in Ovariectomized Mice 36

3.1 Introduction 36

3.2 Materials and Methods 39

3.3 Results..... 47

3.4 Discussion 53

Chapter 4 Human Follicles in Encapsulated Ovarian Cortex are Protected From T-Cell Infiltration in Immunocompetent Mice. 57

4.1 Introduction..... 57

4.2 Materials and Methods 58

4.3 Results..... 66

4.4 Discussion 71

Chapter 5 Conclusions and Future Directions 75

5.1 Summary of findings..... 75

5.2 Future directions..... 77

Appendices 81

Bibliography 107

List of Tables

Table 2.1 Donor Information 15

Appendix Table A.1 Complete list of human donor information 82

Appendix Table B.1 Chapter three complete donor information 93

Appendix Table B.2 Chapter three donor information by mouse 94

Appendix Table C.1 Chapter four complete donor information 97

Appendix Table D.1 All mouse and implant information 102

List of Figures

Figure 1.1 Menstrual Cycle. Human hormone levels and the ovarian cycle are shown over a standardized 28-day menstrual cycle. Adapted from BioRender.[86,113] 3

Figure 1.2 Hormone regulation in the HPG axis. Feedback varies at different parts of the menstrual cycle. Figure adapted by Eric Wong from Silverthron Human Physiology[20]. 4

Figure 1.3 Donor metrics. Age and BMI are plotted (A) showing the diversity of donors, where each point in this graph represents a single donor. The points that are filled in represent the donors whose tissue was utilized throughout this work. The donor tissue was received from across the United States (B). Each pin represents one, two, three, or four (red, orange, green, and blue respectively) donors. 9

Figure 1.4 Representative histological images from each human donor. Each panel is numbered with their donor number. All scale bars are 100μm. 11

Figure 2.1 Overview of human tissue processing and implantation. Tissue received from UNOS donors (A) was processed to isolate the ovaries (B). Ovarian cortex tissue approximately 10mm x 10mm x 1mm is removed (C), then cut to approximately 1mm x 10mm x 1mm (D), and finally cut to approximately 1mm x 1mm x1mm (E). The small tissues are encapsulated in the hydrogel capsule (F) and implanted subcutaneously (G). Removal of the capsules from the subcutaneous space (H) was conducted at various time points. The capsules were removed from the mice (I, J) and then fixed for histological processing and staining. 16

Figure 2.2 Description of implanted tissue groups. Tissue processing was conducted as shown in part (A). Cortical tissue strips were cut into squares either as fresh tissue (Donors 1 and 2) or post-cryopreservation (Donors 3 and 4). Capsules and control tissue were implanted in mice. The total number of capsules/strips at each time point are shown in part (B). 19

Figure 2.3 Donor metrics and initial histology. The donor tissues used in this study were selected from a bank from donors with various ages and BMI values (A). Follicle density values were calculated for each donor from fresh/fixed tissues (B). The large differences in average follicle density between donors is supported by histological images (C–N). Representative images from Donor 1 (C–E), Donor 2 (F–H), Donor 3 (I–K), and Donor 4 (L–N) show stark differences in follicle distribution at low magnification (C, F, I, L). Increased magnification shows the presence of primordial (E iii., K i., N i), primary (E i., H iv., K ii.), and secondary (H ii.) follicles. Scale bars represent 200μm for

C, F, I, and L. Scale bars represent 100μm for D, G, J, and M. Scale bars represent 50μm for all others. 25

Figure 2.4 Follicles in fresh tissue survive up to one month. Representative images from non-encapsulated fresh tissue samples (A-C) and encapsulated fresh tissue samples (D-F) are shown here. These samples were removed from mice at various time points of 3 days (A, D), 1 week (B, E), and 1 month (C, F). Scale bars represent 100mm for inserts and 50mm for all others. Black arrow heads (➤) indicate follicles, asterisks (✻) indicate the PEG capsule, and dashed black lines (---) indicate the human ovarian tissue border with surrounding murine tissue after implantation. 27

Figure 2.5 Follicles in slow frozen tissue survive up to one month. Follicle density values (A) are determined from histological images (C–L). Non-implanted thawed/fixed tissue (B) is a control for non-encapsulated groups (C–G) and encapsulated groups (F–L). These samples were removed from mice at various time points of 1 day (C, H), 3 days (D, I), 1 week (E, J), 2 weeks (F, K), and 1 month (G, L). Scale bars represent 100μm for inserts and 50μm for all others. Black arrow heads (➤) indicate follicles, asterisks (✻) indicate the PEG capsule. 28

Figure 2.6 Follicles in vitrified tissue survive up to three months. Follicle density values (A) are determined from histological images (C–F). Non-implanted thawed fixed tissue (B) is a control for non-encapsulated groups (C, D) and encapsulated groups (E, F). These samples were removed from mice at various time points of 2 months (C, E) and 3 months (D, F). Scale bars represent 100μm for inserts and 50μm for all others. Black arrow heads (➤) indicate follicles, asterisks (✻) indicate the PEG capsule, and dashed black lines (---) indicate the human ovarian tissue border with surrounding murine tissue after implantation. 30

Figure 3.1 Experimental design. NSG mice were implanted with human cortical ovarian tissue (encapsulated or non-encapsulated) and followed out to twenty weeks (A). Donor ovaries (B) are de-cortified (C) and cryopreserved until use. After thawing, tissue is encapsulated in the immune-isolating capsule (D) and is implanted (E). Encapsulated tissue samples (F,G) and non-encapsulated tissue samples (H,I) were removed from the subcutaneous space. Panels G and H show gross morphological changes indicating antral follicles are present. Scale bar represents 1cm A-G, and 5mm for H & I. 40

Figure 3.2 Donor Tissue Characterization. Representative histological images from fresh fixed human ovarian cortex from each donor utilized in this study is shown in A-H. The follicle densities for each donor are shown in I. The distribution of donor tissue among each group is shown in J, with the average age for each group shown in K. 48

Figure 3.3 Encapsulated and non-encapsulated grafts restore endocrine function. Endocrine function of the grafts was measured with 4 metrics (A): vaginal opening (VO), estrous cyclicity (EC), estradiol levels (E2), and follicle stimulating hormone (FSH) levels. Green indicates ovarian endocrine function, and gray/black represents no

endocrine function. The increase in VO and EC color indicates increasing function. E2 is anticipated to increase until it reaches a constant level, and FSH is anticipated to take the longest before starting to decrease to physiological normal levels. In ovariectomized mice we expect no VO and EC, low estradiol and elevated FSH. With functioning ovarian tissue, the VO has the fastest onset, followed with regular ECs, increase in E2 and decrease in FSH. In our study there is a resumption of cyclicity around five weeks for mice with non-encapsulated (B) and encapsulated (C) samples. Trends between non-encapsulated and encapsulated groups were similar when looking at the percent of mice that had entered estrus (D) and the number of cycles achieved in each cohort (E). Estradiol measurements were determined from terminal blood serum (F, G). Analysis shows that there is no significant difference in estradiol levels between groups when comparing cohorts (F). Additionally, mice that received grafts showed statistically significant more estradiol than controls (G). Blood serum collected every other week shows a trend of decreasing FSH levels in week 18 (H). 49

Figure 3.4 Antral Follicle Characterization. Antral follicles from non-encapsulated (A-E) and encapsulated (F-H) tissue. Scale bar represents 1mm (A, F), 500μm (B, D, G), or 100μm (C, E, H). Oo: oocyte, Cu: cumulus granulosa cells, An: antrum, Mu: mural granulosa cells, Th: theca layer, Bv: blood vessel, ✻: PEG capsule, (⋯) indicates the theca cell layer, (- - -) indicates granulosa cell layer..... 51

Figure 4.1 Experimental design and tissue processing. Balb/c mice were implanted with human cortical ovarian tissue (encapsulated or non-encapsulated) and followed out to six weeks (A). Donor ovaries (B) are de-cortified (C) and cryopreserved until use. After thawing, tissue is encapsulated in the immune-isolating capsule (D) and is implanted subcutaneously. Non-encapsulated tissue grafts (E) and encapsulated tissue grafts (F) were removed from the subcutaneous space. Scale bar represents 1cm B-D, and 5mm for E & F..... 59

Figure 4.2 Donor tissue follicle density shows heterogeneity. Representative histological images from fresh fixed human ovarian cortex from each donor utilized in this study is shown in A-F. The follicle densities for all donors are shown in G. Metrics for the donors used in this study are shown in H. 66

Figure 4.3 Short-term histology shows follicles persist after 6-week post implantation. Representative histological images from non-encapsulated (A, C, E) and encapsulated (B, D, F) samples. Non-encapsulated samples show an increase in fibrous stroma as time goes on, with the 6-week samples showing morphologically irregular follicles (E). Encapsulated samples show consistent stromal cell density, and 6-week samples show morphologically normal follicles (F). Black arrow heads (➤) indicate follicles, asterisks (✻) indicate the PEG capsule. Scale bars are 100μm for insets and 500μm for all others..... 67

Figure 4.4 T-cell staining indicates immune-isolating capsule is functioning. Whole slide scans of non-encapsulated (A-F) and encapsulated (G-L) samples show T-cell infiltration in non-encapsulated samples at each timepoint. Lack of staining shows

capsules preclude T-cell infiltration. Black arrow heads (➤) indicate follicles, asterisks (✻) indicate the PEG capsule. Scale bars are 100μm for high magnification images and 1mm for all others. 69

Figure 4.5 Long-term studies in immunocompetent mice shows grafts can support tissue and gonadal hormone function. Experimental design (A) shows some mice were euthanized early, which are collectively termed Group 1. Mice that had implants through the entire 22 weeks are termed Group 2. Examples of each type of implant are shown (B,C). Estrous cyclicity (D) shows mice entered estrus over the study period. All but one mouse entered estrus as shown in E. Estrous cyclicity is supported with upward trends in terminal serum estradiol levels (F). Histological images (G, H) show immune cell infiltration (G) or the presence of early-stage follicles (H). This is supported with IHC showing CD4+ staining (I) in Group 1 samples, and lack of staining in Group 2 (J). CD8+ staining is weak to absent in both groups (K, L). Black arrow heads (➤) indicate follicles, asterisks (✻) indicate the PEG capsule. Scale bars are 500μm in low magnification images and 100μm in high magnification images. 70

Appendix Figure B.1 Chapter three estrous plots for each mouse in the study ... 95

Appendix Figure B.2 Non-antral follicles in stimulated mice 96

Appendix Figure C.1 Chapter four estrous plots for all mice 98

List of Appendices

Appendix A: Human Tissue Donor Information 82

Appendix B: Chapter Three Supplemental Materials..... 93

Appendix C: Chapter Four Supplemental Material 97

Appendix D: Additional Insights 99

Abstract

The increase in pediatric cancer survivorship has concurrently resulted in growing numbers of young women suffering from premature ovarian insufficiency (POI) due to the gonadotoxic effects of chemotherapy and/or radiation. The loss of ovarian endocrine function and inability to undergo physiological puberty experienced by patients with POI is currently treated with hormone replacement therapy (HRT), which does not recapitulate physiological ovarian function and supplies only a fraction of hormones. We hypothesized that a cell-based therapy could fully recapitulate ovarian physiology and promote pubertal development in adolescent girls with POI. The long-term goal of this work is the development of an immune-isolating capsule for implantation of donor ovarian tissue to restore ovarian endocrine function in females with POI.

Previous work has demonstrated that a poly(ethylene glycol) (PEG)-based capsule with a degradable core and non-degradable shell supported encapsulated murine ovarian allografts and prevented infiltration of immune cells. The work described in this dissertation focused on translating the immune-isolating technology to be used with human ovarian tissue and investigating survival and function of the encapsulated human ovarian tissue. The objectives of the work described in this dissertation were to (1) develop an encapsulation method for human ovarian tissue, (2) investigate the ability of the encapsulated tissues to interact with the host hormones to allow for antral follicle growth, and (3) evaluate whether growing human follicles remain protected from host

rejection. We have demonstrated that human ovarian tissue survived the encapsulation process. Additionally, we conducted *in vivo* studies using fresh, vitrified, and slow frozen tissue subcutaneously implanted in mice, removing viable implants up to twelve weeks later.

To address differences between murine and human ovarian tissue, specifically the heterogeneity of follicle distribution in human tissue, we increased the volume of the human graft by a factor of 20. We demonstrated that this modification maintained healthy stromal tissue with no signs of fibrosis. Next, we tested whether encapsulated human follicles could resume folliculogenesis, reach antral stages and secrete gonadal hormones. Ovariectomized immunocompromised mice subcutaneously implanted with immune-isolated human ovarian xenografts for 20 weeks (1) resumed estrous cyclicity (100% of the mice), (2) had significantly increased estradiol levels, and (3) had downward trending levels of follicle stimulating hormone after 18 weeks. Furthermore, large antral follicles (~3mm in diameter) were present in encapsulated and non-encapsulated tissues.

Lastly, we investigated whether the immune-isolating capsule could protect human ovarian tissue xenografted in immunocompetent mice, which is a significantly more rigorous model. Analysis of the xenografts retrieved 6 weeks post implantation confirmed preclusion of CD4+/CD8+ T-cell infiltration and presence of ovarian follicles with normal morphology in the encapsulated tissue. The encapsulated human xenografts restored regular estrous cyclicity, increased levels of estradiol reaching pre-ovariectomy levels, and normal growing follicles persisted for 22 weeks.

In summary, this work supported our hypothesis that encapsulated immune-isolated donor ovarian grafts remained protected from immune rejection, responded to

circulating gonadotropins, and delivered gonadal hormones at physiological levels with reciprocal feedback with the rest of the body. The findings in this work support the use of a cell-based therapy for POI patients and provides a basis for large animal studies.

Chapter 1 Introduction

1.1 Endocrine complications are a result of anticancer treatments in adolescence.

The pediatric and adolescent cancer survival rates have increased significantly over the past 50 years. From 1970 to 2020 the death rate has declined from 6.3 to 1.9 per 100,000 for children and from 7.2 to 2.6 per 100,000 for adolescents[1]. While having cancer in remission is a significant milestone for these patients, it is important to consider their quality of life (QoL) after remission. Chemotherapy and radiation are particularly harmful to the gonads and can delay or prevent these survivors from entering puberty[2–4]. For females, anticancer treatments cause damage to the ovaries primarily at the follicle level, resulting in follicle death and/or premature activation[5–7].

The follicle is the functional unit of the ovary and has two critical functions: fertility and hormone production. Girls are born with approximately 2 million follicles, termed the primordial follicle (PMF) reserve, which is non-renewable and continuously depletes over the course of life[8]. Anticancer treatments that damage the PMF reserve may cause decreased fertility and endocrine function. Approximately half of the pediatric cancer survivors will experience endocrine complications[6,9]. Premature ovarian insufficiency (POI) is one of the most significant endocrine complications of anticancer therapy for young patients and is diagnosed when follicle stimulating hormone (FSH) levels are above 40mIU/L, and spontaneous amenorrhea occurs for at least four months[10].

1.2 Folliculogenesis is disrupted after gonadotoxic treatment.

Dysregulation of folliculogenesis, caused by chemotherapy and radiation, usually manifests as a lack of proper recruitment of primordial follicles, oocyte maturation, and gonadal hormone production[11]. Primordial follicles are activated and recruited to the growing pool in waves[12]. The gradual recruitment of follicles sustains decades of fertility and ovarian endocrine function for the female starting at puberty and gradually diminishing, ceasing at menopause. Follicles that are activated undergo the process of folliculogenesis, which is of critical importance to the follicle's function of hormone production and fertility[13].

The follicle is comprised of three main cell types: the oocyte (female gamete), granulosa (GCs) and theca cells (TCs)[13]. Activated primordial follicles gradually progress through the primary, secondary, antral, and pre-ovulatory stages[13]. Primary follicles are characterized by a single layer of cuboidal GCs surrounding the oocyte, which continue to proliferate as the follicle enters the secondary stage, when the theca layer also begins to develop[13,14]. Follicles continue to mature and begin to rely more on gonadotropin stimulation rather than paracrine signaling[15]. Throughout the process of folliculogenesis, the oocyte and GCs remain avascular, depending entirely on diffusion of nutrients from the extrafollicular space. As the follicle continues to grow, antrum formation allows the follicle to overcome the limits of diffusion through GCs to the oocyte, while the theca layer develops a rich network of blood supply around the follicle[16]. When the follicle reaches 2mm in diameter in humans it is considered pre-ovulatory and it continues to grow[17], culminating with ovulation of one dominant follicle. Post-ovulation, the GCs luteinize forming the corpus luteum[14] (**Figure 1.1**).

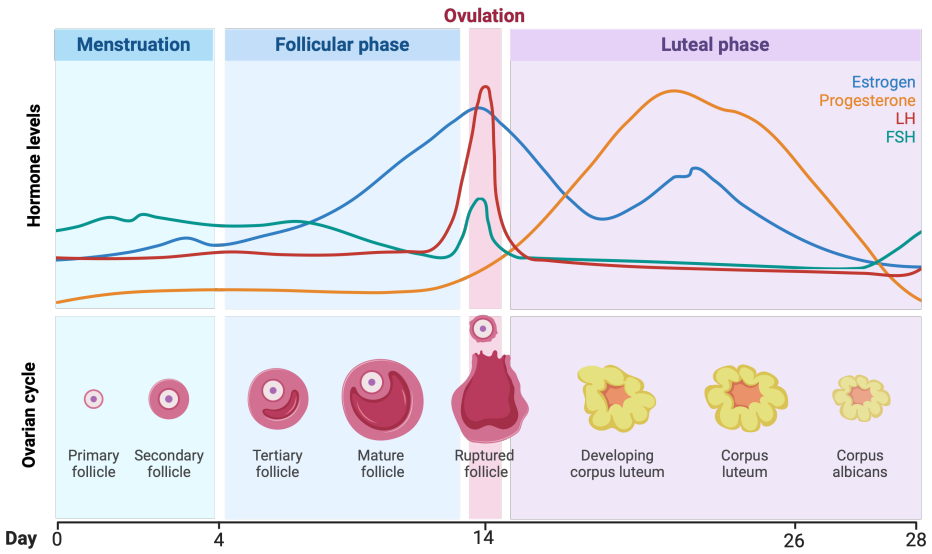

Figure 1.1 Menstrual Cycle. Human hormone levels and the ovarian cycle are shown over a standardized 28-day menstrual cycle. Adapted from BioRender.[86,113]

As with most biological systems, form follows function. The interactions between the oocyte, GCs, and TCs are of critical importance to promote female fertility and endocrine function. The interaction between GCs and TCs results in the production of estradiol explained by the two-cell two-gonadotropin theory[13,14]. In this theory, luteinizing hormone (LH) stimulates TCs to produce androstenedione, which is then transported across the basement membrane to the GCs[18]. Estradiol is produced from androstenedione under FSH stimulation[13]. After ovulation the luteinized GCs and TCs switch to producing progesterone[13]. The process of gonadal hormone production is regulated via the hypothalamus-pituitary-gonadal (HPG) axis. Gonadotropin releasing hormone (GnRH) in the hypothalamus is released to induce the anterior pituitary to produce FSH and LH, which then interact with follicular GCs and TCs[19]. The HPG axis is regulated via multiple feedback loops mediated by multiple hormones (estrogen, inhibin, activin, follistatin, and progesterone). Estrogen and progesterone can act at the pituitary or hypothalamus level of the axis and predominantly have a negative effect on FSH, LH

and GnRH production; however, estrogen can also exert positive feedback at the hypothalamus in the late follicular phase that results in the LH surge necessary for ovulation[20] (**Figure 1.2**).

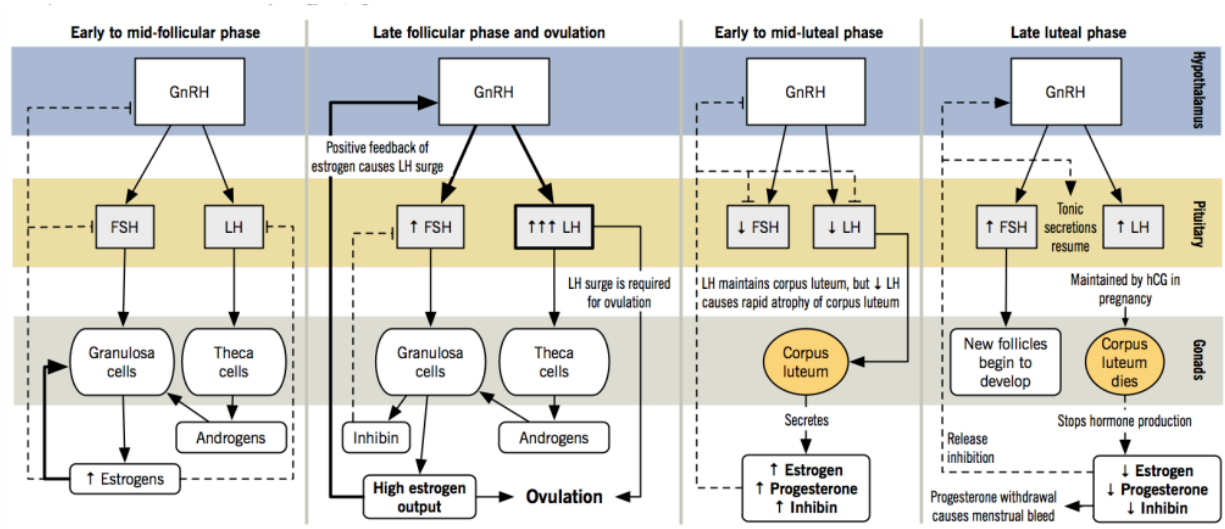

Figure 1.2 Hormone regulation in the HPG axis. Feedback varies at different parts of the menstrual cycle. Figure adapted by Eric Wong from Silverthron Human Physiology[20].

1.3 Hormone replacement therapy has limitations that could be addressed with encapsulated ovarian allografts.

The negative effects of gonadotoxic treatments on the PMF reserve and folliculogenesis lead to POI in adolescent patients and inability to start their puberal development[21,22]. In the long term, the lack of gonadal hormones and elevated unregulated levels of gonadotropins leads to detrimental health outcomes including cardiac disease, osteopenia, growth hormone dysfunction, reduced neuroprotective effects, negative impacts on T-cell function, premature epiphyseal closure, as well as changes to food intake and serum leptin levels[21–26]. Hormone replacement therapy (HRT) is the only existing, yet off-label, treatment to induce puberty in girls with POI[27]. HRT was initially developed to help alleviate negative side effects associated with low estrogen

production (cardiovascular risks, osteopenia, etc.) in menopausal women[28]. HRT includes estrogen and usually contains progesterone. This treatment comes in a variety of forms (pill, transdermal (TD) patch, gels, and creams), with the most widely used method of HRT administration for puberty induction involving a TD patch to deliver 17β-oestradiol and an oral pill delivery of progesterone[29]. However, the use of HRT for puberty induction has yet to be evaluated[29]. Some long-term studies have been used to determine the safety of HRT, but this has been nearly exclusively for evaluating the safety of HRT for menopausal women[30]. Furthermore, because HRT was not designed for induction of puberty, properly dosed treatments are not currently available, meaning these patients must cut pills or TD patches to get an appropriate dose[31]. In addition to having to modify dosages, the doses themselves can vary on a week-to-week basis, making patient compliance a concern. As a result, HRT delivers non-physiological levels of gonadal hormones in a continuous manner, in contrast to physiological cyclicity (**Figure 1.1**), with minimal crosstalk and responsiveness from other endocrine target tissues that are responsive to gonadal hormones, such as fat, cardiovascular, nervous, and musculoskeletal tissues[32].

We hypothesized that allografted ovarian tissue encapsulated in an immune-isolating capsule for pubertal induction would address the limitations of HRT, improve pubertal development, and minimize long-term complications. As with any therapy requiring dosing, HRT requires time for the buildup of delivered hormones. Once that level is reached, the daily fluctuations in hormone levels are largely constant[32]. In contrast, GnRH, FSH, LH, estradiol, and progesterone hormone profiles are of a cyclic nature, repeating approximately every 28 days with each menstrual cycle. Moreover, these

hormones have pulsatility over the course of 24 hours resulting in peaks throughout the day[33]. This cyclic and pulsatile hormone profile is not conserved with the use of HRT but could be better realized with a cell-based therapy. Encapsulated and implanted ovarian allografts would present a unique opportunity to not only eliminate the need for dose modification, but also eliminate the concern of compliance. Finally, and perhaps most importantly, a cell-based therapy using ovarian tissue would restore the physiological ovarian hormone milieu including concentration, composition, pulsatility, reciprocity, and increased estradiol before the LH surge. Because of the unique advantages of a cell-based therapy as compared to HRT, the aim of this dissertation work is to contribute to the development of a method allowing for hormone delivery at *physiologically* relevant levels (i.e. proper cyclicity and pulsatility) and improve patient compliance. This therapy could then lead to overall improved QoL for patients with POI.

1.4 Evaluating the efficacy of immune-isolation technology in ovarian allograft transplantation.

In this thesis I investigated whether implanted immune-isolated ovarian allografts survived and functioned in ovariectomized hosts. Immune-isolation allows transplantation of allogeneic cells/tissue while precluding immune cell infiltration and permitting diffusion of nutrients and signaling molecules in and out of the device[34]. This technology also allows implantation of donor tissue without the detrimental side effects of immunosuppressants typically needed to prevent immune rejection of donor tissues. While there is some debate on which immune cell components are critical to modulate, T-cells must be prevented from entering the device as any contact with the encapsulated cells/tissue will result in rejection[35,36]. Other immune components such as antibodies

(Abs), complement, and cytokines may also be critical in modulating the immune response[36]. This technology has been under investigation for other applications, such as islet cell implantation for those with diabetes, but has yet to be leveraged to treat POI.

The choice of material for the capsule is of utmost importance because ovarian follicles dramatically increase in size during folliculogenesis. Thus, the capsule would need to have the ability to allow for expansion while maintaining physical integrity and protecting the tissue from an immune response. The Shikanov lab and others in the field have developed and characterized multiple hydrogels for encapsulation and 3D follicle culture *in vitro,* including alginate,[37,38,39] alginate-matrigel,[40] fibrin,[37,41] fibrin-alginate,[37,42,43] and poly(ethylene glycol) (PEG)[44,45]. With the goal of implanting this capsule *in vivo,* the material property of being non-degradable, such as alginate, is an attractive option as it would enhance the immune-isolating capability; however, the ability for growing follicles to modify their surrounding environment is limited in non-degradable matrices. Fibrin is degradable and has previously been used for follicle transplants *in vivo* but it degrades too fast and may not preclude immune cell infiltration[46]. Alternatively, the PEG formulations described by Shikanov *et al.* (2011) and Tomaszewski *et al.* (2019) allow for tunable degradation and further modifications to preclude immune cell infiltration[44,45].

Day *et al*. developed a PEG-based dual capsule with a degradable core and non-degradable shell[47–50]. To optimize the immune-isolating properties of the shell, various PEG formulations and photoinitiators were investigated[50]. Studies indicated that PEG-vinyl sulfone (PEG-VS) formed at a sufficiently fast rate to maintain viability of the live tissue suspended within the PEG-VS solution. Additionally, this material demonstrated

minimal local inflammatory reaction *in vivo* post-implantation[51]. Based off these findings the non-degradable shell (PEG-ND) was formulated from 4-arm PEG-VS cross-linked via the photoinitiator Irgacure 2959, with N-vinyl-2-pyrrolidone (NVP) added for enhanced gelation. The final concentrations of each component are (1) PEG at 5% (w/v), (2) NVP at 0.1% (v/v), and (3) Irgacure 2959 at 0.4mg/100μL[48]. To support follicle expansion a degradable core (PEG-D) surrounding ovarian tissue was prepared from 8-arm PEG-VS cross-linked with a biodegradable peptide Ac-GCYK↓NSGCYK↓NSCG (YKNS, ↓ indicates cleavage sites). The final concentration of PEG-VS is 5% (w/v) and the ratio of PEG:YKNS is such that the ratio of -VS:-SH groups is 1:1[48]. Previous work by Day *et al.* has characterized the use of this capsule with murine tissue where the dual PEG capsule was shown to preclude an allo-specific immune response, allow for murine follicle growth, and restore the estrus cycle in mice[48,47].

1.5 Translating the immune-isolating dual capsule for human ovarian allografts.

The specific goal of this dissertation work was to translate the dual-capsule design for use with human ovarian tissue. The use of human ovarian tissue presented different challenges for capsule design compared to murine ovaries. First, human ovarian cortical tissue, where most PMFs are present, contains a significantly greater number of stromal cells which contribute to greater tissue density. This differs from murine ovaries that are relatively homogenous throughout the ovary[52]. Second, the distribution of follicles in human ovarian tissue is significantly more heterogeneous, compared to mice, which requires encapsulation and implantation of larger tissue fragments. Third, while primordial murine and human follicles start at approximately the same size (17-44μm), human follicles reach significantly greater diameters at the antral and pre-ovulatory stages (up to

2cm in humans compared to 500μm in mice), requiring additional capsule design optimization[53].

Healthy ovarian tissue from reproductive aged women is scarce and this work has relied entirely on the donation of ovarian tissue from deceased donors. We obtained human ovarian tissue from Organ Procurement Organization (OPO), International Institute for the Advancement of Medicine (IIAM), which coordinated collection and delivery of fresh ovaries to our lab. The Shikanov lab began receiving tissue in January 2019 and currently has ovarian tissue stored from 46 donors. These donors range from ages 16-40, have BMIs that range from 17 to 50, and come from 12 different states as shown in **Figure 1.3**. The cortical tissue from each donor is carefully characterized for follicle density and distribution, with detailed images of histological sections presented in **Figure 1.4**, and de-identified donor information is summarized in **Appendix Table A.1**, including age, weight, height, BMI, ovary volume, and cross-clamp time (time at which the organ is cut from blood/oxygen supply). Using this donated tissue, we demonstrate in

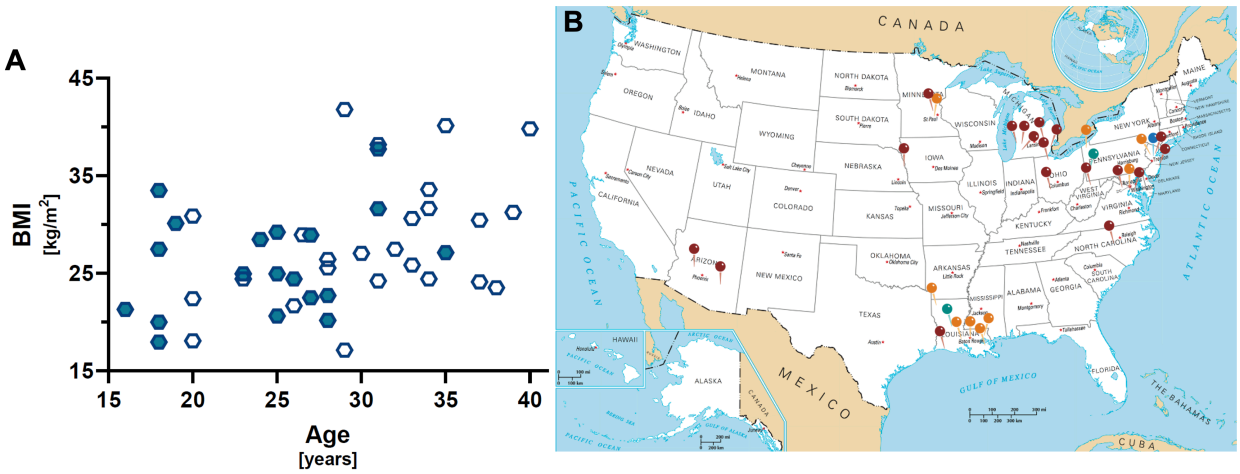

Figure 1.3 Donor metrics. Age and BMI are plotted (A) showing the diversity of donors, where each point in this graph represents a single donor. The points that are filled in represent the donors whose tissue was utilized throughout this work. The donor tissue was received from across the United States (B). Each pin represents one, two, three, or four (red, orange, green, and blue respectively) donors.

Chapter 2 that human ovarian tissue survived the encapsulation process initially developed for encapsulation and implantation of murine tissue; furthermore, we conducted *in vivo* studies using fresh, vitrified, and slow frozen human tissue subcutaneously implanted in immunocompromised mice, showing follicle survival in implants removed up to twelve weeks later. To address differences between murine and human ovarian tissue, specifically the heterogeneity of follicle distribution in human tissue, we optimized the capsule design. We increased human graft volume by a factor of 20 compared to murine allografts and demonstrated that the stromal tissue remained healthy with no signs of fibrosis. In Chapter 3 we aimed to test whether encapsulated human follicles could resume folliculogenesis, reach antral stages and secrete gonadal hormones. After ovariectomizing immunocompromised mice and subcutaneously implanting human ovarian samples, we evaluated estrous cyclicity, serum hormone levels, and graft histology. We found over a 20-week period that (1) estrous cyclicity resumed in all mice, (2) estradiol levels increased significantly with graft implantation, and (3) follicle stimulating hormone levels trended downward after 18 weeks. Furthermore, large antral follicles (~3mm in diameter) were present in encapsulated grafts and non-encapsulated controls.

Chapter 4 details our evaluation of the immune-isolating capacity of the capsule with human ovarian tissue xenografted in immunocompetent mice. Analysis of the xenografts retrieved after 6 weeks confirmed the protection of human ovarian tissue with complete preclusion of CD4+/CD8+ T-cell infiltration and ovarian follicles with normal morphology in the encapsulated tissue. Implantation of the encapsulated human xenografts in ovariectomized immunocompetent mice for 22 weeks restored regular

estrous cyclicity, increased levels of estradiol reaching pre-ovariectomy levels, and normal growing follicles persisted in the immune-isolating capsule.

The work detailed in this dissertation is a significant step toward translating this technology to the clinic. It is the first time human ovarian tissue has been used with this dual capsule. Additionally, we have shown that encapsulated immune-isolated donor ovarian allo- and xenografts remained protected from immune rejection, responded to circulating gonadotropins, and secreted gonadal hormones at physiological levels with reciprocal feedback with the rest of the body.

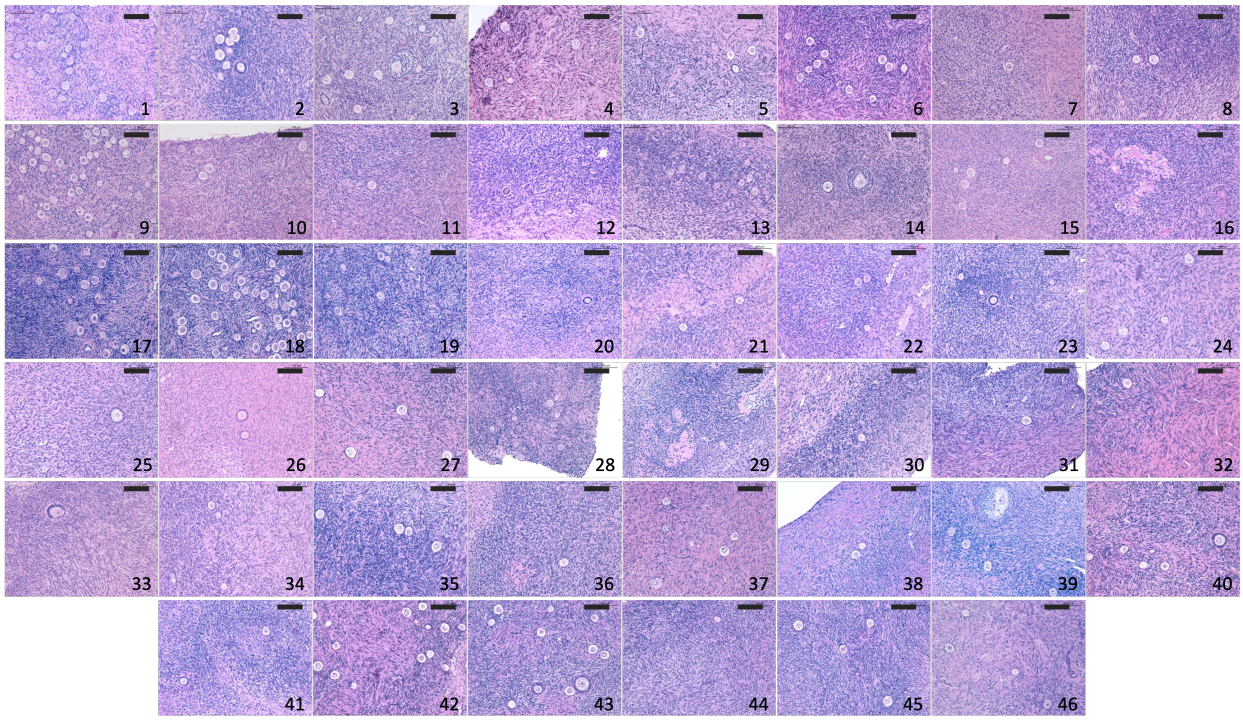

Figure 1.4 Representative histological images from each human donor. Each panel is numbered with their donor number. All scale bars are 100μm.

Chapter 2 Human Ovarian Follicles Xenografted in Immunoisolating Capsules Survive Long Term Implantation in Mice

2.1 Introduction

Over 500,000 survivors of pediatric cancers live in the United States today[54]. Due to advances in anticancer therapy, the 5-year survival rate for pediatric cancer patients reached nearly 85% in 2016, which is a significant increase from 50% in the 1970s [54,55]. This population will continue to grow as the incidence rate of pediatric cancers continues to increase, with an estimated 10,500 new diagnoses in 2021 for children aged 0-14[55]. Unfortunately, chemotherapy and radiation can have detrimental effects on male and female gonads, which may result in delayed or completely absent pubertal development[2]. The delay or absence of pubertal development negatively impacts patient quality of life and carries long-term health risks associated with decreased bone strength and endocrinopathies[56]. The standard of care for puberty induction in adolescent girls with premature ovarian insufficiency (POI) is hormone replacement therapy (HRT), which was developed to treat postmenopausal symptoms in mature women and does not recapitulate physiologic cyclic and pulsatile hormonal patterns found in healthy, reproductive aged women[57,58]. HRT delivers constant doses of estrogen and progesterone, reconstituting ovarian function only partially[28], and precluding ovarian-body homeostasis. Furthermore, the long-term safety and efficacy of HRT to induce puberty has yet to be established[29].

To address the lack of available treatments to induce physiological puberty in adolescent girls with POI, we have developed an immunoisolating hydrogel-based capsule for implantation of donor ovarian tissue without the need for immunosuppression[47,48,50]. Multiple biomaterials have been investigated for supporting follicle growth *in vitro* and *in vivo*, including alginate[37–39], alginate-matrigel[40], fibrin[37,41], fibrin-alginate[37,42,43], and poly(ethylene glycol) (PEG)[45,59]. Here we utilize a system comprised of ovarian tissue surrounded by a degradable PEG hydrogel that promotes follicle growth and expansion. The degradable PEG hydrogel core is surrounded by a non-degradable PEG shell that prevents infiltration of immune cells while allowing diffusion of oxygen, nutrients, and hormones. Our previous studies with these PEG capsules and murine ovarian tissue grafts demonstrated that (1) follicles survive and undergo folliculogenesis for at least 60 days, (2) the capsule prevents immune cell infiltration, and (3) the estrus cycle is restored after encapsulated allogenic tissue is implanted in ovariectomized mice[47].

It remains unknown whether the immunoisolating capsule can support the survival of human ovarian tissue *in vivo*, a key step towards translating this technology to clinical use. Despite many similarities with murine physiology, human ovarian tissue carries some significant morphological differences. Human ovarian tissue is heterogenous with respect to stromal tissue structure, stromal cell and follicle distribution. The majority of primordial follicles are found in the cortex surrounded by a dense stromal tissue, while more mature follicles are found closer to the medulla. In contrast, murine ovarian tissue is more homogeneous, with densely packed follicles present throughout the entire ovary and surrounded by significantly looser stroma [60]. Furthermore, follicle density varies between

different donors, the right and left ovary from the same donor, and different locations in the cortex from the same ovary[61]. Lastly, murine and human primordial follicles are approximately the same size (~30μm), but the terminal diameter of pre-ovulatory follicles in mice is only ~400μm, while human follicles reach a much larger terminal diameter ranging from 2,000 to 20,000μm[62]. Keeping these differences in mind, the main objective of this study was to investigate whether follicles in human ovarian tissues survive the encapsulation process and maintain viability after implantation. We encapsulated human ovarian tissue from donors in a dual-layered PEG capsule and implanted these capsules subcutaneously into non-obese diabetic/severe combined immunodeficient gamma (NSG) mice and evaluated follicle survival in fresh and cryopreserved human ovarian tissue that was either encapsulated or non-encapsulated.

2.2 Materials and Methods

2.2.1 Collection of Human Ovarian Tissue

Organ procurement for research purposes followed standardized protocols in place at the International Institute for the Advancement of Medicine (IIAM) and the associated Organ Procurement Organization (OPO) involved in the harvest. For this study ovaries were procured from four deceased donors (age range: 18-26 years) by the IIAM, see **Table 2.1** for additional donor information. Before cross-clamp, the organs were perfused with either Belzer University of Wisconsin® Cold Storage Solution (Bridge of Life, SC, USA), Custodiol® HTK (Histidine-Tryptophan-Ketoglutarate) Solution (Essential Pharmaceuticals, NC, USA), or SPS-1 Static Preservation Solution (Organ Recovery Systems, IL, USA). Organs were placed in perfusion solution and shipped on ice. De-

identified donor information is summarized in **Table 2.1**, including age, weight, height, BMI, and cross-clamp time (time at which the organ is cut from blood/oxygen supply). Cold ischemic time (CIT) was calculated as the time interval between cross-clamp time of the donor (and subsequent cessation of arterial blood flow to the ovaries) in the operation room and start time of the tissue harvest subsequent to arrival at the laboratory.

2.2.2 Ethical Approval Process

Table 2.1 Donor Information

Donor No.	Age (years)	Height (cm)	Weight (kg)	BMI	Ethnicity	Cause of Death	Storage Solution	Right Ovary Size (cm)	Left Ovary Size (cm)	Cardiac arrest/ downtime	Cross-clamp Date and Time*	Cold Ischemic Time** (hours)
1	26	157	60.2	24.42	Black or African American	Anoxia	UW	4*2*1	4*2*1	YES 30 minutes	7/24/2019 16:27	9.8
2	18	160	70.3	27.46	Black or African American	Anoxia	UW	3*1*0.5	3*1.5*0.5	NO	10/14/2019 6:03	18.8
3	18	162.56	52.8	19.98	White	Head trauma	HTK	4*3*1.2	NA	NO	1/9/2019 17:22	7.9
4	23	165	67.9	24.94	White	Head trauma	UW	4*2.5*1.7	3.5*2*1.2	YES 10 minutes	12/19/2019 15:46	5.1

UW: University of Wisconsin Solution
HTK: Histidine-Tryptophan-Ketoglutarate Solution
* Time at which the organ is cut from blood/oxygen supply
** Time between cross-clamp and the beginning of tissue processing

The IIAM procures tissue and organs for non-clinical research from Organ Procurement Organizations (OPOs), which comply with state Uniform Anatomical Gift Acts (UAGA) and are certified and regulated by the Centers for Medicare and Medicaid Services (CMS). These OPOs are members of the Organ Procurement and Transplantation Network (OPTN) and the United Network for Organ Sharing (UNOS) and operate under a set of standards established by the Association of Organ Procurement Organizations (AOPO) and UNOS. Informed, written consent from the deceased donor's family was obtained for the tissue used in this publication. A biomaterial transfer

agreement is in place between IIAM and the authors that restricts the use of the tissue for pre-clinical research that does not involve the fertilization of gametes. The use of deceased donor ovarian tissue in this research is categorized as 'not regulated', per 45 CFR 46.102 and the 'Common Rule', as it does not involve human subjects and complies with the University of Michigan's IRB requirements as such.

2.2.3 Tissue processing

All tissue processing was done aseptically in a biosafety cabinet. After receiving donor tissue, the ovaries were separated from other reproductive tissues (i.e. the uterus, fallopian tubes) (**Figure 2.1, B**). The ovaries were decortified using a custom cutting guide (Reprolife Japan, Tokyo) to remove 1 µm thick cortex pieces that were approximately 10mmx10mm squares (**Figure 2.1C, Figure 2.2A**). The squares were then cut into approximately 1mm wide strips, 10mm in length and 1mm thick (**Figure 2.1D, Figure**

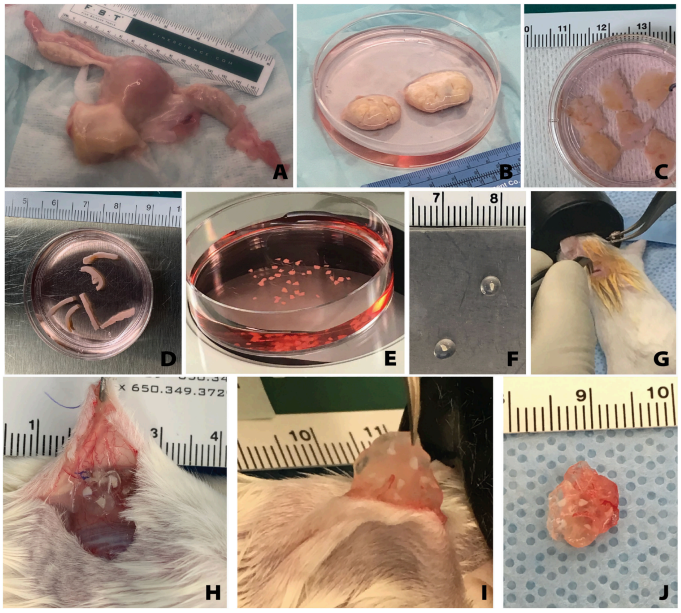

Figure 2.1 Overview of human tissue processing and implantation. Tissue received from UNOS donors (A) was processed to isolate the ovaries (B). Ovarian cortex tissue approximately 10mm x 10mm x 1mm is removed (C), then cut to approximately 1mm x 10mm x 1mm (D), and finally cut to approximately 1mm x 1mm x1mm (E). The small tissues are encapsulated in the hydrogel capsule (F) and implanted subcutaneously (G). Removal of the capsules from the subcutaneous space (H) was conducted at various time points. The capsules were removed from the mice (I, J) and then fixed for histological processing and staining.

2.2A) using a McIlwain Tissue Chopper (The Mickle Laboratory Engineering Co. Ltd., Surrey, UK) and aseptically transferred into holding media (Quinn's Advantage Medium with HEPES (QAMH), 10% Quinn's Advantage Serum Protein Substitute (SPS), CooperSurgical, Måløv, Denmark). The tissue was divided into three groups: 1) Encapsulation of fresh tissue pieces followed by immediate implantation in mice; 2) Fixation using Bouin's fixative (Ricca Chemical, USA) or 4% paraformaldehyde (PFA) (AlfaAesar, USA), and stored overnight at 4°C; 3) Cryopreservation using either slow freezing or vitrification methods.

2.2.4 Cryopreservation

2.2.4.1 Slow Freezing:

The methods as described by Xu et al. were used for slow freezing [63]. Briefly, strips of cortical tissue approximately 1mm x 10mm x 1mm were placed into cryovials (Nunc, Roskilde, Denmark) filled with pre-cooled cryoprotectant media (QAMH, 10% SPS, 0.75M dimethyl sulfoxide (DMSO) (Sigma Aldrich, St. Louis, USA), 0.75M ethylene glycol (Sigma Aldrich, St. Louis, USA), 0.1M sucrose (Sigma Aldrich, St. Louis, USA), and equilibrated at 4°C for at least 30 minutes. After equilibration, cryovials were loaded into the Cryologic Freeze Control System (Cryologic, Victoria, Australia). Vials were then frozen via the following protocol: samples were (1) cooled from 4°C to -9°C at a rate of -2°C /min (2) equilibrated for 6 min at -9°C (3) seeded manually using large swabs cooled by submersion in liquid nitrogen (4) held for 4 min at -9°C (5) cooled to -40°C at a rate of -0.3°C/min and (6) plunged into liquid nitrogen and stored in a cryogenic storage dewar until thawed for use.

2.2.4.2 Vitrification

The methods as described by Kagawa et al. were used for vitrification, with minor changes to the timing [64]. Briefly, strips of tissue approximately 1mm x 10mm x 1mm were first transferred to an equilibration solution (7.5% ethylene glycol, 7.5% DMSO, and 20% SPS) for 25 minutes and then transferred to a vitrification solution (20% ethylene glycol, 20% DMSO, 0.5M sucrose, and 20% SPS) until the tissue sank to the bottom of the vial, indicating saturation with the solution. Each strip was placed on a 25 µm thick copper cryostrip (Lyon Industries, South Carolina, USA), which was then submerged in liquid nitrogen for approximately 30 seconds. Strips were transferred into a cryovial (Nunc, Roskilde, Denmark) filled with and submerged in liquid nitrogen. Samples were stored in liquid nitrogen until thawed for use.

2.2.5 Thawing Tissue

2.2.5.1 Slow Frozen Tissues:

The process described by Xu et al. was followed with minimal changes [63]. Briefly, vials with ovarian tissue were removed from liquid nitrogen and placed in a 37°C bath. Once the cryoprotectant media in the vial had thawed, the tissue was removed from the vial and put into Thaw Solution One (1M DMSO, 0.1M Sucrose, 10% SPS in QAMH) for ten minutes. Tissue was then incubated sequentially in Thaw Solution Two (0.5M DMSO, 0.1M Sucrose, 10% SPS in QAMH), Three (0.1M Sucrose, 10% SPS in QAMH), and Four (10% SPS in QAMH) for ten minutes each. All thaw solutions were maintained at room

temperature during this process. Tissue strips were cut into cubes measuring approximately 1mm3 while still in Thaw Solution Four.

A

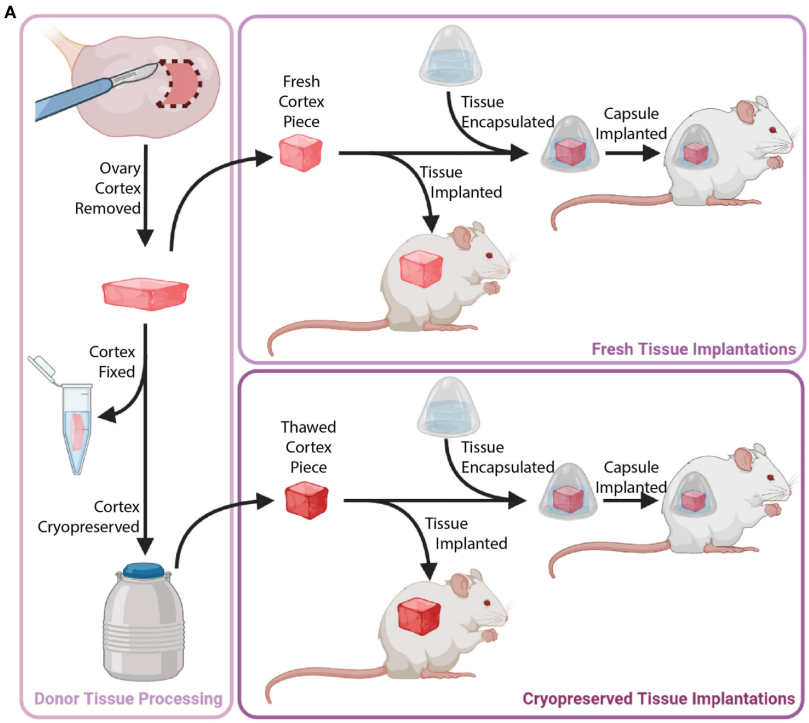

B

	3 days	1 week	2 weeks	1 month	2 month	3 months
# Capsules (donor)	50 (2,4)	50 (2,4)	30 (4)	70 (1,2,3,4)	20 (3)	20 (3)
# Strips (donor)	5 (2,4)	5 (2,4)	3 (4)	7 (1,2,3,4)	2 (3)	2 (3)

Figure 2.2 Description of implanted tissue groups. Tissue processing was conducted as shown in part (A). Cortical tissue strips were cut into squares either as fresh tissue (Donors 1 and 2) or post-cryopreservation (Donors 3 and 4). Capsules and control tissue were implanted in mice. The total number of capsules/strips at each time point are shown in part (B).

2.2.5.2 Vitrified Tissues

The process described by Lee et al. was followed, with minor modifications [65]. The cryovials with ovarian cortex strips were removed from liquid nitrogen. The copper supports with tissue were immediately transferred into Thaw Solution One (1mg/mL Human Serum Albumin (HSA) (MilliporeSigma, MA, USA) and 1M sucrose in QAMH). Copper supports were removed, and the tissue was incubated at 37°C for three minutes. Tissue was transferred to Thaw Solution Two (1mg/mL HSA and 0.5M sucrose in QAMH)

for 5 minutes at room temperature. Tissue was then transferred to Thaw Solution Three (1mg/mL HSA in QAMH), brought up to 37°C, and cut into cubes measuring approximately 1mm3.

2.2.6 Encapsulation

The pieces of ovarian cortical tissue (1mm^3) (**Figure 2.2A)** were maintained in the final thaw solution media (Solution 4 for slow freezing, Solution 3 for vitrification) at 37°C until encapsulation (**Figure 2.1E**). The PEG core was prepared by cross-linking 8-arm PEG-VS (40 kDa, Jenkem Technology, Beijing, China) (5% w/v) with plasmin sensitive peptide (Ac-GCYK↓NSGCYK↓NSCG, MW 1525.69 g/mol, > 90% Purity, Genscript, ↓ indicates the cleavage site of the peptide). The PEG shell was prepared with 4-arm PEG-VS (20 kDa, Jenkem Technology) (5% w/v), Irgacure 2959 (Ciba, Switzerland, MW = 224.3) (0.4% w/v), and N-vinyl-2-pyrrolidone (Sigma-Aldrich, St. Louis, USA) (0.1% v/v). The tissue was then placed in a 4μL droplet of degradable PEG core pre-cursor solution. After five minutes of crosslinking the core was transferred into 10μL of non-degradable PEG shell pre-cursor solution. The shell was cross-linked via UV light at constant intensity (4.4mW/cm^2, 6 minutes). Encapsulated tissue (**Figure 2.1F, Figure 2.2A**) was maintained in Leibovitz L-15 media (Gibco, USA) at 37°C until implantation.

2.2.7 Subcutaneous Implantation

Animal experiments for this work were performed in accordance with the protocol approved by the Institutional Animal Care and Use Committee (IACUC) at the University of Michigan (PRO00007716 & PRO00009635). The IACUC guidelines for survival surgery

in rodents and the IACUC Policy on Analgesic Use in Animals Undergoing Surgery were followed for all procedures.

Female NSG mice (strain 005557, The Jackson Laboratory, Bar Harbor, ME, USA) 6-8 weeks old were anesthetized using isoflurane (2-3%) via inhalation. Mice were given preemptive analgesics (Carprofen, RIMADYL, Zoetis, USA, 5mg/kg body) via subcutaneous injection. An incision was made in the medial/dorsal skin. Nine to ten PEG capsules, along with an equivalent amount of non-encapsulated tissue (as a control), were inserted into the dorsal subcutaneous space in the mouse (**Figure 2.1G**). The control graft was inserted subcutaneously and sutured using 5/0 absorbable sutures (AD surgical) to the subcutaneous tissue to ensure graft recovery. Using 5/0 absorbable sutures the incision was closed, with special attention paid to avoid suturing capsules/control tissue. Mice recovered in a clean cage and were monitored post-operatively for 7-10 days.

2.2.8 Implant Removal

Mice were anesthetized using isoflurane as described above. An incision was made in the medial/dorsal skin, avoiding implanted grafts. The encapsulated and control grafts were removed (**Figure 2.1H-J**), placed in either Bouin's fixative or 4% PFA overnight at 4°C, washed, and stored in 70% ethanol or PBS, depending on respective fixative.

2.2.9 Histology

All samples were processed at the Histology Core in the Dental School at the University of Michigan. The paraffin embedded tissue blocks were serially sectioned at a thickness of 5μm and stained with hematoxylin and eosin.

2.2.10 Follicle Counting

Slides were viewed using a brightfield microscope (Leica DM 1000, Germany) at 20 or 40x magnification. Encapsulated tissue and control non-encapsulated grafts were analyzed for follicle density. Every 16th section was analyzed for follicles for all groups. For slow frozen encapsulated tissue groups between 6 and 17 sections were analyzed per mouse (n=3 mice per time point). For slow frozen non-encapsulated control tissue between 5 and 14 sections were analyzed per mouse (n=3 mice per time point). In the slow frozen groups, each data point represents the follicle density calculated from all capsules retrieved from each mouse. For vitrified encapsulated tissue groups between 4 and 10 sections were analyzed per mouse (n=2 mice per time point). For vitrified non-encapsulated control tissue between 5 and 8 sections were analyzed per mouse (n=2 mice per time point). In the vitrified groups, each data point represents the follicle density calculated from all capsules retrieved from each mouse. For fresh fixed tissue, between 8 and 12 sections were analyzed per donor where each data point represents the follicle density calculated from a single analyzed section. Follicles were counted manually, and follicle stage was identified using standard morphological guidelines [17]. All primordial and primary follicles were counted for each analyzed section. Preantral and antral were counted only after comparing the location of the follicle in the tissue and follicle size in preceding and subsequent sections to avoid “double counting”. Density measurements

were calculated using an estimated area (1mm^2 per section) based on the approximate geometry of the sample, and the estimated tissue section thickness. The follicle density values reported in this study are all normalized to the same volume.

2.2.11 Statistical Analysis

Statistical analysis was performed using GraphPad Prism software. A 1-way ANOVA was used for fresh tissue analysis comparing follicle density between donors. Tukey's comparison test was used for implanted tissue analysis to a evaluate differences in follicle density across two variables (time and encapsulation). The results were considered statistically significant when $p < 0.05$.

2.3 Results

2.3.1 Fresh donor tissue prior to processing reveals donor heterogeneity.

First, we analyzed the follicle density in ovarian cortex from each donor to benchmark a starting point for the grafts. In this study we used ovarian tissue from 4 young healthy deceased donors, ranging from 18 to 26 years old. Inherently, human ovarian cortex varies greatly between donors and location in the ovary. As expected, all donor tissues displayed a high degree of heterogeneity between different strips and various locations in the same cortical strip from the same donor as well as across different donors. The average follicle density in ovarian tissue from Donor 1, 26 years old and BMI of 24.4, was 361 ± 304 follicles/mm^3 (average ± standard deviation). The average follicle density in the ovarian cortex of Donor 2, 18 years old and BMI 27.5, was 1528 ± 528 follicles/mm^3. Donor 3, 18 years old and BMI of 20, had an average follicle density of 4414 ± 521 follicles/mm^3. Donor 4, 25 years old and BMI of 24.9, had an average follicle density

of 464 ± 152 follicles/mm^3 (**Figure 2.3A, B**). Donor 3 had the greatest follicle density, 4414 ± 521 follicles/mm^3 ($p<0.0001$) compared to the other three donors. The follicle density of Donor 2 was greater compared to the lower follicle densities of Donors 1 and 4 ($p <0.0001$). The follicle densities of Donors 1 and 4 were relatively similar and not significantly different. Histological images from each donor showed multiple primordial and primary follicles (**Figure 2.3C-N**). The cortical stroma had regions of densely packed primordial follicles with oocytes surrounded by a single layer of flat squamous granulosa cells (**Figure 2.3E iii., Figure 2.3K i., Figure 2.3N i**.). In addition to primordial follicles, primary and small preantral follicles were also identified in the ovarian tissue from all donors. Primary follicles showed the characteristic oocyte surrounded by a single layer of cuboidal granulosa cells (**Figure 2.3E i., Figure 2.3H iv., Figure 2.3K ii.**), while preantral follicles had a few layers of granulosa cells surrounding the oocyte (**Figure 2.3H ii**.).

A

Donor No.	Age (years)	BMI (kg/m2)
1	26	24
2	18	27
3	18	20
4	23	25

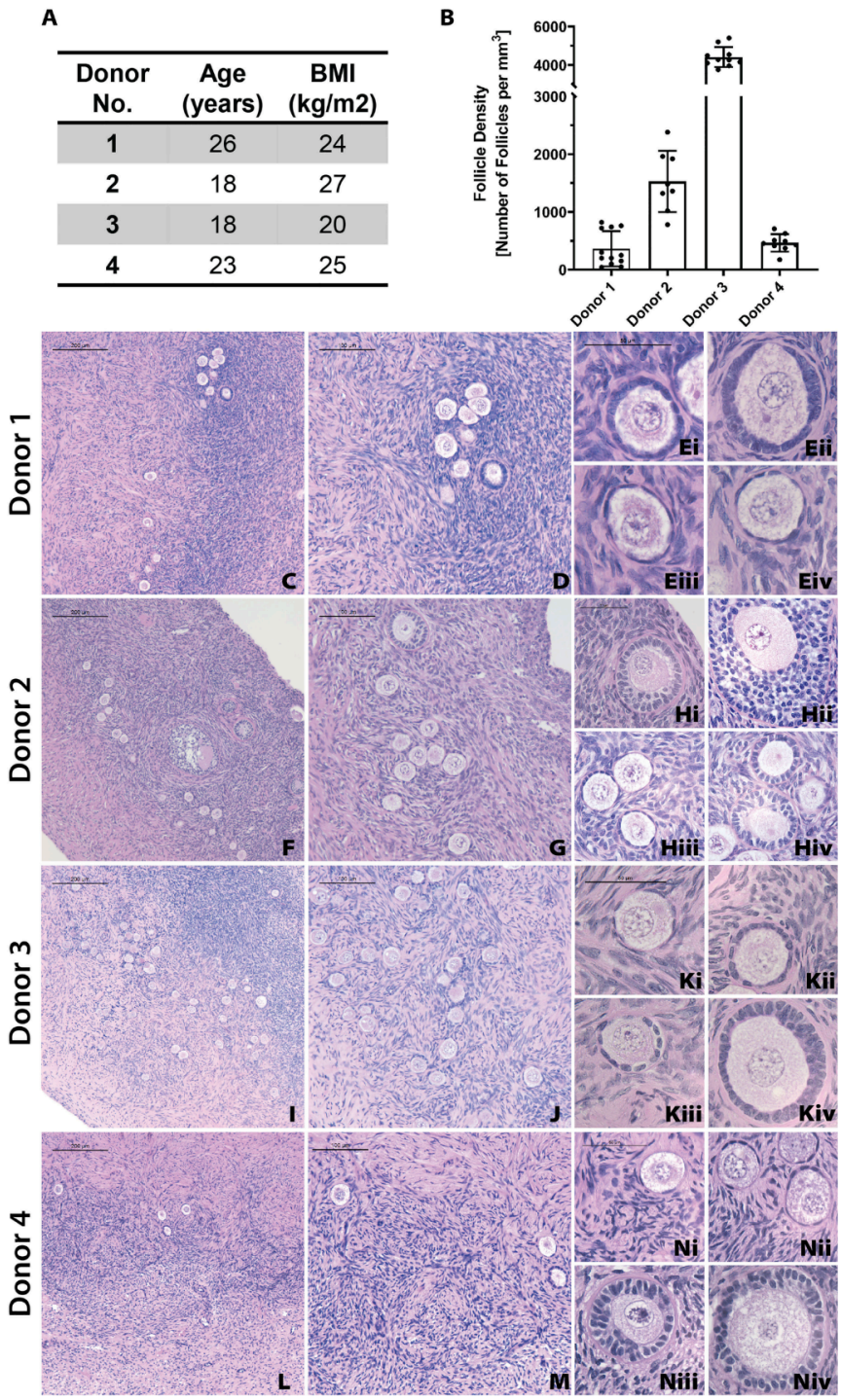

Figure 2.3 Donor metrics and initial histology. The donor tissues used in this study were selected from a bank from donors with various ages and BMI values (A). Follicle density values were calculated for each donor from fresh/fixed tissues (B). The large differences in average follicle density between donors is supported by histological images (C–N). Representative images from Donor 1 (C–E), Donor 2 (F–H), Donor 3 (I–K), and Donor 4 (L–N) show stark differences in follicle distribution at low magnification (C, F, I, L). Increased magnification shows the presence of primordial (E iii., K i., N i), primary (E i., H iv., K ii.), and secondary (H ii.) follicles. Scale bars represent 200μm for C, F, I, and L. Scale bars represent 100μm for D, G, J, and M. Scale bars represent 50μm for all others.

2.3.2 Follicles in encapsulated fresh ovarian cortical tissues survive for at least one month after implantation in NSG mice

Grafting of non-encapsulated human ovarian tissue is a gold standard for restoration of fertility in human patients and animal models[66]. However, whether encapsulated human ovarian allograft survives encapsulation and implantation has yet to be demonstrated. Here, we investigated whether the encapsulation of fresh ovarian cortical tissue in a hydrogel decreases follicle survival and longevity after implantation in mice and compared to non-encapsulated fresh tissue. Immediately after receiving and processing ovaries from Donors 1 and 2, we encapsulated and implanted ovarian cortical tissues in mice with nine to ten capsules per animal for time periods of 3 days (n=2 mice), 1 week (n=2), and 1 month (n=3) (**Figure 2.4D-F respectively**). A non-encapsulated cortical strip measuring 1mm x 10mm x 1mm was implanted in each mouse and served as a control (**Figure 2.4A-C**). Recovery of the capsules from the subcutaneous space was reasonably straightforward as the capsules typically clumped together (**Figure 2.1J**). Eight to ten capsules were recovered in six out of seven mice (no capsules were recovered from one animal, possibly due to degradation). Non-encapsulated control tissue was recovered in all seven mice. Eight to twenty-six sections for each implant type (encapsulated or non-encapsulated) were analyzed using bright field microscopy to assess follicle survival. Multiple follicles at different stages ranging from primordial to antral were present in retrieved encapsulated tissue from all time points up to a month post implantation within the same capsule (**Figure 2.4F**). Nuclear staining of the encapsulated tissue retrieved after 3 days and 1 week identified the presence of multiple stromal cells around the follicles. The encapsulated tissue had multiple surviving follicles

after 1 month, however qualitative analysis showed a decrease in number of stromal cells. Overall, we concluded that follicle survival in human ovarian cortex was not decreased by the encapsulation process and was similar to the non-encapsulated controls.

2.3.3 Slow frozen, short-term implanted tissues tolerate encapsulation and survive to the same extent as non-encapsulated tissue following implantation

The next objective was to determine whether encapsulation of cryopreserved ovarian tissue using the slow freezing approach, similar to the current clinical practice recommended for fertility preservation in pediatric patients, negatively affected follicle survival. Ovarian cortical strips from Donor 4 that had previously been slow frozen, were thawed and encapsulated. Multiple capsules and all non-encapsulated tissues were recovered in all 20 mice. There was no statistically significant difference in follicle density

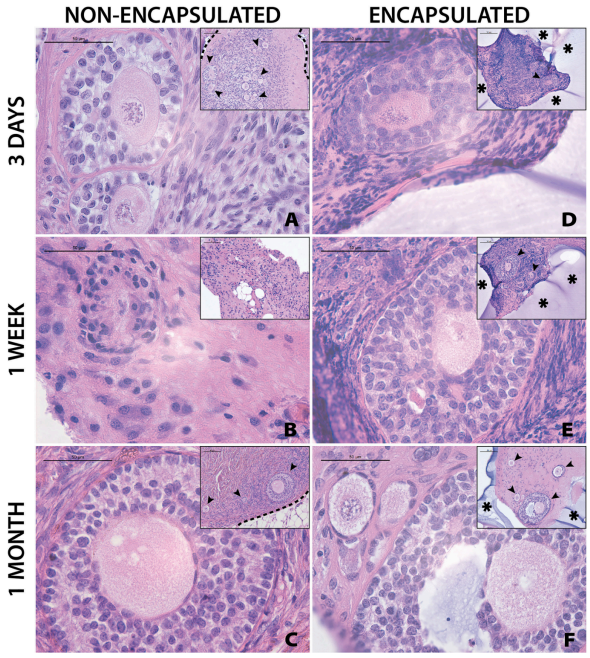

Figure 2.4 Follicles in fresh tissue survive up to one month. Representative images from non-encapsulated fresh tissue samples (A-C) and encapsulated fresh tissue samples (D-F) are shown here. These samples were removed from mice at various time points of 3 days (A, D), 1 week (B, E), and 1 month (C, F). Scale bars represent 100mm for inserts and 50mm for all others. Black arrow heads (➤) indicate follicles, asterisks (✻) indicate the PEG capsule, and dashed black lines (---) indicate the human ovarian tissue border with surrounding murine tissue after implantation.

between encapsulated and non-encapsulated grafts at any time point (**Figure 2.5A**). For the 1-day time point, the follicle density was 24 ± 21 follicles/mm^3 (average ± standard deviation) in the non-encapsulated graft and 90 ± 60 in the encapsulated tissue. For the 3-days' time point, the average follicle density was 30 ± 21 and 73 ± 35, for the 1-week time point, the average follicle density was 28 ± 23 and 80 ± 43, for the 2-weeks' time point, the average follicle density was 25 ± 18 and 89 ± 51 for the 1-month time point, the

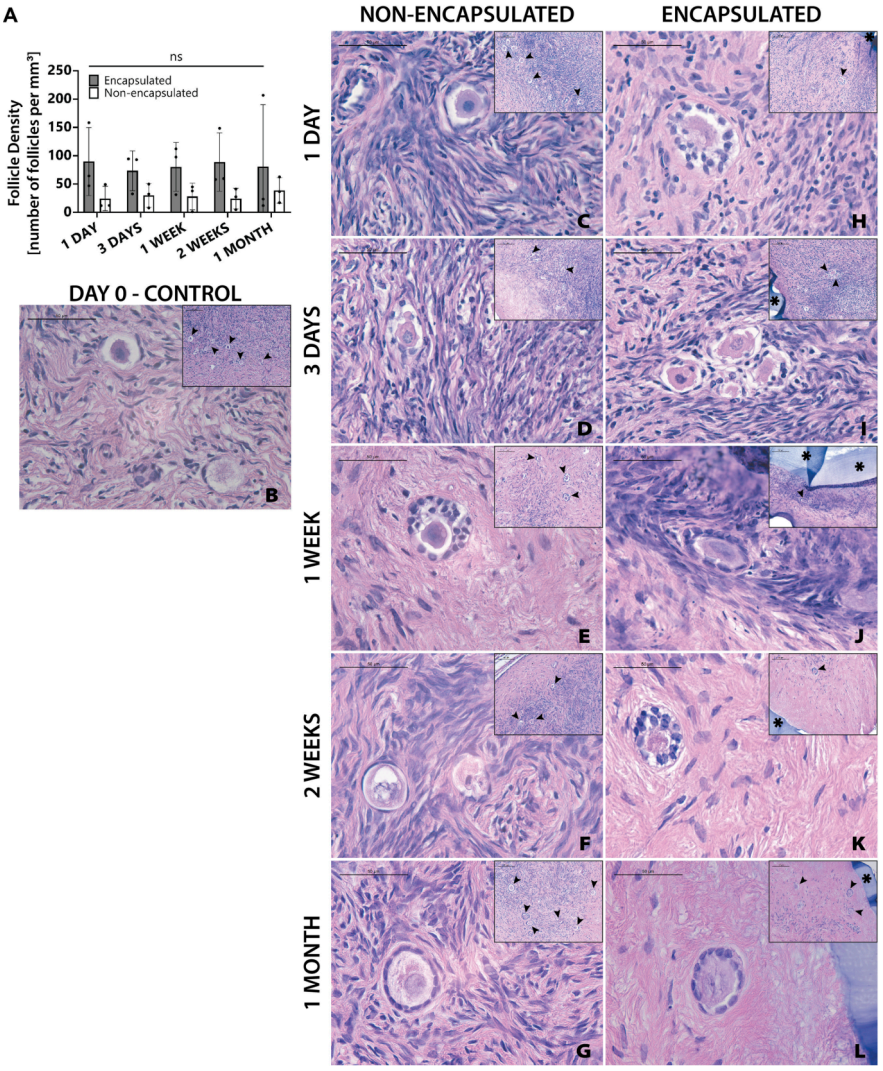

Figure 2.5 Follicles in slow frozen tissue survive up to one month. Follicle density values (A) are determined from histological images (C–L). Non-implanted thawed/fixed tissue (B) is a control for non-encapsulated groups (C–G) and encapsulated groups (F–L). These samples were removed from mice at various time points of 1 day (C, H), 3 days (D, I), 1 week (E, J), 2 weeks (F, K), and 1 month (G, L). Scale bars represent 100μm for inserts and 50μm for all others. Black arrow heads (➤) indicate follicles, asterisks (✻) indicate the PEG capsule.

average follicle density was 39 ± 22 and 81 ± 109, respectively. The difference in follicle density was not statistically significant between different time points, nor was it different when comparing between encapsulated and non-encapsulated groups at each time point. These findings suggest that after slow freezing (1) human ovarian follicles tolerate encapsulation in the dual-layered PEG hydrogel capsule and (2) encapsulated human ovarian tissue survives to the same extent as non-encapsulated tissues when implanted in mice.

Although follicle numbers were not significantly different between groups, we also wanted to probe whether there were any differences between groups in terms of the quality of the stromal compartment. Qualitative histological analysis of tissue fixed immediately post-thawing (**Figure 2.5B**) and tissue fixed after implantation showed similar distribution of stromal cells (marked with hematoxylin). Furthermore, similar stromal cell densities were evident across time points, as well as between encapsulated (**Figure 2.5H-L**) and non-encapsulated groups (**Figure 2.5C-G**) at the same time points, except for the 1-month encapsulated tissue (**Figure 2.5L**). The 1-month encapsulated tissue had less cellular staining around the follicles and more fibrous portions of the extracellular matrix (stained pink with eosin). Furthermore, the types of follicles seen in encapsulated and non-encapsulated groups at various time points were comparable, with primordial and primary follicles being the most prevalent. Taken together, these observations support the hypothesis that follicles can survive slow freezing before encapsulation and survive up to one month *in vivo*.

2.3.4 Vitrified, long-term implanted tissues tolerate encapsulation and survive up to three months in vivo

The final objective of this study was to investigate whether the two clinically available cryopreservation methods, slow freezing and vitrification specifically, have different outcomes of follicle survival in grafted tissue following encapsulation and implantation. Vitrified tissue from Donor 3 was encapsulated and implanted in mice for 2 and 3 months. Non-encapsulated, 1mm^3 grafts served as controls. Two months after implantation the average follicle density was 17 follicles/mm^3 in the non-encapsulated grafts and 2 follicles/mm^3 in the encapsulated tissue. For the 3-month time point, the average follicle density was 57 follicles/mm^3 in the non-encapsulated graft and 22 follicles/mm^3 in the encapsulated tissue (**Figure 2.6A**). Vitrified tissue had greater cell density in the stroma (**Figure 2.6B**) than frozen tissue before implantation (**Figure 2.5B**). Encouragingly, follicles in implanted tissues survived up to three months post-

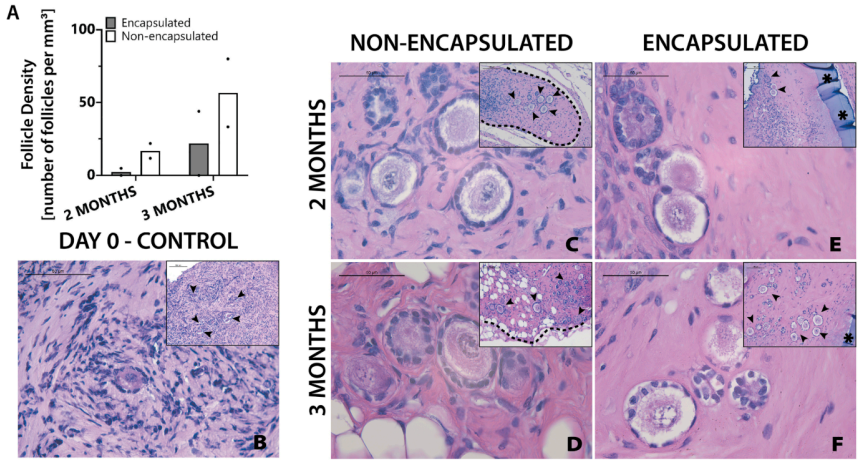

Figure 2.6 Follicles in vitrified tissue survive up to three months. Follicle density values (A) are determined from histological images (C–F). Non-implanted thawed fixed tissue (B) is a control for non-encapsulated groups (C, D) and encapsulated groups (E, F). These samples were removed from mice at various time points of 2 months (C, E) and 3 months (D, F). Scale bars represent 100μm for inserts and 50μm for all others. Black arrow heads (➤) indicate follicles, asterisks (✻) indicate the PEG capsule, and dashed black lines (---) indicate the human ovarian tissue border with surrounding murine tissue after implantation.

implantation, but the surrounding stroma had lower cell density compared to tissue prior to implantation (**Figure 2.6C-F**); the decrease in stroma cell density was observed in all implanted groups, similarly to the one-month time point for encapsulated slow frozen tissue (**Figure 2.5L**) In comparison to other slow frozen tissue, vitrified groups similarly have a follicle pool comprised predominantly of primordial and primary follicles. Based on our findings, we concluded that follicles and ovarian stromal cells tolerate vitrification before encapsulation and survive up to three months *in vivo*.

2.4 Discussion

Previously, using PEG-based immunoisolating capsules we have demonstrated that the capsule protected murine ovarian allografts in immune competent and sensitized murine hosts and promoted folliculogenesis up to antral stages after single and repeated implantations [47]. Despite mice and humans having similar hypothalamus-pituitary-gonad axis regulation, circulating cytokines and hormones, and developmental stages of follicular differentiation, existence of other physiological and anatomical differences between human and murine ovarian tissues necessitates further investigation to determine translatability of the use of immunoisolating capsules from mouse to human tissues. One example of the challenges working with human tissue is that human primordial follicles are spread heterogeneously in the stroma of ovarian cortex and require normalization of the follicle counts in each graft. The heterogeneity of human tissue introduced significant variance into our quantification of follicle density. To control for this, encapsulated tissues and corresponding non-encapsulated tissue originating from the same donor were included within same groups to minimize the impact of inherent heterogeneity between donors. Tissue pieces placed in the encapsulated groups and

non-encapsulated groups were randomized to minimize skewing of results due to heterogeneity present in a single ovary. Even with these adaptations it is uncertain if differences seen are an artifact of tissue heterogeneity or are a result of tissue treatment; persistence of a large variability resulting in largely qualitative methods of analysis. One option to minimize the effect of heterogeneity on follicle density analysis is to significantly increase the number of human donors and recipient mice. Another option is to use cryopreserved tissues that would have undergone a thorough characterization prior to xenografting, allowing for donors with similar follicle densities to be used in the same study.

Ovarian tissue cryopreservation (OTC) enables preservation of many thousands of primordial follicles all at once without the need of ovarian stimulation and can be performed at any age from early prepubertal years to late thirties. Slow freezing and vitrification of ovarian tissues are the two most studied methods of cryopreservation. The majority of clinical data, such as the rates of live births [67–69], the efficiency and safety of OTC in terms of follicle survival and patients' outcomes after transplantation, is available for slow freezing methods, which was considered experimental for a few decades and was recently clinically approved [70]. Slow freezing in general uses a low amount of cryoprotective agents to reduce cell toxicity. This method utilizes standardized equipment and detailed cooling protocols such that there is decreased variability between operators, as well as between batches. On the downside, slow freezing poses the risk of intracellular ice crystal formation, which can be minimized by manual seeding at the media/air interface [71,72]. Vitrification, another cryopreservation method, is currently only approved for embryo and egg cryopreservation[73]. It utilizes greater concentrations of

cryoprotectants that prevent ice crystal formation. Vitrification does not require standardized equipment, which results in some variability between operators and batches. So far, this method has been clinically approved for oocyte and embryo cryopreservation but is still considered experimental for OTC. Possibly, in the future, it may become clinically approved for OTC as well.

Both cryopreservation methods have been shown to have negligible impact on follicle count as compared to fresh tissue [74] and ensure the survival of primordial follicles, which are critical for the application described in this study; dormant primordial follicles in the implanted encapsulated tissue functions as the ovarian reserve, determining the quality and the lifespan of the encapsulated tissue. Additionally, OTC allows important screening for disease or infection and analysis of the follicle density in the donor tissue that would not be possible with fresh tissue. While some reports show that vitrification results in (1) decreased primordial follicle DNA damage and (2) better outcomes for stromal tissue [75], others indicate that slow freezing is superior for (1) preserving primordial follicles, (2) preventing DNA damage, and (3) promoting follicular cell proliferation [65]. Comparison of the survival of slow frozen and vitrified tissues with fresh tissues used as controls showed fresh tissues to have more mature (i.e. secondary/antral) follicles, as expected. More mature follicles contain oocytes that are more metabolically active and antral follicles contain the cumulus-oocyte complex, resulting in decreased cryoprotectant agent penetration and therefore increased probability of ice crystal formation [76]. Our observation that the stroma in slow frozen tissues (**Figure 2.5**) is less fibrous as compared to vitrified tissues (**Figure 2.6**) is somewhat unexpected since the literature indicates that vitrification typically has better stromal cell survival [75]. The most likely explanation for

these differing results is that there was more variability between operators during the vitrification process. Notably, an important finding from the present study is that follicles can survive the process of cryopreservation and survive for at least 30 days *in vivo*, regardless of cryopreservation method.

Encapsulation may slow down the diffusion of nutrients, yet it is necessary to prevent rejection of the grafts. Our comparison of tissues that underwent the encapsulation process to tissues that did not, found that the follicle densities of non-encapsulated tissues were not higher than the follicle densities in encapsulated tissues. Qualitative examination of the implants also indicates minimal differences between encapsulated and non-encapsulated tissues at early time points, but larger differences begin to appear starting around one month. The main change observed is a decrease in stromal cell density in encapsulated tissues. This trend is emphasized by greater areas of fibrous stromal extracellular matrix, the mostly eosin-stained matrix without visible nuclei. The relative similarities between short term implants and subsequent differences in long term implants indicate that the process of encapsulation is not harmful to human tissues. It is hypothesized that as time goes on the rate of diffusion of nutrients is inadequate to support these tissues.

In conclusion, we have shown that an immunoisolating dual PEG capsule supported follicle survival in human ovarian xenografts up to 90 days *in vivo*. The process of encapsulation did not decrease follicle density compared with non-encapsulated grafts. Cryopreservation of ovarian cortical strips allowed for thorough analysis of follicular density to ensure graft longevity. Moving forward towards clinical translation of this technology, a greater scale of characterization of the donor tissue and optimization of the

PEG shell to increase diffusion and increase stromal cell survival at later time points, should be done.

Chapter 3 Human Ovarian Tissue Encapsulated in an Immune-Isolating Hydrogel Restores Ovarian Endocrine Function in Ovariectomized Mice

3.1 Introduction

The population of pediatric cancer survivors continues to grow with an estimated 9,000 new diagnoses in 2024 for children aged 0-14, resulting in more children and teenagers being diagnosed with and surviving cancer, and living into adolescence and adulthood[77,78]. While having cancer in remission is a significant milestone, it is important to consider the patient's quality of life after treatment. Chemotherapy and radiation are particularly harmful to the nonrenewable follicular reserve in the ovaries[5]. Damage to the ovaries may result in delayed or absent pubertal development in these survivors, with 50% of this population experiencing endocrine complications and infertility[5–7,79]. The lack of gonadal hormones leads to a cascade of other negative outcomes including cardiac disease, osteopenia, growth hormone dysfunction, lack of neuroprotective effects, as well as dysregulated T cell function, premature epiphyseal closure, dysregulated food intake and serum leptin levels[80–85]. The widespread systemic impact of the lost ovarian endocrine function demonstrates the importance of ovaries and hormonal feedback in female pediatric cancer survivors.

Hormone replacement therapy (HRT) is the only existing clinically approved treatment to induce puberty in adolescent patients in remission who experience premature ovarian insufficiency (POI) [27,86]. Using HRT for puberty induction in adolescent girls with POI has multiple limitations[87–91]. First and most importantly, HRT supplies only

two hormones, estradiol and progesterone, at steady levels lacking the pulsatility and fluctuations normally present during the menstrual cycle[88–90]. Second, the levels of hormones delivered with HRT are not regulated by the hypothalamic–pituitary–gonadal (HPG) axis and cannot engage with any other reciprocal physiological feedback systems with the rest of the body. Third, exogenous delivery of steroid hormones has been associated with higher risk of anxiety and suicide, particularly for adolescents[91]. Lastly, the long-term safety and efficacy of HRT for puberty induction has yet to be evaluated in adolescent girls requiring the HRT treatment for decades to compensate for the loss of gonadal steroids.[18]

As an alternative for HRT, here we investigated whether implanted donor ovarian tissue could restore the lost ovarian endocrine milieu and the physiological and cyclical reciprocal feedback in the HPG axis by producing missing endogenous hormones in response to circulating gonadotropins. In the past decade implantation of autologous human ovarian cortex has been successful for fertility restoration and can be offered to pediatric patients and women unable to undergo ovarian stimulation[92,93]. Fresh ovarian tissue transplantation was first shown to be successful in 2005 with documented restoration of fertility and endogenous endocrine function[94]. Investigation of cryopreserved tissue function after transplantation showed increased oestrogen levels in 75% of participants, decreased follicle stimulating hormone (FSH) in 72% of participants, decreased luteinizing hormone (LH) in 67% of participants, and the return of menses in 72% of participants[94]. Pooling data from all participants (n=568 women), regardless of the graft being fresh or cryopreserved, Khattak *et al*. concluded that FSH and LH returned to physiological levels 19 weeks after implantation, and menses returned after 18 weeks[94].

However, the use of autologous tissues for pediatric survivors is limited due to the possibility of reintroducing cancer cells potentially harbored in the tissue, especially in patients with hematologic cancers, and is limited to patients who cryopreserved their tissue prior to gonadotoxic treatment, which is far from a widespread practice. In contrast, the immune-isolated donor ovarian tissue would allow for safe and accessible treatment that could restore physiological ovarian endocrine function without immunosuppressive therapy.

Human ovarian tissue has been successfully xenografted from days to months in ovariectomized or intact immunocompromised mice, such as NOD scid gamma (NSG), severe combined immunodeficiency disease (SCID), and congenitally athymic nude mice (nu/nu), often with exogenous stimulation (human menopausal gonadotropin or FSH), and varying grafting locations (intraperitoneal, subcutaneous, intramuscular, and in ovarian bursa)[95]. We have developed an immune-isolating capsule that would allow implantation of donor tissue in an immunocompetent host without the need of immunosuppression. Our previous work demonstrated that a poly(ethylene glycol) (PEG)-based hydrogel capsule with a degradable core and a non-degradable shell supported growth and function of murine follicles in the encapsulated allogeneic tissue while precluding immune cell infiltration and rejection of the allograft[96,97]. However, to mitigate the heterogeneous nature of the human ovarian cortex and variable follicle distribution we increased the volume of the graft from 1mm^3 to 19.6mm^3 and tested whether encapsulated human follicles could resume folliculogenesis, reach antral stages and secrete gonadal hormones. After ovariectomizing immunocompromised mice and subcutaneously implanting encapsulated human ovarian cortical tissues, we evaluated

estrous cyclicity, serum hormone levels, and graft histology. As controls we used non-encapsulated size-matched cortical pieces also xenografted subcutaneously. We found over a 20-week period that (1) estrous cyclicity resumed in all mice (2) estradiol levels increased significantly with graft implantation, and (3) FSH levels trended downward after 18 weeks. Morphological analysis of the encapsulated grafts and non-encapsulated controls confirmed the presence of large antral follicles, ~3mm in diameter, responsible for the hormone production. This work demonstrates, for the first time that the survival and function, including hormone production and folliculogenesis, of encapsulated human ovarian tissue was not affected by the lack of direct vascularization and was similar to the non-encapsulated controls. Furthermore, we demonstrated that human ovarian tissue, either encapsulated or non-encapsulated controls, integrated into the mouse HPG axis, responding to circulating host's gonadotropins and secreting estradiol in response.

3.2 Materials and Methods

3.2.1 Collection of Human Ovarian Tissue

Organ procurement was conducted as previously described[98]. Briefly, organs involved in ovarian cortex harvesting were obtained followed standardized protocols in place at the International Institute for the Advancement of Medicine (IIAM) and the associated Organ Procurement Organization (OPO) for research purposes. This study utilized ovaries procured by the IIAM from eight deceased donors ranging between16-31 years old. Organs were placed in storage solution and shipped on ice. Storage solutions were either normal saline or Belzer University of Wisconsin® Cold Storage Solution. De-identified donor information is summarized in **Appendix Table B.1**, including age, weight, height, BMI, and cross-clamp time (time at which the organ is cut from blood/oxygen

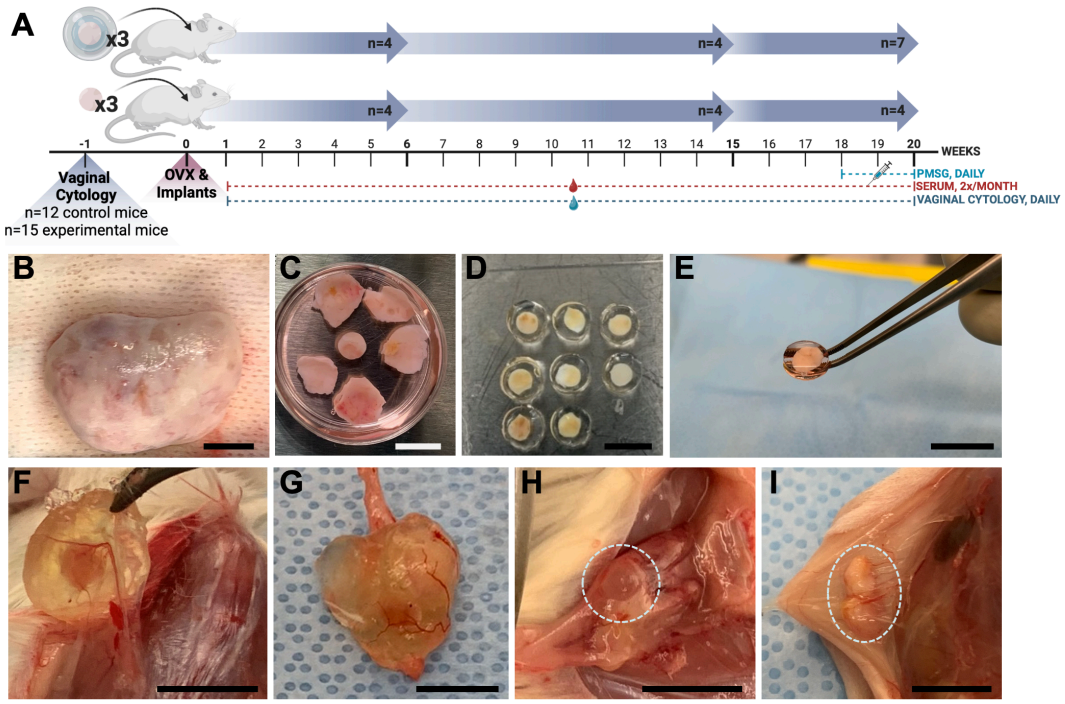

Figure 3.1 Experimental design. NSG mice were implanted with human cortical ovarian tissue (encapsulated or non-encapsulated) and followed out to twenty weeks (A). Donor ovaries (B) are de-cortified (C) and cryopreserved until use. After thawing, tissue is encapsulated in the immune-isolating capsule (D) and is implanted (E). Encapsulated tissue samples (F,G) and non-encapsulated tissue samples (H,I) were removed from the subcutaneous space. Panels G and H show gross morphological changes indicating antral follicles are present. Scale bar represents 1cm A-G, and 5mm for H & I.

supply). Cold ischemic time (CIT) was calculated as the time interval between cross-clamp time of the donor (and subsequent cessation of arterial blood flow to the ovaries) in the operation room and start time of the tissue harvest after arrival at the laboratory.

3.2.2 Ethical Approval Process

As stated previously[98], the IIAM procures tissue and organs for non-clinical research from Organ Procurement Organizations (OPOs), which comply with state Uniform Anatomical Gift Acts (UAGA) and are certified and regulated by the Centers for Medicare and Medicaid Services (CMS). These OPOs are members of the Organ Procurement and Transplantation Network (OPTN) and the United Network for Organ Sharing (UNOS) and operate under a set of standards established by the Association of

Organ Procurement Organizations (AOPO) and UNOS. Informed, written consent from the deceased donor's family was obtained for the tissue used in this publication. A biomaterial transfer agreement is in place between IIAM and the authors that restricts the use of the tissue for pre-clinical research that does not involve the fertilization of gametes. The use of deceased donor ovarian tissue in this research is categorized as 'not regulated', per 45 CFR 46.102 and the 'Common Rule', as it does not involve human subjects and complies with the University of Michigan's IRB requirements as such.

3.2.3 Tissue Processing

All tissue processing was done aseptically in a biosafety cabinet. After receiving donor tissues, the ovaries were separated from other reproductive tissues (i.e. the uterus, fallopian tubes) (**Figure 3.1B**). The ovaries were de-cortified using a custom cutting guide (Reprolife Japan, Tokyo) to make squares measuring 10mmx10mm and approximately 1 mm thick (**Figure 3.1C**). The squares were then aseptically transferred into holding media (Quinn's Advantage Medium with HEPES (QAMH), 10% Quinn's Advantage Serum Protein Substitute (SPS), CooperSurgical, Måløv, Denmark) before cryopreservation.

3.2.4 Slow Freezing

The methods as described by Xu et al. were used for slow freezing[63]. Briefly, the 10mm x 10mm x 1mm squares of cortical tissue approximately were placed into cryovials (Nunc, Roskilde, Denmark) filled with pre-cooled cryoprotectant media (QAMH, 10% SPS, 0.75M dimethyl sulfoxide (DMSO) (Sigma Aldrich, St. Louis, USA), 0.75M ethylene glycol (Sigma Aldrich, St. Louis, USA), 0.1M sucrose (Sigma Aldrich, St. Louis, USA)), and equilibrated at 4°C for at least 30 minutes. After equilibration, cryovials were loaded

into the Cryologic Freeze Control System (Cryologic, Victoria, Australia). Vials were then frozen via the following protocol: (1) cooling from 4°C to -9°C at a rate of -2°C /min (2) equilibration for 6 min at -9°C (3) manual seeding using large swabs cooled by submersion in liquid nitrogen (4) holding for 4 min at -9°C (5) cooling to -40°C at a rate of -0.3°C/min and (6) storage in liquid nitrogen a cryogenic storage dewar until thawed for use.

3.2.5 Thawing Tissue

The process described by Brunette et al. was followed with minimal changes[98]. Briefly, vials with ovarian tissues were removed from liquid nitrogen and placed in a 37°C bath. Once the cryoprotectant media in the vial had thawed, the tissue was removed from the vial and put into Thaw Solution One (0.5M DMSO, 0.5M ethylene glycol, 0.1M Sucrose, 10% SPS in QAMH) for ten minutes. Tissue was then incubated sequentially in Thaw Solution Two (0.25M DMSO, 0.25M ethylene glycol, 0.1M Sucrose, 10% SPS in QAMH), Three (0.1M Sucrose, 10% SPS in QAMH), and Four (10% SPS in QAMH) for ten minutes each. Thaw solutions were maintained at room temperature, and samples were protected from light and agitated while in thaw solutions. Tissue squares were biopsy punched into disks measuring approximately 5mm in diameter while still in Thaw Solution Four (**Figure 3.1C**).

3.2.6 Encapsulation

The disks of ovarian cortical tissue (5mm dia.) were maintained in the final thaw solution media (Solution 4) at 37°C until encapsulation. The PEG core was prepared by cross-linking 8-arm PEG-VS (40 kDa, Jenkem Technology, Beijing, China) (5% w/v) with

plasmin sensitive peptide (Ac-GCYK↓NSGCYK↓NSCG, MW 1525.69 g/mol, > 90% Purity, Genscript, ↓ indicates the cleavage site of the peptide). The PEG shell was prepared with 4-arm PEG-VS (20 kDa, Jenkem Technology) (5% w/v), Irgacure 2959 (Ciba, Switzerland, MW = 224.3) (0.4% w/v), and N-vinyl-2-pyrrolidone (Sigma-Aldrich, St. Louis, USA) (0.1% v/v).

The tissue was placed in a mold and 40μL of degradable PEG core pre-cursor solution was added, covering the tissue surface. After five to six minutes of crosslinking the core was removed from the mold and set on top of 70μL of non-degradable PEG shell pre-cursor solution. An additional 30-35μL of non-degradable PEG shell pre-cursor solution was added on top of the core, ensuring complete coverage. The shell was cross-linked via UV light (OmniCure S1500, Excelitas Technologies, USA) at constant intensity (30mW/cm^2) for 45 seconds. Encapsulated tissue (**Figure 3.1D**) was maintained in Leibovitz L-15 media (Gibco, USA) at 37°C until implantation.

3.2.7 Subcutaneous Implantation

Animal experiments for this work were performed in accordance with the protocol approved by the Institutional Animal Care and Use Committee (IACUC) at the University of Michigan (PRO00009635). The IACUC guidelines for survival surgery in rodents and the IACUC Policy on Analgesic Use in Animals Undergoing Surgery were followed for all procedures.

Female NSG mice (strain 005557, The Jackson Laboratory, Bar Harbor, ME, USA) 8-18 weeks old were anesthetized using isoflurane (2-3%) via inhalation. Mice were given preemptive analgesics (Carprofen, RIMADYL, Zoetis, USA, 5mg/kg body) via subcutaneous injection. An incision was made in the medial/dorsal skin. Bilateral

ovariectomies were performed before graft implantation. Three PEG capsules with human cortical issue or three control non-encapsulated tissues were inserted into the dorsal subcutaneous space in the mouse (**Figure 3.1E**). The control graft was inserted subcutaneously and sutured using 5/0 absorbable sutures (AD surgical) to the subcutaneous tissue to ensure graft recovery. Using 5/0 absorbable sutures the incision was closed, with special attention paid to avoid suturing capsules/control tissue. Mice recovered in a clean cage, were given analgesics at 24 hours, and were monitored post-operatively for 7-10 days.

3.2.8 Serum Hormone Analysis

Every two weeks blood was collected from the lateral tail vein. A volume no greater than 1% body weight was collected each time using glass Pasteur pipettes (FisherBrand). At the time of sacrifice, blood was collected via cardiac puncture. Following blood collection, samples were stored at 4 °C overnight, then centrifuged for 15 minutes at 2,000 G. Serum was aliquoted and stored at −80 °C until analysis. The samples were analyzed for mouse FSH and estradiol at the Ligand Assay and Analysis Core Facility at the University of Virginia Center for Research in Reproduction. FSH was analyzed using a radioimmunoassay, with a lower detection limit of 1.9 ng/mL. Estradiol was analyzed using ALPCO ELISA, with a lower detection limit of 5 pg/mL.

3.2.9 Vaginal Cytology

Vaginal cytology was collected daily starting 7 days post-surgery until completion of the study[97,99]. Briefly, sterile saline was used to collect secreted vaginal cells and analyzed to determine which cell types were present. The ratio of various cell types

allowed for staging and determining if estrous cyclicity was occurring. The loss of estrous cyclicity due to ovariectomies was confirmed by a persistence of leukocytes. The cyclical transition of cells from leukocytes to cornified epithelial and then to nucleated epithelial cells signaled resumption of estrous cyclicity.

3.2.10 PMSG Injections

Pregnant Mare Serum Gonadotropins (PMSG, Pregnyl, Merck, USA) injections began on week 18 of the study. Mice were injected with 2IU PMSG each day via intraperitoneal injections. Mice were stimulated until euthanasia at the end of the experiment.

3.2.11 Implant Removal

Implants were removed at 6, 15, or 20 weeks (**Figure 3.1A**). Mice were anesthetized using isoflurane as described above. An incision was made in the medial/dorsal skin, avoiding implanted grafts. The encapsulated (**Figure 3.1F, G**) and control grafts (**Figure 3.1H, I**) were removed and placed in 4% PFA overnight at 4°C, washed, and stored in 70% ethanol.

3.2.12 Histology

All samples were processed at the Histology Core in the Dental School at the University of Michigan. The paraffin embedded tissue blocks were serially sectioned at a thickness of 5μm and stained with hematoxylin and eosin.

3.2.13 Follicle Counting

Slides from fresh fixed ovarian tissue were imaged using a digital slide scanner (Leica Aperio AT2®, Germany) at 20x magnification. Every 8th section was analyzed for the number and stage of follicles present, with 15 to 25 sections analyzed per donor. Each data point represents the follicle density calculated from each section analyzed. QuPath software (v0.2.2) was used for manual follicle counting. Follicle stage was identified using standard morphological guidelines[100]. All primordial and primary follicles were counted for each analyzed section. Preantral and antral were counted only after comparing the location of the follicle in the tissue and follicle size in preceding and subsequent sections to avoid “double counting”. Density measurements were calculated using tissue section area and the estimated tissue section thickness (20μm). The follicle density values reported in this study are all normalized to the same volume.

3.2.14 Statistical Analysis

Statistical analysis was performed using GraphPad Prism software, version 10. To determine whether there was a significant difference between the number of estrus cycles between encapsulated and non-encapsulated groups a two-way ANOVA with Šídák’s multiple comparisons was used. Estradiol levels between ovariectomized controls, non-encapsulated, and encapsulated groups were compared with an one-way ANOVA with Tukey’s multiple comparisons tests. Estradiol levels between non-encapsulated and encapsulated groups at each time point were evaluated with an ordinary one-way ANOVA with Šídák’s multiple comparisons. For all test, results were considered statistically significant when $p < 0.05$.

3.3 Results

3.3.1 Fresh tissue heterogeneity is illustrated, and experimental groups are defined.

We analyzed follicle density in the ovarian tissues from all 8 donors. Representative histological images for each donor used in this study depict the presence of primordial follicles (**Figure 3.2A-H**). Tissue from Donor A (18 years old (y.o.)), B (16 y.o.), and C (25 y.o.) qualitatively show a higher density of primordial follicles, which is supported by follicle density measurements (**Figure 3.2I**) with 662 ± 330, 297 ± 68, and 107 ± 98 (follicles per mm^3) for Donors A, B, and C, respectively. The follicle density for Donors D (27 y.o.), E (18 y.o.), F (25 y.o.), G (31 y.o.), and H (28 y.o.) was lower: 56 ± 35, 54 ± 54, 2 ± 3, 24 ± 15, and 50 ± 51 respectively. To compensate for age and follicular density differences between available donors, mice received tissue from a mix of donors as summarized in (**Figure 3.2J, K**). The average age of donor tissue used was 24 ± 6 years (yrs.) for the non-encapsulated control mice (NE) and 23 ± 6 yrs. for mice receiving encapsulated ovarian tissue (E) for the 6-week cohort, 23.8 ± 5.8 yrs. (NE) and 23.6 ± 6.4 yrs. (E) for the 15-week cohort, and 22.2 ± 5.8 yrs. (NE) and 23 ± 6.2 yrs. (E) for the 20-week cohort. Additional details on which donors were implanted in individual mice can be found in **Appendix Table B.2**.

3.3.2 Estrous cyclicity resumption is the first indication there is interaction between encapsulated grafts and mouse hypothalamus-pituitary axis.

We utilized a range of markers for graft functionality (**Figure 3.3A**), starting with vaginal cytology to establish estrous cyclicity in ovariectomized mice implanted with encapsulated and non-encapsulated ovarian tissue. We saw a variety of cycle frequencies and lengths from each mouse and have shown the most consistent cycling from both the non-encapsulated (**Figure 3.3B**) and encapsulated groups (**Figure 3.3C**). Individual cyclicity data for each mouse from the study are shown in **Appendix Figure**

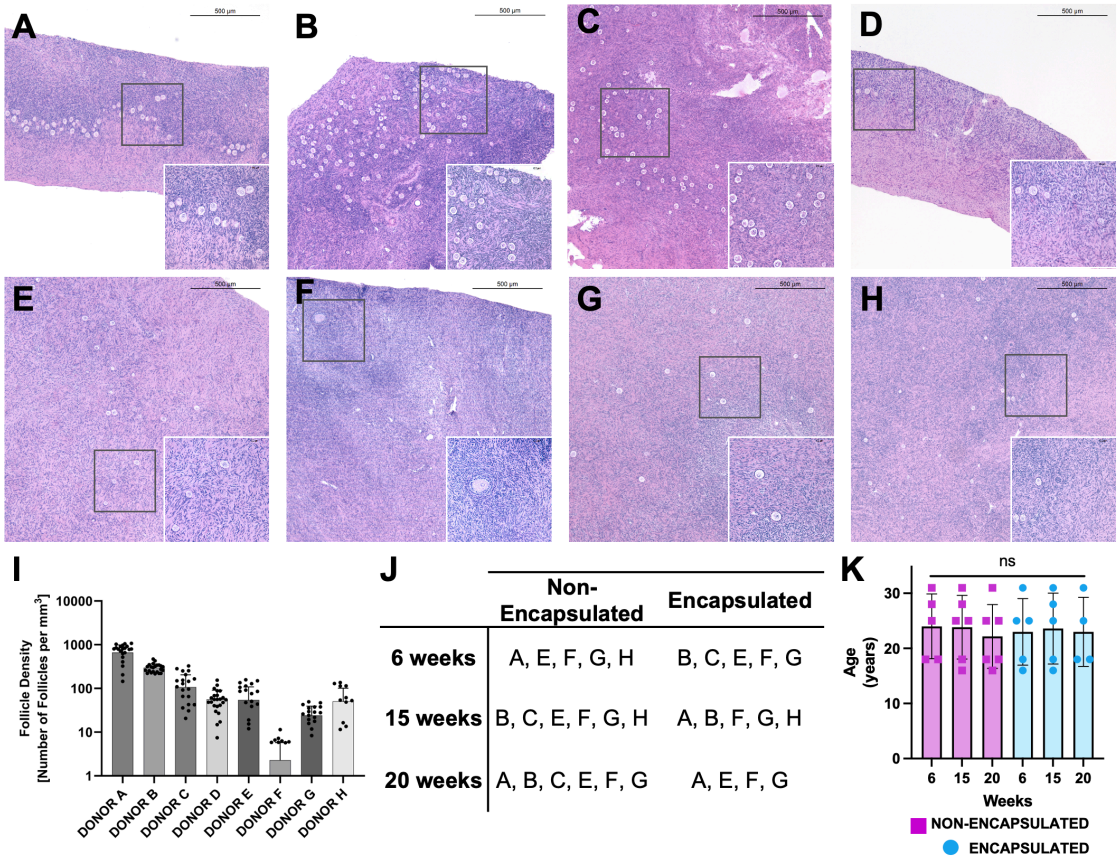

Figure 3.2 Donor Tissue Characterization. Representative histological images from fresh fixed human ovarian cortex from each donor utilized in this study is shown in A-H. The follicle densities for each donor are shown in I. The distribution of donor tissue among each group is shown in J, with the average age for each group shown in K.

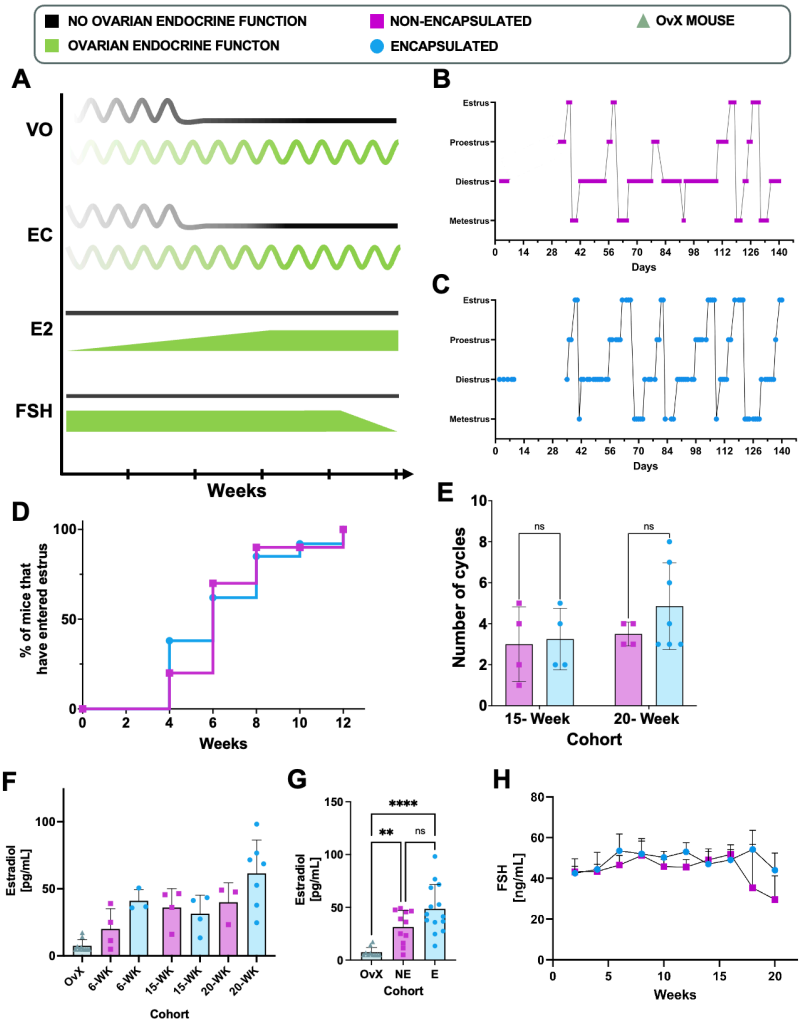

Figure 3.3 Encapsulated and non-encapsulated grafts restore endocrine function. Endocrine function of the grafts was measured with 4 metrics (A): vaginal opening (VO), estrous cyclicity (EC), estradiol levels (E2), and follicle stimulating hormone (FSH) levels. Green indicates ovarian endocrine function, and gray/black represents no endocrine function. The increase in VO and EC color indicates increasing function. E2 is anticipated to increase until it reaches a constant level, and FSH is anticipated to take the longest before starting to decrease to physiological normal levels. In ovariectomized mice we expect no VO and EC, low estradiol and elevated FSH. With functioning ovarian tissue, the VO has the fastest onset, followed with regular ECs, increase in E2 and decrease in FSH. In our study there is a resumption of cyclicity around five weeks for mice with non-encapsulated (B) and encapsulated (C) samples. Trends between non-encapsulated and encapsulated groups were similar when looking at the percent of mice that had entered estrus (D) and the number of cycles achieved in each cohort (E). Estradiol measurements were determined from terminal blood serum (F, G). Analysis shows that there is no significant difference in estradiol levels between groups when comparing cohorts (F). Additionally, mice that received grafts showed statistically significant more estradiol than controls (G). Blood serum collected every other week shows a trend of decreasing FSH levels in week 18 (H).

B.1. The first evidence of cyclicity was recorded 4 weeks post implantation with 20% of mice in the NE group and 38% in the E group cycling (**Figure 3.3D**). By week six post

implantation 70% in the NE group and 62% in the E group cycled. By week eight 90% in the NE and 85% in the E group cycled, and by week ten 90% in the NE and 92% in the E group experienced at least one estrous cycle. All mice achieved estrus by week twelve. The number of cycles per group was analyzed for cohorts that had implants for longer time periods than the twelve weeks it took for all mice to cycle. The number of cycles was not significantly different between NE and E groups in analyzed cohorts (**Figure 3.3E**). The average number of cycles for the 15-week cohort was 3 ± 1.8 for NE and 3.25 ± 1.5 for E. The average number of cycles for the 20-week cohort was 3.5 ± 0.6 for NE and 4.9 ± 2.1 for E.

3.3.3 Elevated levels of systemic estradiol confirm that mouse gonadotropins stimulated the production and secretion of gonadal hormones from implanted ovarian tissue.

To determine whether human ovarian tissue implanted in ovariectomized mice was stimulated by the circulating gonadotropins we analyzed blood serum for systemic levels of estradiol. (**Figure 3.3F**). After 15 weeks post implantation estradiol levels reached 36.1 ± 14.1 pg/mL in the NE group and 31.4 ± 13.9 pg/mL in the E group. After 20 weeks the estradiol levels reached 40.0 ± 14.5 pg/mL (NE) and 61.5 ± 24.92 pg/mL(E), showing upward trends in estradiol levels matching the time it takes for human follicles reach preantral and antral stages. The average levels of estradiol were 31.3 ± 15.9 pg/mL for the NE group and 48.5 ± 23.1 pg/mL for the E group with no significant difference between the groups implanted with human tissue (**Figure 3.3G**) and significantly higher compared to ovariectomized control mice, which average at 7.5 ± 4.5 pg/mL. As expected in ovariectomized mice, the FSH levels increased from ~5-10ng/mL[101] immediately after

ovariectomy and reached an average of 42ng/mL in both groups in the 20-week cohort (**Figure 3.3H**). However, starting at week 18 post implantation, the levels of FSH showed

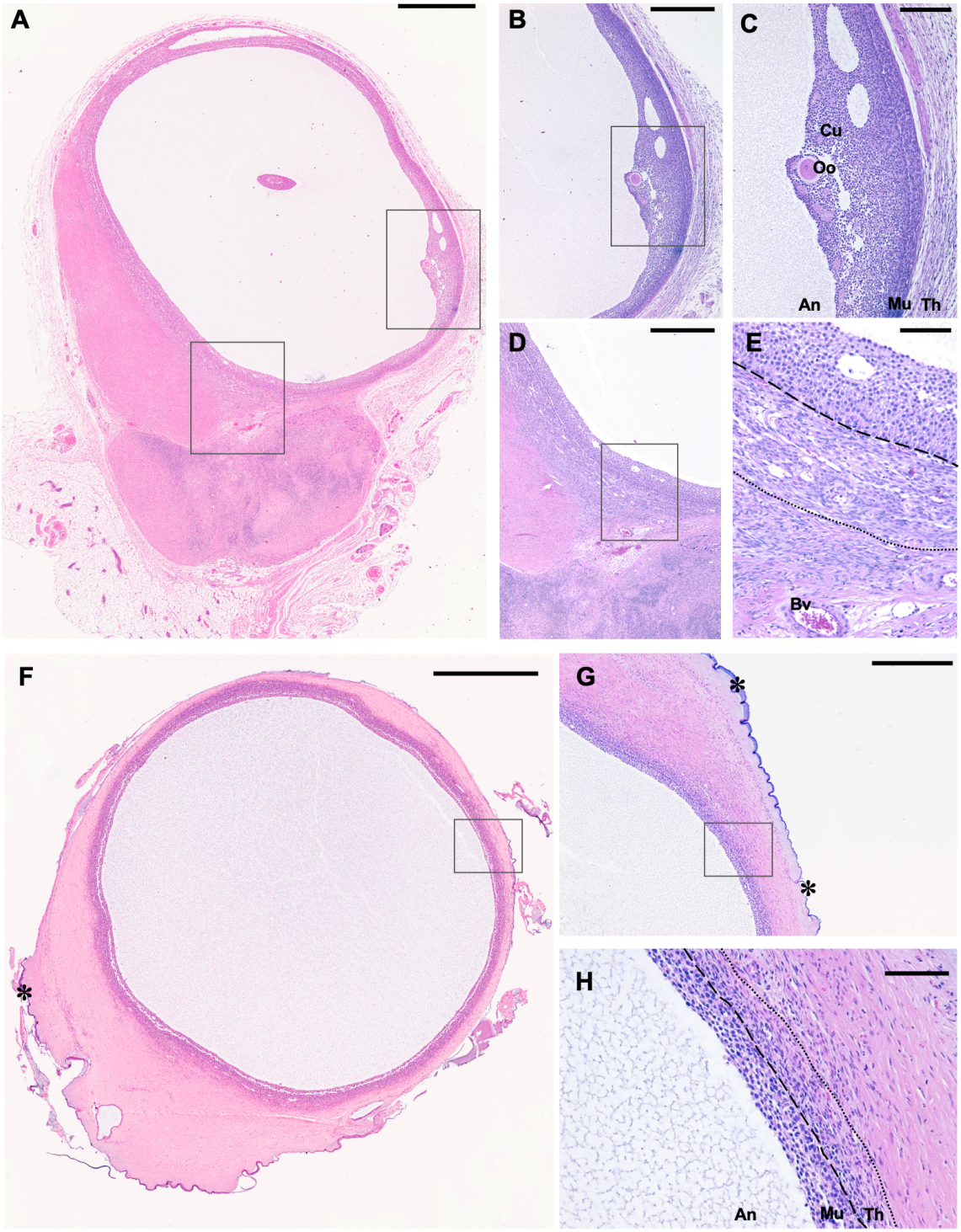

Figure 3.4 Antral Follicle Characterization. Antral follicles from non-encapsulated (A-E) and encapsulated (F-H) tissue. Scale bar represents 1mm (A, F), 500μm (B, D, G), or 100μm (C, E, H). Oo: oocyte, Cu: cumulus granulosa cells, An: antrum, Mu: mural granulosa cells, Th: theca layer, Bv: blood vessel, ✻: PEG capsule, (⋯) indicates the theca cell layer, (- - -) indicates granulosa cell layer.

a downward trend suggesting that the levels of circulating estradiol reached the threshold required to restore the normal physiological negative feedback on the HPG axis.

3.3.4 Antral follicles are present in both non-encapsulated and encapsulated groups.

A histological analysis of retrieved grafts confirmed presence of multiple primordial and primary follicles in in the non-encapsulated and encapsulated groups (**Appendix Figure B.2**), including large antral follicles (**Figure 3.4**). Three antral follicles were observed in the non-encapsulated group, one in the 15-week cohort (800μm in diameter), and two in the 20-week cohort (1.5 mm and 2.5 mm in diameter). One antral follicle was observed in the encapsulated group in the 20-week cohort, measuring 3.5 mm in diameter. The morphology of the antral follicles correlated well with healthy folliculogenesis (**Figure 3.4B, C**). Each antral follicle had a clear antral cavity surrounded by an organized layer of mural granulosa cells, separated from a well-defined theca layer by a basement membrane (**Figure 3.4D, E**). In contrast to the encapsulated tissue, the non-encapsulated graft contained visible blood vessels with red blood cells in them, suggesting revascularization of the grafted tissue by the host vasculature. However, despite the absence of revascularization, critical for prevention of immune rejection, the antral follicles in the encapsulated tissue had a similar organization of granulosa and theca layers (**Figure 3.4G, H**), suggesting normal folliculogenesis despite the lack of direct revascularization.

3.4 Discussion

The data presented in this study demonstrated that human tissue implanted subcutaneously in ovariectomized mice integrated into the mouse HPG axis by responding to the circulating gonadotropins, producing and secreting gonadal steroids. Despite the heterogeneity in follicular density in human donors, all ovariectomized mice implanted with encapsulated or non-encapsulated tissue experienced vaginal opening and at least one estrus cycle confirming sustained folliculogenesis and steroidogenesis in the human tissue. No statistical significance was found in the number of cycles achieved by each mouse when comparing cohorts that received encapsulated and non-encapsulated tissue, indicating the capsule did not interfere with endogenous gonadotropin stimulation and hormone diffusion. Additionally, we see that there was no significant difference in circulating estradiol levels when compared between cohorts.

Function of xenografted human tissue in ovariectomized mice was confirmed by vaginal opening, restoration of estrous cyclicity and presence of circulating estradiol. Intact non ovariectomized mice experience estrous every 4 days, which correlates with the murine follicle development duration. Murine small antral follicles reach preovulatory stages in 4 days, while complete folliculogenesis from primordial stage to ovulation takes 18 days[102]. In contrast, human follicles can take up to 180 days to grow from primordial stages, which are the majority of follicles located in the cortex, to ovulatory stages, taking approximately 3 months to reach 1-2mm in diameter[100]. First, after xenografting human ovarian cortex, we observed changes in vaginal opening and estrous cyclicity around 6-10 weeks. Interestingly, the rate of cycling in ovariectomized mice implanted with human ovarian tissue extended to weeks in our study, confirming that despite being stimulated

by the endogenous gonadotropins human follicles followed their internal biological clock. Mice demonstrated variability in cycle duration and frequency (all variations shown in **Appendix Figure B.1**), with some mice having multiple cycles every few weeks and some mice only experiencing a few cycles. The variation mouse-to-mouse was likely due to the heterogeneity (in both follicle number and maturity) of the grafted tissue, as expected. Mice that took weeks to resume estrus likely contained mostly immature follicles and mice with longer gaps between estruses likely had fewer follicles overall.

Restoration of ovarian endocrine function was also confirmed by the increased levels of estradiol beginning in the sixth week post-implantation, and overall increase in estradiol levels on a cohort level. There was a trend of increasing estradiol levels as the time post-implantation progressed, which was expected as the growing follicles needed time to mature. The additional metric we analyzed was FSH levels, which remained elevated throughout the study, but began to trend downward starting at 18 weeks, suggesting that the levels of estradiol reached sufficient levels for long enough to regain the negative feedback on the hypothalamus and pituitary. Importantly, our data suggests that mouse gonadotropins stimulated folliculogenesis and steroidogenesis in human ovarian tissue and human hormones influenced the reproductive organs causing VO and EC and integrated within the HGP axis. Our data agree with results from Man *et al.*, where serum hormone levels were shown to change with tissue implantation after bilateral oophorectomy[103,104]. Furthermore, our data also demonstrated that there was no significant difference between the encapsulated and non-encapsulated fully vascularized grafts with regards to the onset of graft function and longevity. Interestingly, our results of human ovarian tissue grafted in mice also align with the clinical data reporting that it takes

19 weeks for hormone levels to return to physiological levels in human studies[94]. Lastly, the presence of theca cells in the antral follicles and increased levels of estradiol further confirm normal steroidogenesis and folliculogenesis. According to the two-cell/two-gonadotropin theory, theca cells that convert cholesterol into androstenedione must be present for granulosa cells to make high levels of estradiol[105].

Despite the promising results, our study had a few limitations. First, due to the nature of ovarian follicles and thickness of the human cortex it was impossible to analyze the follicle density without damaging the tissue before implantation. As a result, we were unable to say with certainty how many follicles were implanted in each mouse. A survival dye, such as Neutral red, could be used for follicle counts; however, it would require thinner pieces of tissue which would increase the number of follicles activated due to mechanical stress and excessive manipulation. Follicle activation is of critical concern as too many activated follicles would shorten graft longevity. As a compromise, we minimized the extent of human tissue manipulation and only used donor's age as the determining factor for extrapolating follicle density.

Second, we carried out our study for 20 weeks, attempting to match the duration of the study with human folliculogenesis. Human cortex contains mostly primordial follicles that would only reach antral stages after 20 weeks. As expected, we observed the early signs of endocrine function, including VO, EC and E2, and a downward trend in FSH levels. This duration is in line with the data reported by Khattak et al[94] in human studies, but a longer study would allow us to reach complete restoration of the HPG axis, possibly several waves of activation, and even determine how long it would take to exhaust the implanted follicle reserve and establish a dose-response relationships. Third,

while we have been able to collect hormones from blood serum, we are not able to collect enough to test for multiple hormones, such progesterone, AMH and inhibins, on every blood draw. This was due to the limited blood sampling in a mouse model, and we therefore could only report estradiol levels at terminal time points. The ability to collect more blood serum would allow us to have a more nuanced picture of what was happening with multiple hormones over the duration of this study and their cyclic profiles.

Lastly, we used immunocompromised mice in this study which did not allow us to test the immune-isolating ability of the capsules. Yet, this study still provided important evidence that despite encapsulation and lack of direct revascularization, human ovarian tissue grafts have survived and functioned, relying only on diffusion. The next step would be to evaluate the capsules in an immune competent mouse model that would inform us on capsule's ability to withstand immune rejection and follicle expansion without fail.

In conclusion, we have shown that large human antral follicles could grow in an ovariectomized NSG mouse model. These antral follicles were found in grafts that were both encapsulated and non-encapsuled. Furthermore, estradiol production and estrous cyclicity were observed for both the encapsulated and non-encapsulated groups. This indicates not only that the graft was interfacing with the mouse hypothalamus/pituitary axis, but also indicates the immune-isolating capsule did not preclude hormone diffusion. Now that we have developed a model to grow large follicles in our immune-isolating capsules, we can move on to evaluating the immune-isolating feature.

Chapter 4 Human Follicles in Encapsulated Ovarian Cortex are Protected From T-Cell Infiltration in Immunocompetent Mice.

4.1 Introduction

In the previous chapters we have shown our work with encapsulated human ovarian tissue implanted for short and long term in immunocompromised mice. To address the differences between human and murine follicles we utilized larger pieces (a 20-fold increase in volume) and carried out experiments for 20 weeks in ovariectomized NSG mice. This study has shown that by ovariectomizing the mice we can stimulate human follicles to grow to mature stages resulting in the resumption of estrous cyclicity in all mice, increased estradiol levels with graft implantation, and a downward trend in follicle stimulating hormone levels around week 18 (Chapter 3).

In this work we aim to investigate whether human ovarian tissue remains protected from rejection in the immune-isolating capsule when follicles grow to mature stages in immunocompetent mice. We recognize that the immune response toward a xenograft is anticipated to be stronger compared to an immune response mounted against allogeneic tissue in humans, due to the innate immune system recognizing molecular discrepancies between the host and donor species[106], however we decided to push the capsule to its limits. We evaluated the xenograft response as a proxy for what could happen with allogeneic implant in the future. The rejection of a xenograft graft could happen via hyper acute rejection (HAR) on the order of hours, cellular xenograft rejection (CXR) or acute

humoral xenograft rejection (AHXR) on the order of days to weeks, and chronic rejection on the order of months to years [107,108]. In xenografts, the mechanisms of HAR in a vascularized grafts are well defined, but they have not been fully characterized in cellular rejection[107]. Here we investigated the immune-isolating properties of our capsule by evaluating T-cell infiltration and graft function by assessing estrous cyclicity, serum hormone levels, and histological evaluation of follicles.

4.2 Materials and Methods

4.2.1 Collection of Human Ovarian Tissue

Organ procurement was conducted as previously described[98]. Briefly, ovaries were obtained following standardized protocols in place at the International Institute for the Advancement of Medicine (IIAM) and the associated Organ Procurement Organization (OPO) for research purposes. This study utilized ovaries procured by the IIAM from six deceased donors (age range: 18-27 years). Organs were placed in storage solution and shipped on ice. Storage solutions were either normal saline or Belzer University of Wisconsin® Cold Storage Solution. De-identified donor information is summarized in **Appendix Table C.1**, including age, weight, height, BMI, and cross-clamp time (time at which the organ is cut from blood/oxygen supply). Cold ischemic time (CIT) was calculated as the time interval between cross-clamp time of the donor (and subsequent cessation of arterial blood flow to the ovaries) in the operation room and start time of the tissue harvest after arrival at the laboratory.

4.2.2 Ethical Approval Process

As stated previously[98], the IIAM procures tissue and organs for non-clinical research from Organ Procurement Organizations (OPOs), which comply with state Uniform Anatomical Gift Acts (UAGA) and are certified and regulated by the Centers for Medicare and Medicaid Services (CMS). These OPOs are members of the Organ Procurement and Transplantation Network (OPTN) and the United Network for Organ Sharing (UNOS) and operate under a set of standards established by the Association of Organ Procurement Organizations (AOPO) and UNOS. Informed, written consent from the deceased donor's family was obtained for the tissue used in this publication. A biomaterial transfer agreement is in place between IIAM and the authors that restricts the use of the tissue for pre-clinical research that does not involve the fertilization of gametes.

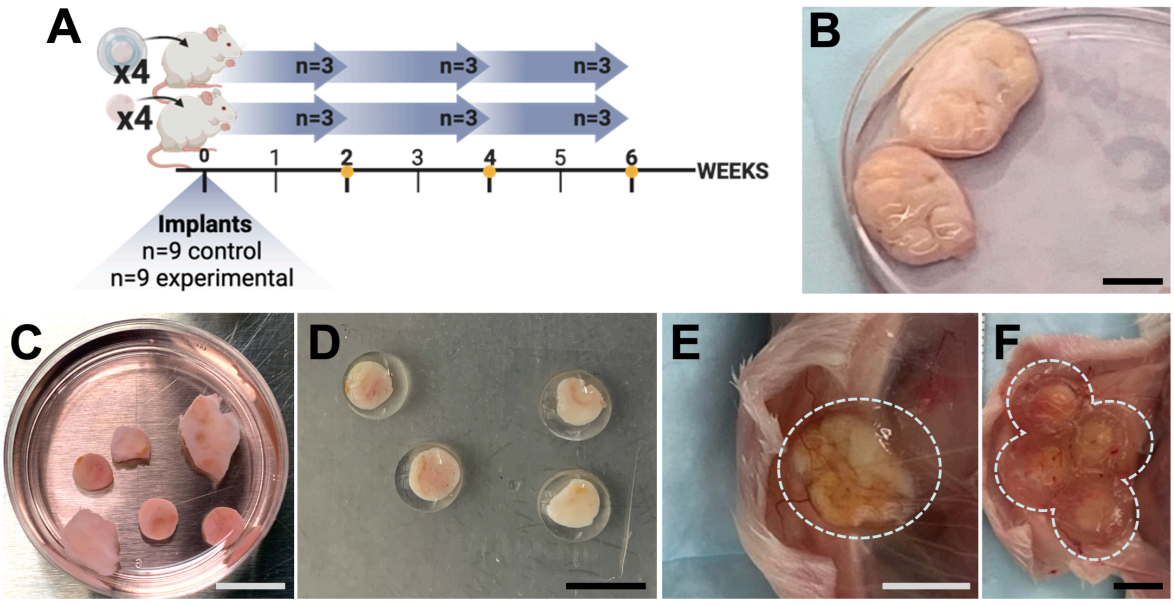

Figure 4.1 Experimental design and tissue processing. Balb/c mice were implanted with human cortical ovarian tissue (encapsulated or non-encapsulated) and followed out to six weeks (A). Donor ovaries (B) are de-cortified (C) and cryopreserved until use. After thawing, tissue is encapsulated in the immune-isolating capsule (D) and is implanted subcutaneously. Non-encapsulated tissue grafts (E) and encapsulated tissue grafts (F) were removed from the subcutaneous space. Scale bar represents 1cm B-D, and 5mm for E & F.

The use of deceased donor ovarian tissue in this research is categorized as 'not regulated', per 45 CFR 46.102 and the 'Common Rule', as it does not involve human subjects and complies with the University of Michigan's IRB requirements as such.

4.2.3 Tissue Processing

All tissue processing was done aseptically in a biosafety cabinet. After receiving donor tissues, the ovaries were separated from other reproductive tissues (i.e. the uterus, fallopian tubes) (**Figure 4.1B**). The ovaries were decortified using a custom cutting guide (Reprolife Japan, Tokyo) to remove approximately 1 mm thick cortex pieces that were approximately 10mmx10mm squares (**Figure 4.1C**). The squares were then aseptically transferred into holding media (Quinn's Advantage Medium with HEPES (QAMH), 10% Quinn's Advantage Serum Protein Substitute (SPS), CooperSurgical, Måløv, Denmark) before cryopreservation.

4.2.4 Slow Freezing

The methods as described by Xu et al. were used for slow freezing [63]. Briefly, squares of cortical tissue approximately 10mm x 10mm x 1mm were placed into cryovials (Nunc, Roskilde, Denmark) filled with pre-cooled cryoprotectant media (QAMH, 10% SPS, 0.75M dimethyl sulfoxide (DMSO) (Sigma Aldrich, St. Louis, USA), 0.75M ethylene glycol (Sigma Aldrich, St. Louis, USA), 0.1M sucrose (Sigma Aldrich, St. Louis, USA)), and equilibrated at 4°C for at least 30 minutes. After equilibration, cryovials were loaded into the Cryologic Freeze Control System (Cryologic, Victoria, Australia). Vials were then frozen via the following protocol: samples were (1) cooled from 4°C to -9°C at a rate of -2°C /min (2) equilibrated for 6 min at -9°C (3) seeded manually using large swabs cooled

by submersion in liquid nitrogen (4) held for 4 min at -9°C (5) cooled to -40°C at a rate of -0.3°C/min and (6) plunged into liquid nitrogen and stored in a cryogenic storage dewar until thawed for use.

4.2.5 Thawing Tissue

The process of slow frozen tissue thawing described by Brunette et al. was followed for all short term (2, 4, and 6 week) studies[98]. For long term studies the process changed slightly. Briefly, vials with ovarian tissues were removed from liquid nitrogen and placed in a 37°C bath. Once the cryoprotectant media in the vial had thawed, the tissue was removed from the vial and put into Thaw Solution One (0.5M DMSO, 0.5M ethylene glycol, 0.1M Sucrose, 10% SPS in QAMH) for ten minutes. Tissue was then incubated sequentially in Thaw Solution Two (0.25M DMSO, 0.25M ethylene glycol, 0.1M Sucrose, 10% SPS in QAMH), Three (0.1M Sucrose, 10% SPS in QAMH), and Four (10% SPS in QAMH) for ten minutes each. Thaw solutions were kept at room temperature, and samples were protected from light and agitated while in thaw solutions. Tissue squares were cut into disks measuring approximately 5mm in diameter while still in Thaw Solution Four.

4.2.6 Encapsulation

The pieces of ovarian cortical tissue (5mm dia.) were maintained in the final thaw solution media (Solution 4 for slow freezing) at 37°C until encapsulation. The PEG core was prepared by cross-linking 8-arm PEG-VS (40 kDa, Jenkem Technology, Beijing, China) (5% w/v) with plasmin sensitive peptide (Ac-GCYK↓NSGCYK↓NSCG, MW 1525.69 g/mol, > 90% Purity, Genscript, ↓ indicates the cleavage site of the peptide). The

PEG shell was prepared with 4-arm PEG-VS (20 kDa, Jenkem Technology) (5% w/v), Irgacure 2959 (Ciba, Switzerland, MW = 224.3) (0.4% w/v), and N-vinyl-2-pyrrolidone (Sigma-Aldrich, St. Louis, USA) (0.1% v/v).

The tissue was placed in a mold and 40μL of degradable PEG core pre-cursor solution was added, covering the tissue surface. After five to six minutes of crosslinking the core was removed from the mold and set on top of 70μL of non-degradable PEG shell pre-cursor solution. An additional 30-35μL of non-degradable PEG shell pre-cursor solution was added on top of the core, ensuring complete coverage. The shell was cross-linked via UV light (OmniCure S1500, Excelitas Technologies, USA) at constant intensity (30mW/cm^2) for 45 seconds. Encapsulated tissue (**Figure 4.1D**) was maintained in Leibovitz L-15 media (Gibco, USA) at 37°C until implantation.

4.2.7 Subcutaneous Implantation

Animal experiments for this work were performed in accordance with the protocol approved by the Institutional Animal Care and Use Committee (IACUC) at the University of Michigan (PRO00009635 and PRO00011284). The IACUC guidelines for survival surgery in rodents and the IACUC Policy on Analgesic Use in Animals Undergoing Surgery were followed for all procedures.

Female Balb/c mice (strain 000651, The Jackson Laboratory, Bar Harbor, ME, USA) 12-16 weeks old were anesthetized using isoflurane (2-3%) via inhalation. Mice were given preemptive analgesics (Carprofen, RIMADYL, Zoetis, USA, 5mg/kg body) via subcutaneous injection. An incision was made in the medial/dorsal skin. Bilateral ovariectomies were performed before graft implantation for long term studies, otherwise ovaries were left intact. Four PEG capsules or four control non-encapsulated tissues were

inserted into the dorsal subcutaneous space in the mouse. The control graft was inserted subcutaneously and sutured using 5/0 absorbable sutures (AD surgical) to the subcutaneous tissue to ensure graft recovery. Using 5/0 absorbable sutures the incision was closed, with special attention paid to avoid suturing capsules/control tissue. Mice recovered in a clean cage, were given analgesics at 24 hours, and were monitored post-operatively for 7-10 days.

4.2.8 Serum Hormone Analysis

Every two weeks blood was collected from the lateral tail vein of mice. A volume no greater than 1% body weight was collected each time using glass Pasteur pipettes (FisherBrand). At the time of sacrifice, blood was collected via cardiac puncture. Following blood collection, samples were stored at 4 °C overnight, then centrifuged for 15 minutes at 2,000 G. Serum was aliquoted and stored at −80 °C until analysis. The samples were analyzed for mouse FSH and estradiol at the Ligand Assay and Analysis Core Facility at the University of Virginia Center for Research in Reproduction. FSH was analyzed using a radioimmunoassay, with a lower detection limit of 0.016 ng/mL. Estradiol was analyzed using ALPCO ELISA, with a lower detection limit of 5 pg/mL.

4.2.9 Vaginal Cytology

As described previously, vaginal cytology was collected daily starting 7 days post-surgery until completion of the study[97,99]. Briefly, sterile saline was used to collect secreted vaginal cells and analyzed to determine which cell types were present. The ratio of various cell types allowed for staging and determining if estrous cyclicity was occurring. The loss of estrous cyclicity as a result of ovariectomies was confirmed by a persistence

of leukocytes. The cyclical transition of cells from leukocytes to cornified epithelial and then to nucleated epithelial cells signaled resumption of estrous cyclicity.

4.2.10 Implant Removal

Implants were removed at various time points (**Figure 4.1A**). Mice were anesthetized using isoflurane as described above. An incision was made in the medial/dorsal skin, avoiding implanted grafts. The control grafts (**Figure 4.1E**) and capsules (**Figure 4.1F**) were removed and placed in 4% PFA overnight at 4°C, washed, and stored in 70% ethanol.

4.2.11 Histology

All samples were processed at the Histology Core in the Dental School at the University of Michigan. The paraffin embedded tissue blocks were serially sectioned at a thickness of 5μm and stained with hematoxylin and eosin.

4.2.12 Follicle Counting

Slides from fresh fixed ovarian tissue were imaged using a digital slide scanner (Leica Aperio AT2®, Germany) at 20x magnification. Every 8th section was analyzed for follicles, with 25 sections analyzed per donor. Each data point represents the follicle density calculated from each section analyzed. QuPath software (v0.2.2) was used for manual follicle counting. Follicle stage was identified using standard morphological guidelines[100]. All primordial and primary follicles were counted for each analyzed section. Preantral and antral were counted only after comparing the location of the follicle in the tissue and follicle size in preceding and subsequent sections to avoid “double counting”. Density measurements were calculated using tissue section area and the estimated

tissue section thickness (20μm). The follicle density values reported in this study are all normalized to the same volume.

4.2.13 Immunohistochemistry Staining

Slides were incubated at 60°C then deparaffinized in xylenes. Samples went through a hydration series before antigen retrieval using antigen Retrieval Buffer (100X Tris-EDTA Buffer, pH 9.0; Abcam, #ab94681) at 97°C. Slides were washed with TBS-T and blocked using KPL Universal Block (Sera Care, #5560-0009) at room temperature. Primary antibodies used for CD4 and CD8 staining were rabbit monoclonal anti-mouse CD4 (Abcam, #ab183685), 1:1000 and rabbit polyclonal anti-mouse CD8 (Abcam, #ab203035), 1:500, respectively. Primary antibodies were diluted in Lab Vision™ Antibody Diluent OP Quanto (Thermo Scientific, #TA-125-ADQ) and added to slides for one hour at room temperature. Secondary antibodies (goat anti-rabbit Ig, Human ads-HRP (Southern Biotech, #4010-05)) were added for 15 minutes at a dilution of 1:100 or 30 minutes at a dilution of 1:50 for CD4 and CD8 samples, respectively. Slides were then incubated with DAB (Betazoid DAB Chromogen Kit, BioCare Medical, #BDB2004L) for 10 minutes at room temperature. Samples were then counterstained with Hematoxylin 2 (Fisher Scientific, #220-102), dehydrated in an ethanol series, clarified in xylene, and mounted with Permount Mounting Media (Fisher Scientific, #SP15-100).

4.2.14 Statistical Analysis

Statistical analysis was performed using GraphPad Prism software, version 10. Estradiol levels were evaluated with an one-way ANOVA with Šídák's multiple comparisons. Results were considered statistically significant when $p < 0.05$.

4.3 Results

4.3.1 Donor tissue is characterized for experimental design.

This study utilized tissue from six donors (**Figure 4.2**). The histology images from each donor qualitatively show a range of follicle densities (**Figure 4.2A-F**), which is supported by the quantification of these densities as shown in **Figure 4.2G**. The follicle density was 107 ± 98, 56 ± 35, 54 ± 54, 42 ± 33, 156 ± 65, and 106 ± 50 follicles per mm^3 for Donors A, B, C, D, E, and F, respectively. Donor age and BMI are listed in **Figure 4.2H**. Donors A-C were utilized in short term studies and Donors D-F were utilized in long term studies.

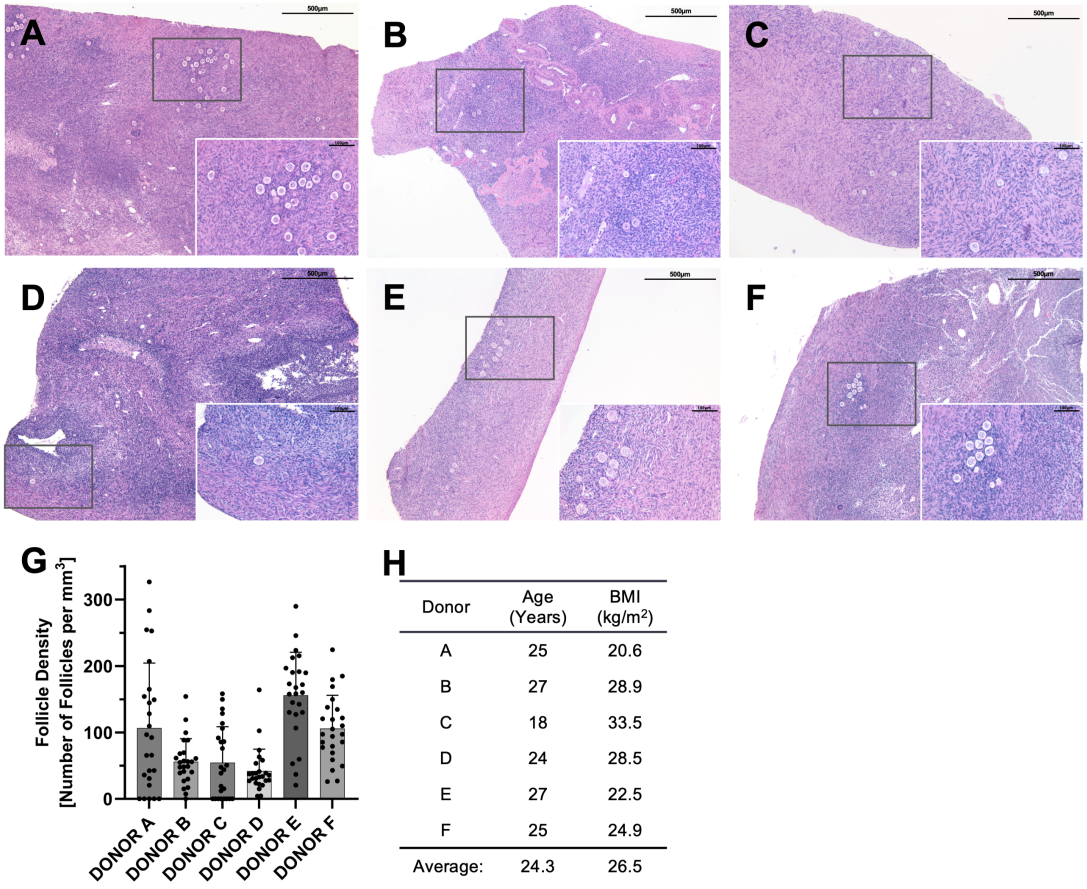

H

Donor	Age (Years)	BMI (kg/m^2)
A	25	20.6
B	27	28.9
C	18	33.5
D	24	28.5
E	27	22.5
F	25	24.9
Average:	24.3	26.5

Figure 4.2 Donor tissue follicle density shows heterogeneity. Representative histological images from fresh fixed human ovarian cortex from each donor utilized in this study is shown in A-F. The follicle densities for all donors are shown in G. Metrics for the donors used in this study are shown in H.

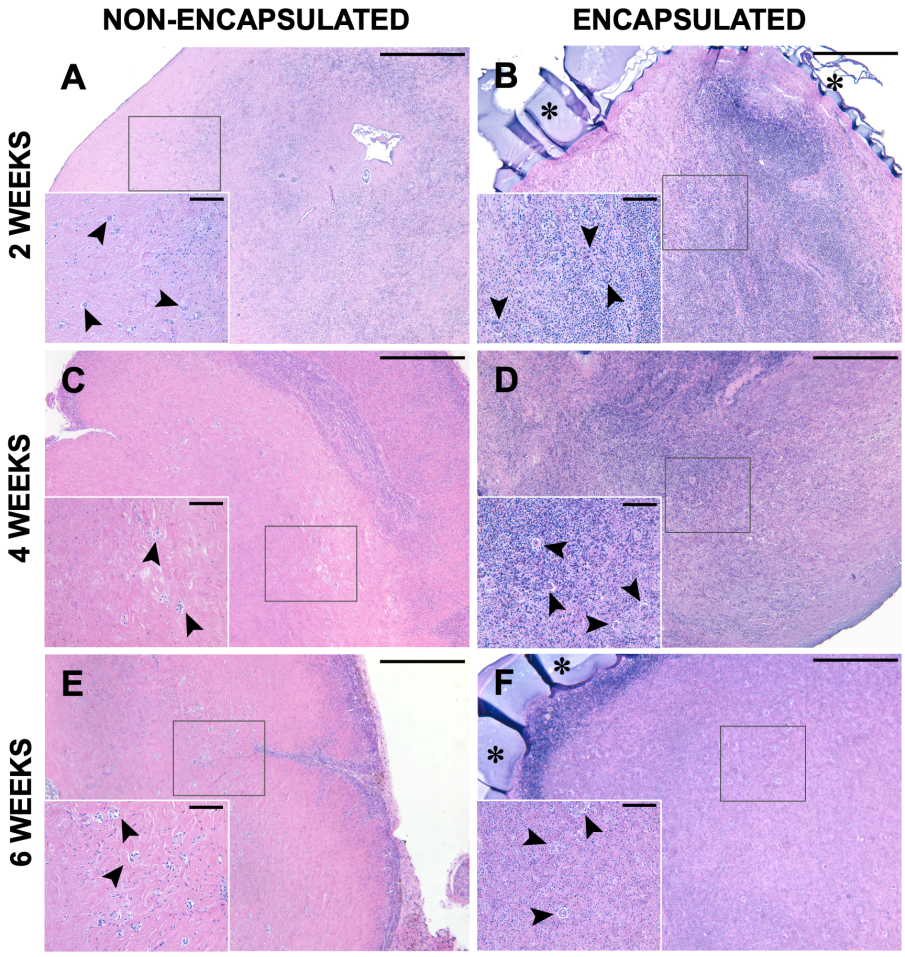

Figure 4.3 Short-term histology shows follicles persist after 6-week post implantation. Representative histological images from non-encapsulated (A, C, E) and encapsulated (B, D, F) samples. Non-encapsulated samples show an increase in fibrous stroma as time goes on, with the 6-week samples showing morphologically irregular follicles (E). Encapsulated samples show consistent stromal cell density, and 6-week samples show morphologically normal follicles (F). Black arrow heads (➤) indicate follicles, asterisks (✻) indicate the PEG capsule. Scale bars are 100μm for insets and 500μm for all others.

4.3.2 Short-term studies indicate the immune-isolating capsule precludes T-cell infiltration.

Histological processing of grafts implanted in immunocompetent mice for 2 weeks (**Figure 4.3A, B**), 4 weeks (**Figure 4.3C, D**), or 6 weeks (**Figure 4.3E, F**) shows a stark difference between non-encapsulated (**Figure 4.3A, C, E**) and encapsulated (**Figure 4.3B, D, F**) grafts. Follicles in non-encapsulated grafts show morphological signs of

atresia, and the tissue stroma is largely acellular and fibrous. In contrast, follicles in encapsulated graphs show normal morphology and cellular stroma. Staining for CD4+ and CD8+ T-cells is shown in **Figure 4.4**. Images of the whole sample and higher magnification images clearly show positive staining of T-cells for non-encapsulated samples (**Figure 4.4A-F**) at all time points. No evidence of infiltrating T cells was found in encapsulated samples (**Figure 4.4G-L**) at all time points.

4.3.3 Long-term studies show graft interaction with host Hypothalamus-Pituitary axis via estrous cyclicity and serum estradiol levels.

Long term studies were designed for 22 weeks of implantation (**Figure 4.5A**). 4 out of 9 mice were euthanized early due to adverse effects near the grafting site, with 5 mice completing the 22-week study. For all mice in the study, samples from mice that completed the 22-week study remained largely intact (**Figure 4.5B**) while those in the early euthanasia group were falling apart (**Figure 4.5C**). A representative cyclicity plot (**Figure 4.5D**) showed an initial estrus stage at 7 weeks and second estrus at 18 weeks. The cyclicity plots from all other mice can be found in **Appendix Figure C.1**. Even with some implants looking damaged, 8 out of 9 mice entered estrus at least once; the mice began entering estrus in week 6 (11%), with additional mice entering estrus in week 7 (78%), and one mouse entering estrus in week 18 (**Figure 4.5E**).

Serum estradiol measurements were split into mice that were euthanized early (Group 1 (G1), **Figure 4.5F**) and those that completed the full 22 weeks (Group 2 (G2), **Figure 4.5F**). The estradiol levels showed an upward trend as samples were left in mice for longer, with the average estradiol level of 11 ± 4.5 pg/mL and 32 ± 49 pg/mL in G1

and G2, respectively. The average values for each group also showed a higher average level compared to ovariectomized controls (6 ± 1.8 pg/mL).

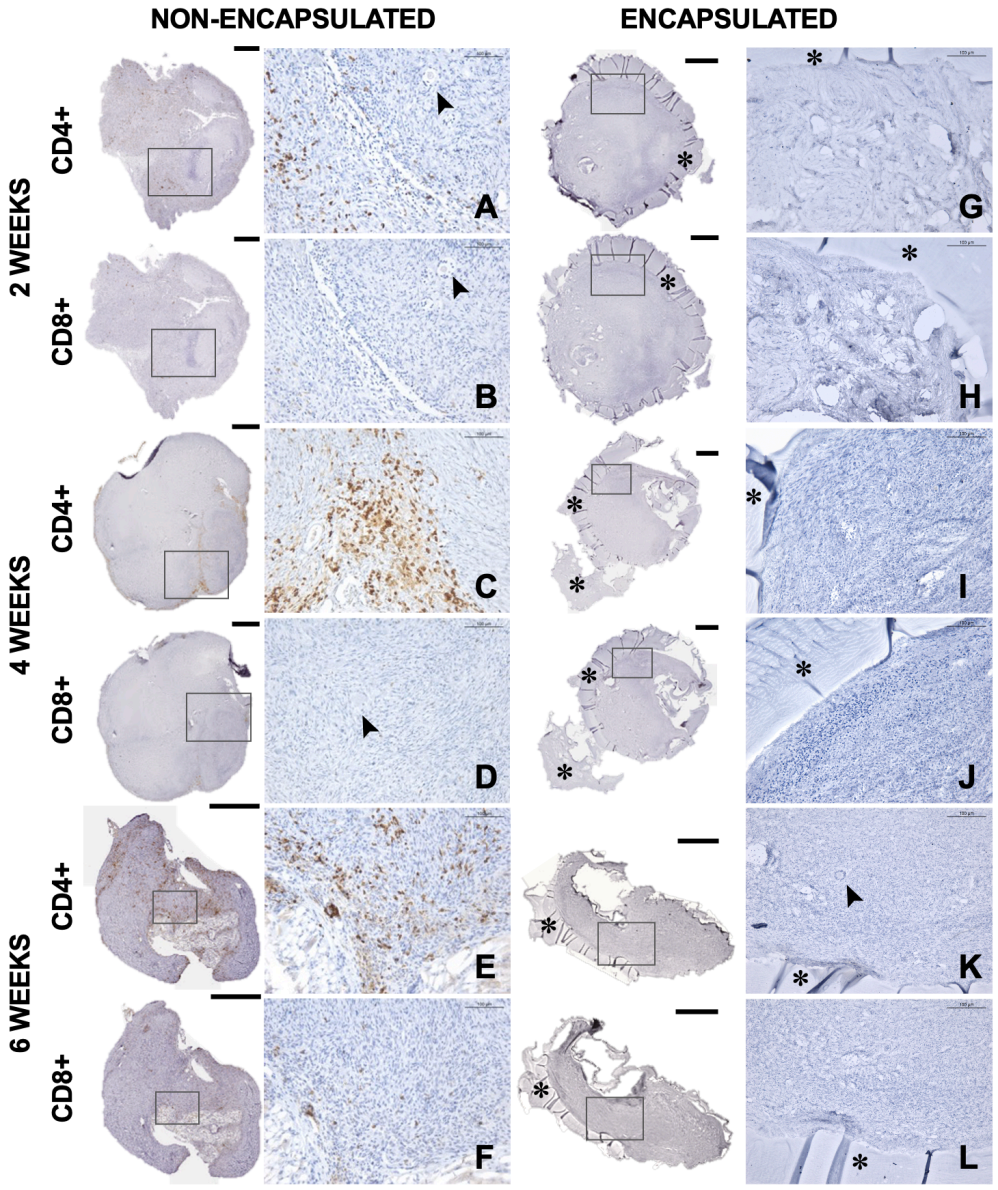

Figure 4.4 T-cell staining indicates immune-isolating capsule is functioning. Whole slide scans of non-encapsulated (A-F) and encapsulated (G-L) samples show T-cell infiltration in non-encapsulated samples at each timepoint. Lack of staining shows capsules preclude T-cell infiltration. Black arrow heads (➤) indicate follicles, asterisks (✻) indicate the PEG capsule. Scale bars are 100μm for high magnification images and 1mm for all others.

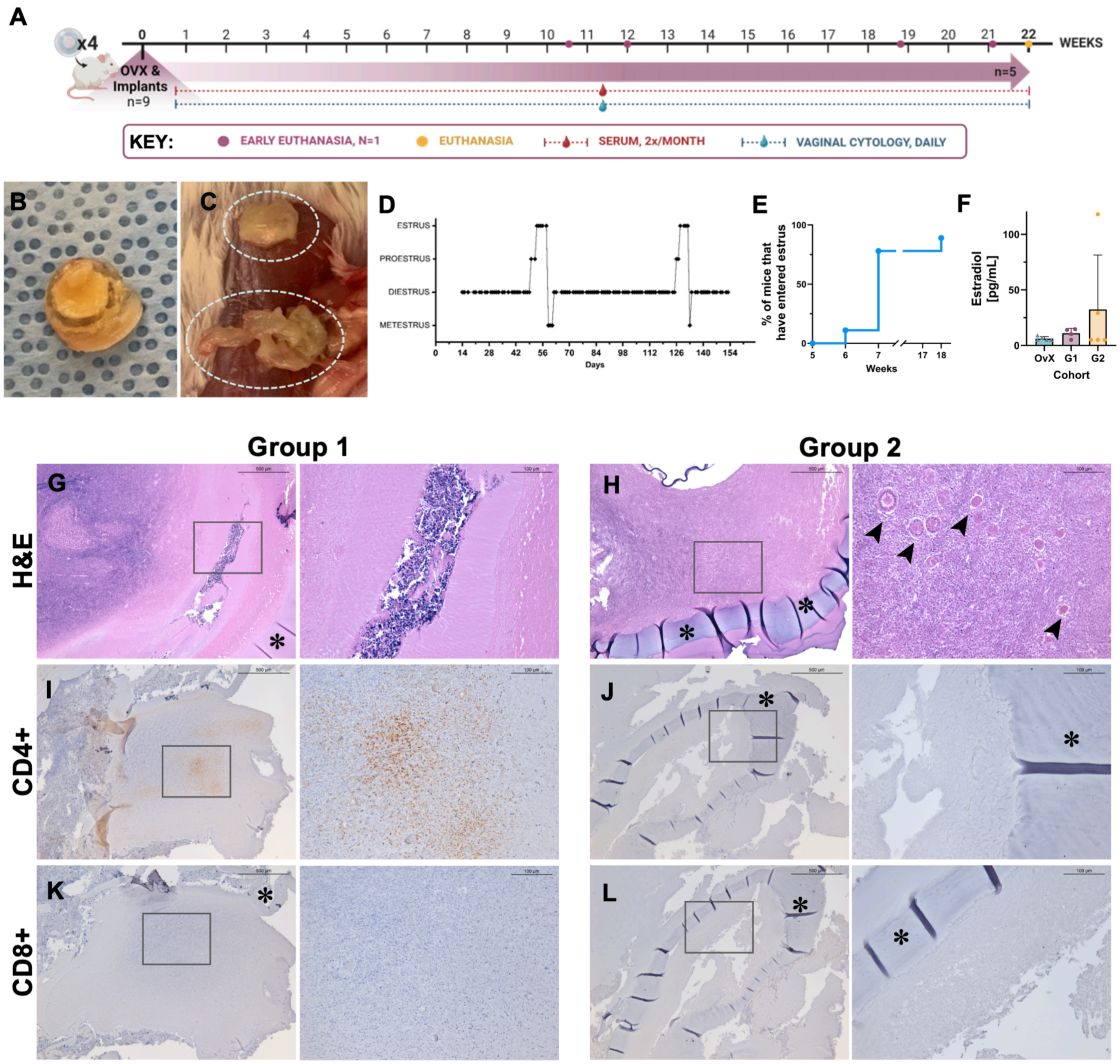

Figure 4.5 Long-term studies in immunocompetent mice shows grafts can support tissue and gonadal hormone function. Experimental design (A) shows some mice were euthanized early, which are collectively termed Group 1. Mice that had implants through the entire 22 weeks are termed Group 2. Examples of each type of implant are shown (B,C). Estrous cyclicity (D) shows mice entered estrus over the study period. All but one mouse entered estrus as shown in E. Estrous cyclicity is supported with upward trends in terminal serum estradiol levels (F). Histological images (G, H) show immune cell infiltration (G) or the presence of early-stage follicles (H). This is supported with IHC showing CD4+ staining (I) in Group 1 samples, and lack of staining in Group 2 (J). CD8+ staining is weak to absent in both groups (K, L). Black arrow heads (➤) indicate follicles, asterisks (✻) indicate the PEG capsule. Scale bars are 500μm in low magnification images and 100μm in high magnification images.

4.3.4 Histological analysis indicates early-stage follicles persist after 22 weeks.

Histological analysis of long-term capsules shows two main outcomes. Group 1 is comprised of capsules that came from mice that needed to be euthanized early (**Figure 4.5C, G, I, K**). Group 2 is comprised of capsules that came from mice that had implants

until 22 weeks and protected the graft (**Figure 4.5B, H, J, L**). Tissue from Group 1 showed infiltration of immune cells when evaluated using morphological analysis in H&E (**Figure 4.5G**), and strong CD4+ staining is observed in the tissue (**Figure 4.5I**). These samples did not contain strong staining or CD8+ cells (**Figure 4.5K**). Conversely, Group 2 shows early-stage follicles are present at 22 weeks (**Figure 4.5H**), and there is no observed CD4+ or CD8+ staining (**Figure 4.5J, L**).

4.4 Discussion

The main goal of this study was to evaluate the immune-isolating properties of the capsule. We began this study by characterizing the donor tissue used in both short-term and long-term studies. There is clear heterogeneity between donors, as expected. In short term studies, Donors A-C were randomized between all groups. We began with short term studies to evaluate if there was hyper acute or acute rejection of the grafts. As expected, we saw the non-encapsuled controls showing signs of rejection as early as 2 weeks with follicle morphology showing signs of follicular degeneration or apoptosis. This trend was continued at the 4- and 6-week time points with follicles in the 6-week grafts showing significant morphological changes and fibrous stroma. Conversely, the encapsulated tissue showed healthy follicle morphology and cellular stroma throughout 6-weeks.

In addition to follicle morphology, we wanted to evaluate cellular graft rejection and conducted staining for CD4+ and CD8+ T-cells. We saw stronger CD4+ staining than CD8+ staining across all time points, with more CD8+ staining in week 6 samples. We hypothesize that since CD8+ T-cells are responsible for inducing apoptosis or cell lysis, while CD4+ T-cells release cytokines to induce an immune response and help activate

CD8+ T-cells, this result indicates that as CD4+ T-cells arrive at the tissue they are just starting to augment the immune response at week 2.

The long-term studies were designed using tissue from Donors D-F and intended to show capsule function with large volumetric changes in follicle size. We were encouraged to see early signs of graft function, indicating the immune-isolating capacity of the capsule, when estrous cyclicity was observed, indicating that estradiol was being produced and diffusing out of the graft. We were also interested to see a similar trend compared to short term IHC staining where CD4+ T-cells were present in Group 1, but no positive staining for CD8+ T-cells was observed. Mice that exhibited ulceration of the skin, possibly due to a large number of capsules, were euthanized earlier and the capsules retrieved from these mice did not stay intact. Further studies are needed to determine if there were cracks due to follicle expansion allowing for immune cell infiltration, graft rejection, and skin lesions or if capsules were swelling with follicle expansion and putting pressure on the skin, causing itching and graft damage.

This study has provided valuable insight into whether the immune-isolating capsule could protect human ovarian tissue xenograft implanted in an immunocompetent mouse. Despite pushing the limits of macroencapsulation we recognize a few limitations. First, graft rejection is predominantly regulated via T-cells, but other factors are likely at play including innate immune cells[108]. Additional studies to indicate if host-released cytokines near the capsule, or complement, have any effect on graft function to help to further elucidate the capsule function. Second, assuming there is a cellular response to damage-associated molecular patterns during implantation, it is possible that immune cells near the capsule will react to peptide hormones being produced by the graft. Although PEG is

widely considered an inert material[109,110], and has been used in many applications, there is still some concern for an immune response to the material[111]. Initial capsule design evaluated various PEG capsule formations, however the PEG-VS shell utilized in this work showed the least amount of capsule formation[51]. While capsule formation was limited in this study, the impact of this capsule on tissue health and function has yet to be investigated.

Third, we observed a resumption of estrous cyclicity, but no large antral follicles were observed. It is hypothesized that follicles are maturing, producing estradiol, and then undergoing atresia. Investigating the graft composition at intermediate time points would allow a more nuanced analysis on the stages of folliculogenesis within the capsule. Finally, the long-term goal of this capsule is for allograft use, not xenograft use. We are aware that this xenograft model has a stronger response in some ways than the allo-response, but these responses are different[106]. While previous work has shown the capsules protect murine grafts from the allo-response, these studies did not include human follicles that can reach 2mm in diameter. Understanding the immune response with large volumetric changes in follicle size is critical to fully evaluate any possibility of capsule fracture.

In conclusion, we aimed to evaluate the immune-isolating capacity of the capsule with human ovarian tissue xenografted in immunocompetent mice. Analysis of the xenografts retrieved after 6 weeks confirmed the protection of human ovarian tissue with complete preclusion of CD4+/CD8+ T-cell infiltration and showed ovarian follicles with normal morphology in the encapsulated tissue. Implantation of the encapsulated human xenografts in ovariectomized immunocompetent mice for 22 weeks restored regular

estrous cyclicity, increased levels of estradiol reaching pre-ovariectomy levels, and normal growing follicles persisted in the immune-isolating capsule.

Chapter 5 Conclusions and Future Directions

5.1 Summary of findings

The first experimental question we sought to answer was whether the PEG capsule developed for murine tissue would support the survival and function of human ovarian cortical tissue while maintaining immune isolation. We began by using identical methods as had previously been used with murine tissue, only changing the source of the tissue from rodent to human. It was shown that the process of encapsulation did not decrease follicle density compared with non-encapsulated grafts. Furthermore, the dual PEG capsule supported follicle survival in human ovarian xenografts up to 90 days *in vivo*. Cryopreservation of ovarian cortical strips allowed for thorough analysis of follicular density to ensure graft longevity, as well as move the technology closer to how it would be used clinically. The next objective was to mitigate the variability between human ovarian tissue grafts stemming from the inherent heterogeneity of the human ovarian cortical tissue between donors and even withing the same ovary. The size of the graft was increased to a volume 20 times larger than the original tissue volume, which also required increasing the capsule size. This change in size was critical and required additional design changes, including flipping capsules over to fully crosslink the capsule. We concluded that the capsule design was sufficient for use with human ovarian tissue and that it would serve as the basis for all studies to come.

The next experimental question was whether the human follicles would be able to grow, how to stimulate this growth, and whether circulating gonadotropins in a mouse would suffice. As described in the introduction, mature follicles require endocrine signaling to mature to multi-layer and antral follicle sizes. Multiple stimulation protocols using exogeneous gonadotropins were tested, however the most effective approach was implanting grafts in ovariectomized mice, with high levels of endogenous murine FSH to act on the human grafts. We have shown that human follicles grew and reached antral stages in an ovariectomized NSG mouse model. Moreover, these antral follicles were found in grafts that were both encapsulated and non-encapsulated. Additionally, significant estradiol production and regular estrous cyclicity were observed for both the encapsulated and non-encapsulated groups. This indicates not only that the graft is interfacing with the mouse hypothalamus/pituitary axis, but also proves that the immune-isolating capsule does not preclude bidirectional exchange of hormones via diffusion. This is a critical feature if this technology is to be translated for clinical use. Once we developed a model to grow large follicles in our immune-isolating capsules, we were able to move on to evaluating the immune-isolating feature.

The final experimental question was to determine if the immune-isolating capsule was functioning as anticipated with respect to preventing immune cell infiltration. Immune-isolating capsules and control tissue were implanted subcutaneously in immunocompetent mice. Analysis of xenografts retrieved after 6 weeks confirmed the protection of human ovarian tissue with complete preclusion of CD4+/CD8+ T-cell infiltration and showed ovarian follicles with normal morphology in the encapsulated tissue. Implantation of the encapsulated human xenografts in ovariectomized

immunocompetent mice for 22 weeks restored regular estrous cyclicity, increased levels of estradiol, and normal growing follicles persisted in the immune-isolating capsule. Furthermore, CD4+/CD8+ T-cells were not observed in grafts that were implanted for 22 weeks. Without the ability to protect the graft from the immune system this technology would require patients to use immunosuppressive medication, one of the main strengths of this technology.

In conclusion, we have demonstrated the translatability of this technology to the clinic. We have shown that the capsule materials and encapsulation methods used do not damage follicle viability, that human ovarian follicles can grow up to 3mm in size, and that even with growing follicles the tissue is protected from cell-based immune rejection. This work can be used as a basis for additional large animal studies. Additionally, it can serve a basis for using these materials in other immune-isolating applications.

5.2 Future directions

This work has shed some light on how this technology can be translated to the clinic by utilizing human tissue, but it has also generated many new questions. These questions fall into three main categories: (1) biological questions, (2) materials engineering, and (3) manufacturing.

With regards to biology, it will be important to tease out how the follicles in one graft are interacting with follicles in another. Follicle crosstalk is critical for ensuring that follicles activate in waves, maintaining the primordial follicle pool. Sequential follicle activation occurs naturally in the ovaries, but it was unclear if the same process would persist when the ovary is divided, and only small portion is implanted. This work has shown that there are primordial and primary follicles still present after 22 weeks, indicating

they did not all activate at once; however, it would be interesting to evaluate how many follicles underwent atresia and how many are still in a quiescent state. Furthermore, it will be important to determine what happens to the follicles in a capsule where an antral follicle becomes dominant. Will it cause atresia of the other follicles in the graft? If we can model follicle activation rates it would go a long way to determining graft longevity and would give us a better idea of the quantity of tissue that would need to be implanted in a patient. To model activation rates in the capsule samples would need to be removed at more intervals than were used in this work. Follicle classification could be conducted for these samples and compared across timepoints. This approach would require a large number of samples and hosts to get an accurate picture of this process and a large animal model with less ovarian heterogeneity may be necessary.

Another avenue of research would be to look at the presence of other gonadal hormones and reciprocal feedback. Due to the small blood volume in mice, we were unable to run assays to determine the amount of progesterone, activins, inhibins, androstenedione, and other hormones. To fully understand how this graft would function as a replacement for functional ovaries, characterization of corpus lutea and progesterone would be critical. The experiments in NSG mice showed that the estrous cycle began to lengthen, indicating a cycle more on a human menstrual cycle timeline. This begs the question how reciprocal feedback is occurring – how are the estradiol levels produced by the human tissue impacting the hypothalamus and pituitary? Are the other peptide hormones produced by the human tissue interacting with the brain in a similar way as estradiol? The answers to these questions are likely better answered with large animal

studies where larger volumes of blood can be collected, allowing for additional analyses to be performed.

With respect to the immune-isolating properties of the capsule, there are many questions that could be investigated to determine what exactly is happening at the surface of the dual capsule. While only minimal capsule formation was noted in these studies, it will be important to determine whether T-cells surrounding the capsule are releasing chemokines that promote a stronger response at the graft surface. The composition of the PEG hydrogel is widely considered biologically inert, as described in Chapter 4, but the allo- or xenogeneic antigens diffusing through the gel may contribute to an immune response. It would also be interesting to see if there are any host complement proteins in the capsule and get a better idea of the xenograft response in this context. Research on grafting human ovarian tissue into animals is very rare, as most transplant work looks at utilizing other animal tissues in humans (i.e. porcine hearts and kidneys). It could also be interesting to compare grafts between different types of immune compromised mice with varying levels of deficiencies, and it could provide an opportunity to see which components of the innate immune system influence the response to the capsule.

Moving on to materials engineering, there are a lot of opportunities to investigate pore size and see how we can improve diffusion without compromising immune-isolation. This work focused entirely on bulk hydrogels, but it would be interesting to see how changes to pore size or the addition of micropores would impact graft longevity and health. There is some evidence that the limits of oxygen diffusion may be reached in the middle of the tissue graft as it is currently made. In addition to addressing the limits of diffusion, the tunable chemistry and modular design of the hydrogel can support release

of chemokines to further minimize immune response, induce tolerance or deliver factors that can delay premature follicle activation, such as AMH. For example, tolerance induction could potentially be achieved with a slowly degradable capsule that eventually would be vascularized by the host to prevent tissue death and extend function.

The use of 3D printing to get precise capsule dimensions would have a strong impact on scaling up the process. Currently, the manual process of making gels is reproducible, but the exact dimension of the gel on each surface is unknown, which may affect the function of the tissue due to variable access to soluble factors. If the necessary capsule thickness to prevent immune cell infiltration was known, capsules could be made at that exact thickness with a much smaller dimensional tolerance than is possible making them by hand. The manufacturing process for this capsule will be critical for FDA approval and will be critical to delivering the best product possible to the patient. When thinking about translating this technology to people the most likely scenario is that this product will be kept cryopreserved until thawed and implanted. If this is the case, we need to evaluate freezing protocols that not only protect the tissue, but also are suitable to keep the capsule intact.

Appendices

Appendix A: Human Tissue Donor Information

Appendix Table A.1 Complete list of human donor information

Record No.	1	2	3	4	5
Age	18	26	18	26	23
Height (cm)	162.56	157	160	165	165
Weight (kg)	52.8	60.2	70.3	59	67.9
BMI (kg/m^2)	19.981	24.423	27.461	21.671	24.94
Ethnicity	White	Black or African American	Black or African American	White	White
Blood Type	O	O	O	A	O
Cause of death	Head Trauma	Anoxia	Anoxia	Head Trauma	Head Trauma
Storage Solution	HTK	UW	UW	UW	UW
Cross-clamp date/time	1/9/19 17:22	7/24/19 16:27	10/14/19 06:03	10/22/19 03:05	12/19/19 15:46
Placed on ice time	1/9/19 22:30	7/24/19 17:30	10/14/19 07:30	10/22/19 04:25	12/19/19 17:20
Lab start time	1/10/19 01:17	7/25/19 02:15	10/14/19 23:53	10/22/19 17:05	12/19/19 20:52
Right Ovary Size (cm)	4x3x1.2	4x2x1	3x1x0.5	2x1x1	4x2.5x1.7
Right Ovary Volume (ml)	Not Specified	Not Specified	Not Specified	Not Specified	Not Specified
Left Ovary Size (cm)	N/A	4x2x1	3x1.5x0.5	2.5x2x1.5	3.5x2x1.2

Record No.	1	2	3	4	5
Left Ovary Volume (ml)	N/A	Not Specified	Not Specified	Not Specified	Not Specified
CPR administered	No	Yes 30 minutes	No	No	Yes 10 minutes
Cold Ischemic Time (hours)	7.9	9.8	18.8	15.0	5.1

Table A1 cont'd

Record No.	6	7	8	9	10
Age	20	30	28	20	35
Height (cm)	168	173	152	165	160
Weight (kg)	51	80.9	61	84	69.4
BMI (kg/m^2)	18.07	27.031	26.402	30.854	27.109
Ethnicity	White	White	Asian	White	White
Blood Type	O	B	O	O	A1
Cause of death	Head Trauma	ESLD	Anoxia	Anoxia	Cerebrovascular/ Stroke
Storage Solution	NS	NS	HTK	NS	UW
Cross-clamp date/time	3/19/20 13:19	7/16/20 16:52	9/3/20 19:08	9/11/20 00:48	9/26/20 12:46
Placed on ice time	3/19/20 14:30	7/16/20 18:28	9/3/20 22:01	9/11/20 2:05	9/27/20 12:31
Lab start time	3/20/20 10:55	7/16/20 21:45	9/4/20 02:30	9/11/20 17:30	9/27/20 10:45
Right Ovary Size (cm)	3.2x2.4x1.3	2.25x2.5x1.34	3.5x2.25x1	3.7x1.9x0.8	Not Specified
Right Ovary Volume (ml)	5	8	6	4.5	8
Left Ovary Size (cm)	2.9x2x1.5	4x2.75x1.7	N/A	4.5x2x0.6	Not Specified
Left Ovary Volume (ml)	3	9	N/A	4	6
CPR administered	No	No	Yes 10 minutes	Yes 0 minutes	No
Cold Ischemic Time (hours)	22.6	4.9	7.4	17.7	22.0

Table A1 cont'd

Record No.	11	12	13	14	15
Age	37	31	19	28	29
Height (cm)	170	166	163	165	165
Weight (kg)	88	87.1	80	54.9	113.8
BMI (kg/m^2)	30.45	31.608	30.11	20.165	41.8
Ethnicity	Black or African American	White	White	Black or African American	White
Blood Type	O	A	A1	A	A1
Cause of death	Anoxia	Head Trauma	Head Trauma	Head Trauma	Anoxia
Storage Solution	NaCL	NaCL	NS	UW	UW
Cross-clamp date/time	11/9/20 17:50	12/8/20 18:11	12/22/20 21:28	1/27/21 13:10	3/3/21 22:29
Placed on ice time	11/9/20 21:00	12/8/20 22:23	Not Specified	1/27/21 15:05	3/3/21 23:55
Lab start time	11/10/20 18:15	12/9/20 18:49	12/23/20 17:18	1/27/21 20:33	3/4/21 14:56
Right Ovary Size (cm)	Not Specified	3.75x2.5x1	4x2.75x1	3x2x.9	3.5x2.5x2.25
Right Ovary Volume (ml)	Not Specified	6	9	6	7
Left Ovary Size (cm)	Not Specified	6x2.5x1	4x2.5x1	4x3x1.5	3.25x2x1.5
Left Ovary Volume (ml)	Not Specified	8	7	11	4
CPR administered	Yes 9 minutes	Yes 0 minutes ~200 compressions	No	No	No
Cold Ischemic Time (hours)	25.4	26.6	20.8	7.4	16.5

Table A1 cont'd

Record No.	16	17	18	19	20
Age	40	18	16	25	33
Height (cm)	152	165	154.94	173	183
Weight (kg)	92	48.8	51.1	61.7	102.5
BMI (kg/m^2)	39.82	17.925	21.286	20.616	30.607
Ethnicity	White	White	White	White	White
Blood Type	A2	O	A1	O	A1
Cause of death	Anoxia	Anoxia	Anoxia	Anoxia	Anoxia
Storage Solution	NS	NS	NS	NS	UW
Cross-clamp date/time	4/15/21 15:57	5/21/21 10:42	5/25/21 06:58	5/29/21 10:19	6/22/21 14:22
Placed on ice time	4/15/21 17:17	5/21/21 12:45	5/25/21 07:55	5/29/21 10:30	6/22/21 15:37
Lab start time	4/16/21 09:57	5/22/21 09:25	5/25/21 21:20	5/29/21 23:01	6/23/21 08:03
Right Ovary Size (cm)	3x1.5x0.75	4x2x1	2.2x1.7x0.9	4.4 x 2.8 x 1	3 x 1.75 x 1.25
Right Ovary Volume (ml)	2	6	2.5	9	4
Left Ovary Size (cm)	2.25x1.5x1	3.5x2x1	2.4x2x1.5	4.2 x 3.3 x 1.1	3 x 2 x 1.75
Left Ovary Volume (ml)	4	5	5	12	4
CPR administered	Yes, 60 minutes	Yes	Yes, 9 minutes	Yes, 30 minutes	Yes, 35 minutes
Cold Ischemic Time (hours)	18.0	23.7	15.4	13.7	17.7

Table A1 cont'd

Record No.	21	22	23	24	25
Age	27	27	37	18	39
Height (cm)	155	173	160	163	163
Weight (kg)	69.5	86.5	61.7	89	83
BMI (kg/m^2)	28.928	28.902	24.102	33.496	31.239
Ethnicity	White	Black or African American	White	White	White
Blood Type	O	O	A1	A	O
Cause of death	Anoxia	Cerebrovascular / Stroke	Anoxia	Anoxia	Cerebrovascular/ Stroke
Storage Solution	NS	UW	NS	NS	NS
Cross-clamp date/time	6/26/21 13:46	7/20/21 18:54	7/26/21 20:36	7/27/21 08:50	10/12/21 18:07
Placed on ice time	6/26/21 15:35	Not Specified	7/26/21 23:30	7/27/21 10:40	10/12/21 18:57
Lab start time	6/27/21 14:20	7/21/21 15:08	7/27/21 15:15	7/27/21 22:35	10/13/21 08:24
Right Ovary Size (cm)	2.5x1.7x1	3.5x2.5x0.8	3x2x1.5	4x3x1.2	3.8x2.4x1.2
Right Ovary Volume (ml)	2	5	4	9	9
Left Ovary Size (cm)	2.4x1.6x0.9	4x2.3x0.9	2.5x2x1.4	3.5x2.5x1.5	4x2.5x1
Left Ovary Volume (ml)	2	6	3	7	8.5
CPR administered	Yes, Unknown minutes	NO	Yes, 5 minutes	No	No
Cold Ischemic Time (hours)	25.6	21.2	19.7	14.7	14.3

Table A1 cont'd

Record No.	26	27	28	29	30
Age	25	31	28	31	34
Height (cm)	180.34	152	157	160	175.26
Weight (kg)	95	87.2	56	62	75
BMI (kg/m^2)	29.211	37.742	22.719	24.219	24.417
Ethnicity	White	White	White	Black or African American	Black or African American
Blood Type	A2	O	O	O	B
Cause of death	Anoxia	Anoxia	Anoxia	Head Trauma	Anoxia
Storage Solution	NS	UW	NS	NS	Saline
Cross-clamp date/time	1/2/22 13:49	1/14/22 17:26	5/4/22 18:10	5/10/22 16:28	8/31/22 02:44
Placed on ice time	1/2/22 16:00	1/14/22 19:30	5/4/22 20:48	5/10/22 18:00	8/31/22 05:18
Lab start time	1/3/22 14:18	1/15/22 21:07	5/5/22 14:34	5/11/22 21:21	8/31/22 13:12
Right Ovary Size (cm)	4.8x2.7x1.6	4.5x3.25x1.4	3.5x1.9x1	2.4x1.5x1	4.5x2.3x2
Right Ovary Volume (ml)	12	11	5	2	9
Left Ovary Size (cm)	4.2x3.4x0.9	4x2.5x1.5	3.6x3x2	2.5x1.5x1.2	4.6x3x1.9
Left Ovary Volume (ml)	10	9	10	2	12
CPR administered	Yes, 50 minutes	Yes, 25 minutes	Yes, 19 minutes	No	Yes, 2 minutes
Cold Ischemic Time (hours)	25.5	27.7	20.4	29.9	10.5

Table A1 cont'd

Record No.	31	32	33	34	35
Age	24	33	34	27	28
Height (cm)	162	168	155	160.02	165.1
Weight (kg)	74.7	72.6	76	57.6062	69.6
BMI (kg/m^2)	28.464	25.833	31.634	22.497	25.534
Ethnicity	Hispanic/Latino	Asian: Korean	White	Black or African American	Hispanic/Latino
Blood Type	O	O	A	A	O
Cause of death	Head Trauma	Head Trauma	Head Trauma	Head Trauma	Cerebrovascular/ Stroke
Storage Solution	NS	Saline	NS	NS	NS
Cross-clamp date/time	9/21/22 01:43	9/23/22 17:10	11/18/22 16:30	11/25/22 21:37	12/10/22 00:22
Placed on ice time	9/21/22 03:20	9/23/22 18:55	11/18/22 18:10	11/25/22 23:45	12/10/22 02:30
Lab start time	9/21/22 13:51	9/24/22 16:38	11/19/22 12:35	11/26/22 13:29	12/10/22 11:57
Right Ovary Size (cm)	3.1x1x2.2	4x2.1x1.2	3x2x1.4	3x2.2x1	2.7x1.5x1.1
Right Ovary Volume (ml)	3	6	4	4	4
Left Ovary Size (cm)	4x0.8x1.8	3.5x2.25x0.8	3.5x2x1	3.4x2.2x1.1	3.1x2x0.6
Left Ovary Volume (ml)	3	4	4	3	4
CPR administered	No	No	No	No	No
Cold Ischemic Time (hours)	12.1	23.5	20.1	15.9	11.6

Table A1 cont'd

Record No.	36	37	38	39	40
Age	29	34	25	35	23
Height (cm)	175	168	152.4	170	152.4
Weight (kg)	52.4	94.8	57.9	116	56.7
BMI (kg/m^2)	17.11	33.588	24.929	40.138	24.413
Ethnicity	White	Hispanic/Latino	White	Hispanic/Latino	White
Blood Type	A2	A1	O	B	A1
Cause of death	Overdose	Cerebrovascular/ Stroke	Anoxia	Anoxia	Anoxia
Storage Solution	NaCL	UW	NS	NS	NS
Cross-clamp date/time	12/19/22 14:30	1/26/23 09:33	1/27/23 20:09	2/20/23 16:14	2/25/23 17:31
Placed on ice time	12/19/22 15:10	1/26/23 12:00	1/27/23 22:15	2/20/23 18:30	2/25/23 19:15
Lab start time	12/19/22 19:30	1/27/23 08:05	1/28/23 13:30	2/21/23 12:40	2/26/23 14:08
Right Ovary Size (cm)	4x1.7x0.8	4.5x2x1.25	4.5x2.1x0.8	3x3x1.2	2.5x2x1.1
Right Ovary Volume (ml)	4	10	6	6	4
Left Ovary Size (cm)	3.5x1.8x0.9	3.5x2.0x1.0	4.6x2.5x0.7	3x2x1	N/A
Left Ovary Volume (ml)	4	6	7	4	N/A
CPR administered	Yes, 10 minutes	No	Yes, Unknown	No	Yes
Cold Ischemic Time (hours)	5.0	24.5	17.3	20.4	20.6

Table A1 cont'd

Record No.	41	42	43	44
Age	38	20	32	31
Height (cm)	175.26	160	178	142
Weight (kg)	72.2	57.4	87	77
BMI (kg/m^2)	23.506	22.422	27.459	38.187
Ethnicity	White	White	White	White
Blood Type	A2	A2	O	B
Cause of death	Cerebrovascular/ Stroke	Anoxia	Anoxia	Cerebrovascular/ Stroke
Storage Solution	NaCL	NaCL	Servator-B	NSS
Cross-clamp date/time	3/24/23 10:34	8/7/23 14:35	10/9/23 22:32	10/11/23 17:59
Placed on ice time	3/24/23 10:20	8/7/23 15:00	Not Specified	10/11/23 20:15
Lab start time	3/24/23 20:55	8/7/23 20:27	10/10/23 10:10	10/12/23 10:18
Right Ovary Size (cm)	2.7x2x0.9	4.25x2.2x1.5	4x2x0.8	2.5x0.78x2
Right Ovary Volume (ml)	3	14	5	4
Left Ovary Size (cm)	2.9x2.2x1.1	6x2.2x1.5	4.8x2x0.9	2.3x2.0x0.75
Left Ovary Volume (ml)	3	16	5	4
CPR administered	No	Yes 25 minutes	Yes 35 minutes	NO
Cold Ischemic Time (hours)	11.4	5.9	11.6	16.3

Table A1 cont'd

Record No.	45	46
Age	23	22
Height (cm)	165	172
Weight (kg)	138	193
BMI (kg/m^2)	50.689	29.4
Ethnicity	White	White
Blood Type	A1	A
Cause of death	Cerebrovascular/ Stroke	Head Trauma
Storage Solution	NSS	NSS
Cross-clamp date/time	10/25/23 10:13	1/30/24 23:16
Placed on ice time	10/25/23 13:39	Not Specified
Lab start time	10/26/23 09:49	1/31/24 10:32
Right Ovary Size (cm)	3.5x2.7x1.2	3x1.5x1
Right Ovary Volume (ml)	7	5
Left Ovary Size (cm)	4.0x3.0x1.3	2.5x2x0.75
Left Ovary Volume (ml)	7	4
CPR administered	No	Not Specified
Cold Ischemic Time (hours)	23.6	11.3

Appendix B: Chapter Three Supplemental Materials

Appendix Table B.1 Chapter three complete donor information

Donor ID	A	B	C	D	E	F	G	H	Average ± Std. Dev.
Age (years)	18	16	25	27	18	25	31	28	23.5 ± 5.5
Height (cm)	165	155	173	173	163	180	152	157	164.8 ± 9.9
Weight (kg)	48.8	51.1	61.7	86.5	89	95	87.2	56	71.9 ± 19.3
Body Mass Index (kg/m^2)	17.9	21.3	20.6	28.9	33.5	29.2	37.7	22.7	26.5 ± 6.9
Right Ovary Volume (mL)	6	2.5	9	5	9	12	11	5	7.4 ± 3.3
Left Ovary Volume (mL)	5	5	12	6	7	10	9	10	8.0 ± 2.6
Cold Ischemic Time* (hours)	23.7	15.4	13.7	21.2	14.7	25.5	27.7	20.4	20.3 ± 5.3
Cardiac arrest/downtime (minutes)	YES	YES 20	YES 50	NO	NO	YES 15	YES 0	YES 19	
Cross-clamp Date and Time**	5/21/21 10:42	5/25/21 6:58	5/29/21 10:19	7/20/21 18:54	7/27/21 8:50	1/2/22 13:49	1/14/22 17:26	1/14/22 17:26	
Ethnicity	W	W	W	B	W	W	W	W	
Cause of Death	Anoxia	Anoxia	Anoxia	CV/S	Anoxia	Anoxia	Anoxia	Anoxia	
Storage Solution	NS	NS	NS	UW	NS	NS	UW	NS	

B, Black or African American; W, White.
CV/S, cardiovascular/stroke
UW, University of Wisconsin Solution; NS, Normal Saline.
**Time at which the organ is cut from blood/oxygen supply.*
***Time between cross-clamp and the beginning of tissue processing*

Appendix Table B.2 Chapter three donor information by mouse

Group	Time Point	Mouse	Donors
Encapsulated	6 weeks	3	C, F
		10	B, E, F
		20	E, G
		28	E, G
	15 weeks	11	B, F
		15	A, B, F
		21	G, H
		27	G
	20 weeks	5	A, F
		8	F, G
		12	E, F
		13	F
		17	G
		22	G
		25	E, G
Non-Encapsulated	6 weeks	1	A, F
		14	E, F
		18	E, G, H
		24	E, G, H
	15 weeks	4	C, F
		6	B, F
		19	G, H
		23	E, G, H
	20 weeks	2	B, C, G
		7	F, G
		9	B, E, F
		16	A, F

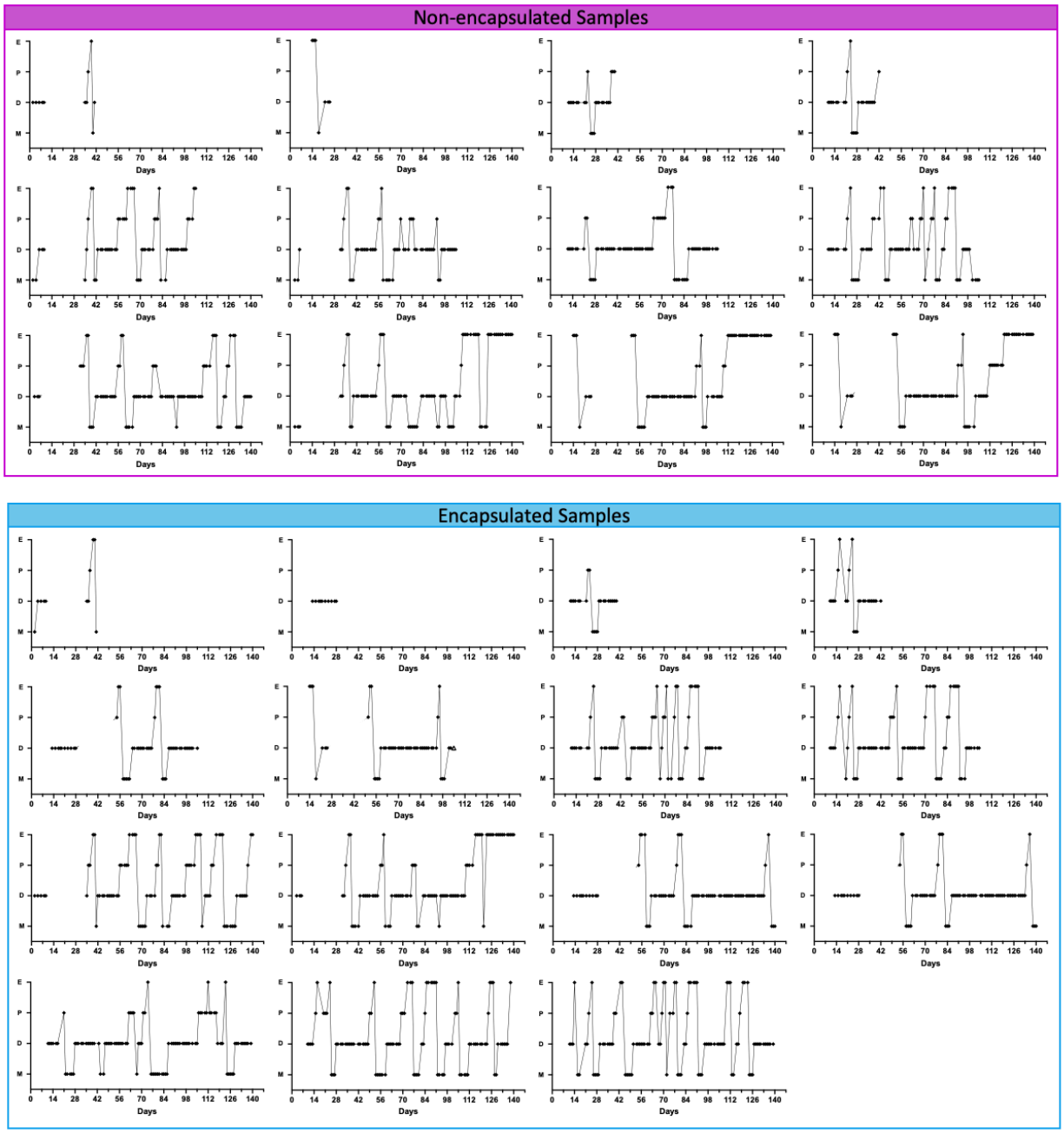

Appendix Figure B.1 Chapter three estrous plots for each mouse in the study

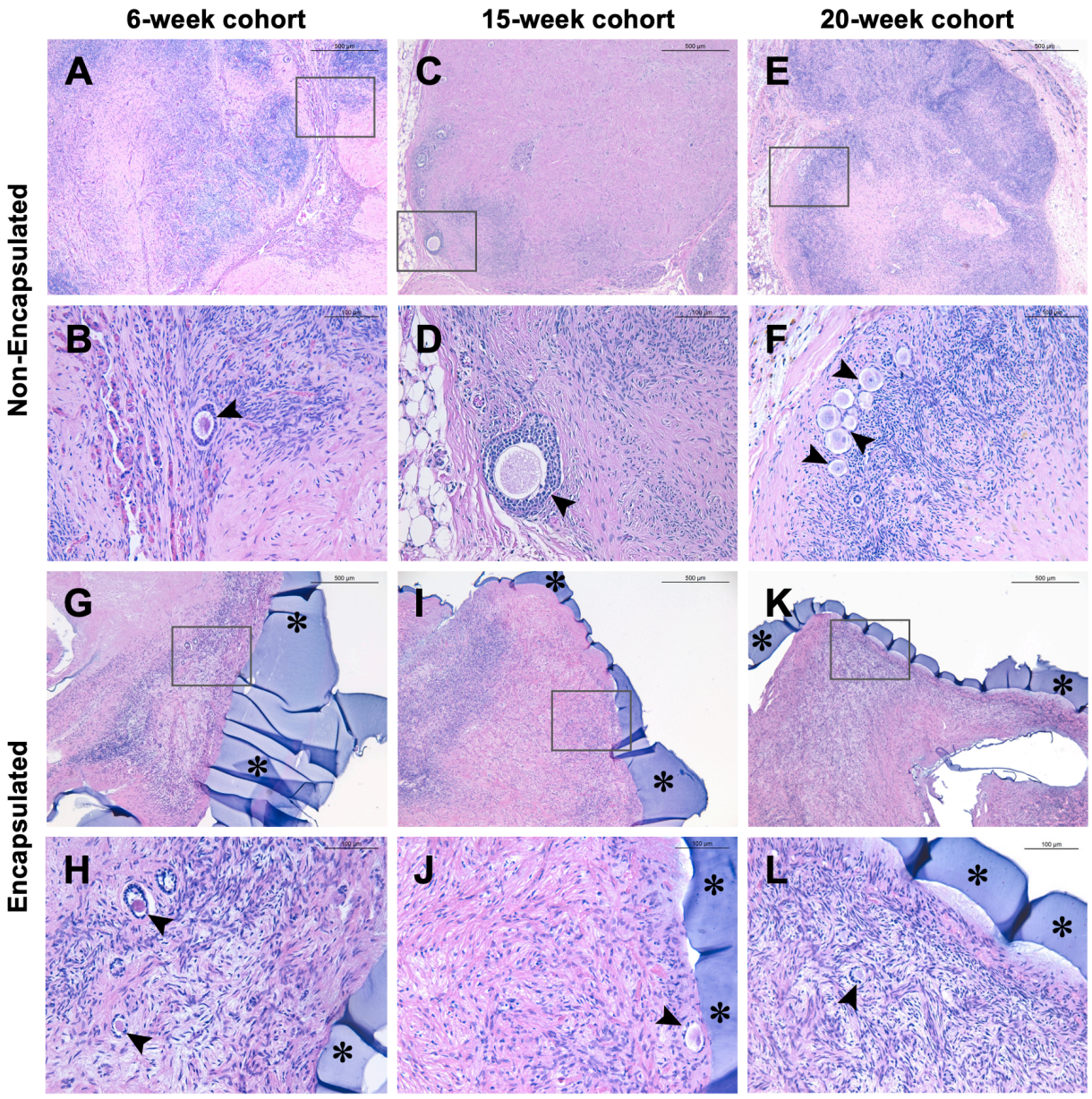

Appendix Figure B.2 Non-antral follicles in stimulated mice

Appendix C: Chapter Four Supplemental Material

Appendix Table C.1 Chapter four complete donor information

Donor No.	A	B	C	D	E	F	Average ± Std. Dev.
Age (years)	25	27	18	24	27	25	24.3 ± 3.3
Height (cm)	173	173	163	162	160	152	163.8 ± 8.1
Weight (kg)	61.7	86.5	89	74.7	57.6	57.9	71.2 ± 14.2
BMI (kg/m^2)	20.6	28.9	33.5	28.5	22.5	24.9	26.5 ± 4.7
Right Ovary Volume (mL)	9	5	9	3	4	6	6.0 ± 2.5
Left Ovary Volume (mL)	12	6	7	3	3	7	6.3 ± 3.3
Cold Ischemic Time* (hours)	13.7	21.2	14.7	12.1	15.9	17.3	15.8 ± 3.2
Cardiac arrest/ downtime (minutes)	YES 50	NO	NO	NO	NO	YES Unknown	
Cross-clamp Date and Time**	5/29/21 10:19	7/20/21 18:54	7/27/21 8:50	9/21/22 1:43	11/25/22 21:37	1/27/23 20:09	
Ethnicity	W	B	W	H	B	W	
Cause of Death	Anoxia	Cerebrovascular /Stroke	Anoxia	Head Trauma	Head Trauma	Anoxia	
Storage Solution	NS	UW	NS	NS	NS	NS	

B, Black or African American; H, Hispanic/Latino; W, White.
UW, University of Wisconsin Solution; NS, Normal Saline.
**Time at which the organ is cut from blood/oxygen supply.*
***Time between cross-clamp and the beginning of tissue processing*

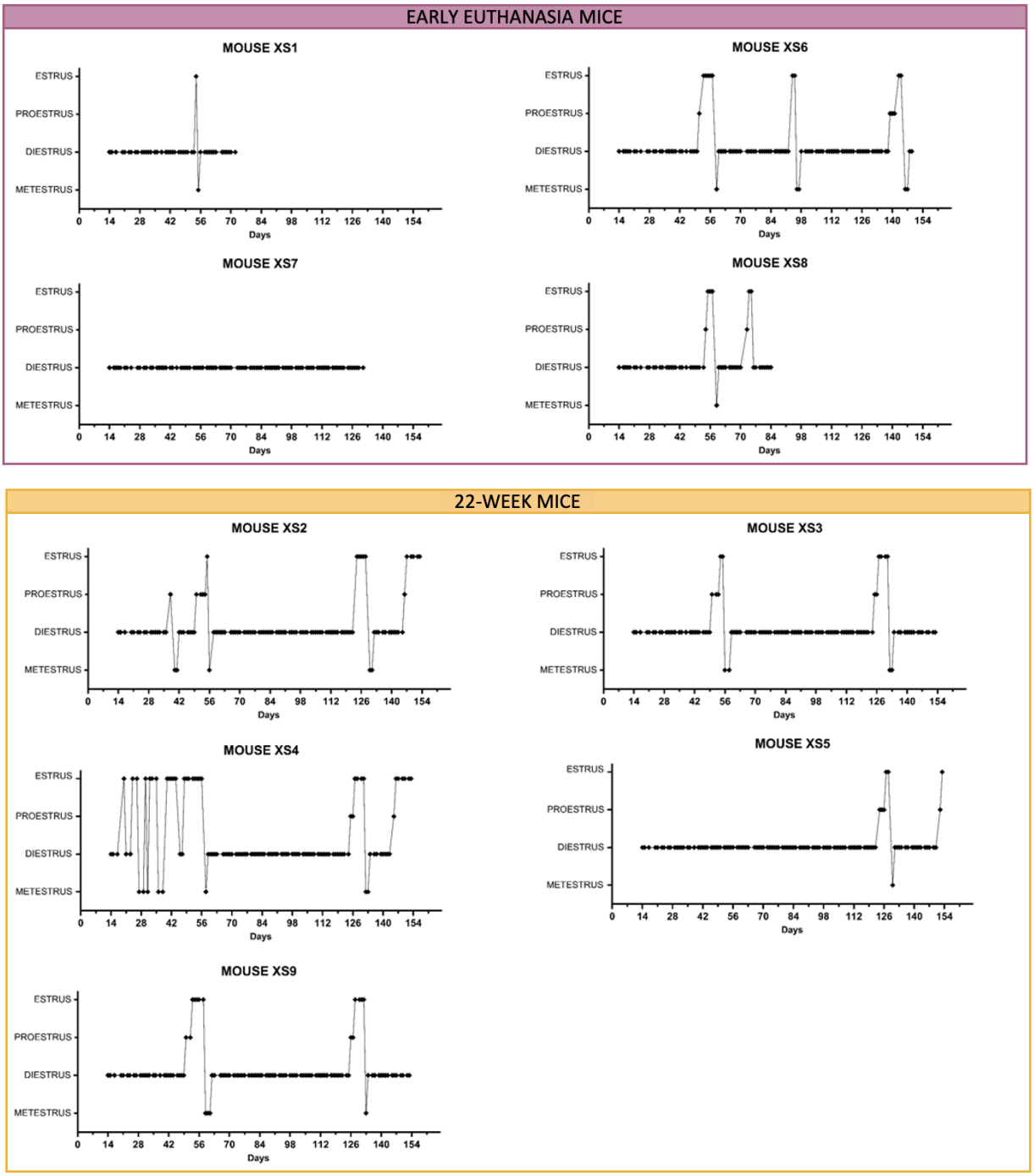

Appendix Figure C.1 Chapter four estrous plots for all mice

Appendix D: Additional Insights

Over the course of my dissertation work there were experiments that did not make it into a manuscript/previous chapter but may be helpful to future students trying to achieve similar goals. All animal experiments detailed here were performed in accordance with the protocol approved by the Institutional Animal Care and Use Committee (IACUC) at the University of Michigan (PRO00007716, PRO00009635, PRO00011284). The IACUC guidelines for survival surgery in rodents and the IACUC Policy on Analgesic Use in Animals Undergoing Surgery were followed for all procedures.

Improving the encapsulation process

After completing the work outlined in Chapter 2, I began to improve the encapsulation method I had used to (1) encapsulate larger pieces of tissue, (2) cut down manufacturing time, and (3) try to develop a process that was more reproducible than the small gels. The first study I conducted was encapsulating pieces of cortex between 0.25 and 0.75 mm^3. I implanted 8 NSG mice with two gels and one piece of control tissue each. These mice were followed for 1 or 4 weeks before conducting histological analysis.

One of the main things I wanted to achieve was more consistent encapsulation. The processes used were highly dependent on the person making the capsules and I began using a PDMS mold to make more consistent gels. It was during the process of using molds and larger pieces of tissue I became aware of a new crosslinking problem. The larger pieces of tissue were impeding the UV light, and the non-degradable PEG

shell was not fully crosslinking underneath the tissue. There was enough crosslinking that I could lift the gel up and out of a mold, but after it was put in media to swell before implantation that loosely crosslinked gel would be destroyed by the swelling. It was at this point that I began the process of flipping the capsules in a mold halfway through crosslinking. I also began testing the UV curing parameters. The work done in Chapter 2 utilized a Spectroline UV lamp that emitted light at 365nm. This lamp was turned on for 6 minutes, which delivered an intensity of 4.4mW/cm^2. A new light was obtained (OmniCure S15000 with standard filter, Excelitas, Technologies, Waltham, MA, USA) that delivered a range of wavelengths (320-500nm), had adjustable intensity levels, and easily adjustable lamp height. The increase in delivered wavelengths resulted in delivering wavelengths that improved molar absorbance of Irgacure 2959[112]. The crosslinking protocol was updated to deliver 30mW/cm^2 for 45 seconds, allowing for a nearly 50% reduction in capsule production time.

After these adjustments I wanted to evaluate the feasibility of removing a single capsule or piece of control tissue from a mouse so I could have enough time points of graft analysis but decrease the number of animals used. I implanted 5 NSG mice with two gels and one piece of control tissue. I took out one gel from each mouse in week one and collected the remaining samples in week four. Unfortunately, the gels tend to clump and getting one out without damaging/disrupting the remaining gel was difficult; additionally, for longer time points the gels can become adhered to the skin or muscle layer making it difficult to extract samples without damaging mouse tissue. Furthermore, there was a worry that the repeated opening and closing of the dorsal skin would cause the mouse to

heal slower. After completing this study, we decided to only collect samples at terminal time points.

Stimulation protocol development

The stimulation protocol described in Chapter 3 utilized the ovariectomized mouse model, however this was not the first protocol tried. The stimulation of human ovarian tissue in murine models is not standard, and methods vary widely across labs. A review on stimulation methods conducted in 2020 by Wall *et al* details the many approaches taken. The first study to look at follicle maturation utilized FSH and human chorionic gonadotropin (hCG) in NSG mice. FSH (Gonal-F, EMD Serano, USA) was injected intraperitoneally every other day for two weeks at 7.5 IU, starting two weeks after graft implantation. This protocol also utilized 20 IU hCG injection 24 hours before euthanasia. Three mice received the FSH and hCG regimen, two mice received saline treatment, and three mice had no treatment. result was no large follicles. A second study utilized protocols found in the review. I began stimulating NSG mice one-week post-implantation with 1 IU of FSH every other day, continuing for 13 or 20 weeks. Similarly, no large follicles were observed.

Appendix Table D.1 All mouse and implant information.

	Lab Donor #	Thaw Media Components	OVX?	Implant Date	Mouse Age @ Implant [months]	Mouse Age @ Implant [weeks]	Mouse Identifier	Mouse Strain	Gels, Tissue, or Both?	Euthanasia Date	Fixative	Implantation Time	Gel Tissue Size	# of Gels	Control Tissue Size	# of pieces of control tissue	Notes
Vitrified Tissue Study	1			4/9/19			H1	NSG	G	5/9/19	Bouins	1mo	1mmx1mmx.5mm	10	NA	NA	gels only in this mouse
	1			4/9/19			H2	NSG	T	5/9/19	Bouins	1mo	NA	NA	1mmx1mmx.5mm	10	tissue only in this mouse
	1			4/11/19			H3	NSG	G	6/5/19	Bouins	2mo	1mmx1mmx.5mm	10	NA	NA	gels only in this mouse
	1			4/11/19			H4	NSG	T	6/5/19	Bouins	2mo	NA	NA	1mmx1mmx.5mm	10	tissue only in this mouse
	1			4/11/19			H5	NSG	G	6/5/19	Bouins	2mo	1mmx1mmx.5mm	10	NA	NA	gels only in this mouse
	1			4/11/19			H6	NSG	T	6/5/19	Bouins	2mo	NA	NA	1mmx1mmx.5mm	10	tissue only in this mouse
	1			4/12/19			H7	NSG	G	7/9/19	Bouins	3mo	1mmx1mmx.5mm	10	NA	NA	gels only in this mouse
	1			4/12/19			H8	NSG	T	7/9/19	Bouins	3mo	NA	NA	1mmx1mmx.5mm	10	tissue only in this mouse
	1			4/12/19			H9	NSG	G	7/9/19	Bouins	3mo	1mmx1mmx.5mm	10	NA	NA	gels only in this mouse
	1			4/12/19			H10	NSG	T	7/9/19	Bouins	3mo	NA	NA	1mmx1mmx.5mm	10	tissue only in this mouse
Fresh Tissue Study	2			7/25/19			FT1	NSG	B	8/22/19	Bouins	4wk	1mmx1mmx.5mm	9	10mmx1mmx.5	1	1 feel on floor; could not locate control tissue
	2			7/25/19			FT2	NSG	B	8/22/19	Bouins	4wk	1mmx1mmx.5mm	10	10mmx1mmx.5	1	
	3			10/15/19			FT6	NSG	B	10/18/19	Bouins	3 days	1mmx1mmx.5mm	10	10mmx1mmx.5	1	
	3			10/15/19			FT7	NSG	B	11/19/19	Bouins	5wks	1mmx1mmx.5mm	10	10mmx1mmx.5	1	Could not locate control tissue
	3			10/15/19			FT8	NSG	B	10/22/19	Bouins	1wk	1mmx1mmx.5mm	10	10mmx1mmx.5	1	
	3			10/15/19			FT9	NSG	B	10/18/19	Bouins	3 days	1mmx1mmx.5mm	10	10mmx1mmx.5	1	
	3			10/15/19			FT10	NSG	B	10/22/19	Bouins	1wk	1mmx1mmx.5mm	10	10mmx1mmx.5	1	
Slow Freezing Study + Stimulation Study 1	5	DMSO	No	2/13/20			H11	NSG	B	2/14/20	PFA	1 day	1mmx1mmx.5mm	10	10mmx1mmx.5	1	
	5	DMSO	No	2/9/20			H12	NSG	B	2/10/20	PFA	1 day	1mmx1mmx.5mm	10	10mmx1mmx.5	1	
	5	DMSO	No	2/12/20			H13	NSG	B	2/13/20	PFA	1 day	1mmx1mmx.5mm	10	10mmx1mmx.5	1	
	5	DMSO	No	2/9/20			H14	NSG	B	2/12/20	PFA	3 days	1mmx1mmx.5mm	10	10mmx1mmx.5	1	
	5	DMSO	No	2/11/20			H15	NSG	B	2/14/20	PFA	3 days	1mmx1mmx.5mm	10	10mmx1mmx.5	1	
	5	DMSO	No	2/12/20			H16	NSG	B	2/15/20	PFA	3 days	1mmx1mmx.5mm	10	10mmx1mmx.5	1	
	5	DMSO	No	2/13/20			H17	NSG	B	2/20/20	PFA	1wk	1mmx1mmx.5mm	10	10mmx1mmx.5	1	
	5	DMSO	No	2/9/20			H18	NSG	B	2/16/20	PFA	1wk	1mmx1mmx.5mm	10	10mmx1mmx.5	1	
	5	DMSO	No	2/12/20			H19	NSG	B	2/19/20	PFA	1wk	1mmx1mmx.5mm	10	10mmx1mmx.5	1	
	5	DMSO	No	2/13/20			H20	NSG	B	2/27/20	PFA	2wk	1mmx1mmx.5mm	10	10mmx1mmx.5	1	
	5	DMSO	No	2/9/20			H21	NSG	B	2/23/20	PFA	2wk	1mmx1mmx.5mm	10	10mmx1mmx.5	1	
	5	DMSO	No	2/9/20			H22	NSG	B	2/23/20	PFA	2wk	1mmx1mmx.5mm	10	10mmx1mmx.5	1	
	5	DMSO	No	2/13/20			H23	NSG	B	3/14/20	PFA	1mo	1mmx1mmx.5mm	10	10mmx1mmx.5	1	STIMULATED
	5	DMSO	No	2/11/20			H24	NSG	B	3/12/20	PFA	1mo	1mmx1mmx.5mm	10	10mmx1mmx.5	1	STIMULATED
	5	DMSO	No	2/11/20			H25	NSG	B	3/12/20	PFA	1mo	1mmx1mmx.5mm	10	10mmx1mmx.5	1	STIMULATED
	5	DMSO	No	2/13/20			H26	NSG	B	3/14/20	PFA	1mo	1mmx1mmx.5mm	10	10mmx1mmx.5	1	NO INJECTION
	5	DMSO	No	2/11/20			H27	NSG	B	3/12/20	PFA	1mo	1mmx1mmx.5mm	10	10mmx1mmx.5	1	SALINE INJECTION
	5	DMSO	No	2/11/20			H28	NSG	B	3/12/20	PFA	1mo	1mmx1mmx.5mm	10	10mmx1mmx.5	1	NO INJECTION
	5	DMSO	No	2/12/20			H29	NSG	B	3/13/20	PFA	1mo	1mmx1mmx.5mm	10	10mmx1mmx.5	1	SALINE INJECTION
	5	DMSO	No	2/12/20			H30	NSG	B	3/13/20	PFA	1mo	1mmx1mmx.5mm	10	10mmx1mmx.5	1	NO INJECTION
Lg Square Pilot	10	DMSO	No	12/2/20			SLH1	NSG	B	12/9/20	Bouins	1wk	~10X5X.5mm	2	~10X5X.5mm	1	
	10	DMSO	No	12/2/20			SLH2	NSG	B	12/30/20	Bouins	4wk	~10X5X.5mm	2	~10X5X.5mm	1	
	10	DMSO	No	12/2/20			SLH3	NSG	B	12/9/20	Bouins	1wk	~10X5X.5mm	2	~10X5X.5mm	1	
	10	DMSO	No	12/2/20			SLH4	NSG	B	12/30/20	Bouins	4wk	~10X5X.5mm	2	~10X5X.5mm	1	
	10	DMSO	No	12/2/20			SLH5	NSG	B	12/9/20	Bouins	1wk	~10X5X.5mm	2	~10X5X.5mm	1	
	10	DMSO	No	12/2/20			SLH6	NSG	B	12/30/20	Bouins	4wk	~10X5X.5mm	2	~10X5X.5mm	1	
	10	DMSO	No	12/2/20			SLH7	NSG	B	12/30/20	Bouins	4wk	~10X5X.5mm	2	~10X5X.5mm	1	
	10	DMSO	No	12/2/20			SLH8	NSG	B	12/9/20	Bouins	1wk	~10X5X.5mm	1	~10X5X.5mm	1	PEG-ND went under the parafilm

Appendix Table D1 Cot'd

	Lab Donor #	Thaw Media Components	OVX?	Implant Date	Mouse Age @ Implant [months]	Mouse Age @ Implant [weeks]	Mouse Identifier	Mouse Strain	Gels, Tissue, or Both?	Euthanasia Date	Fixative	Implantation Time	Gel Tissue Size	# of Gels	Control Tissue Size	# of pieces of control tissue	Notes
Xeno Pilot 1	12	DMSO	No	3/8/21			LX1	C57BL/6	G	3/18/21	Bouins	4 days; 10 days	6mm ø disk	3	6mm ø disk	1	3/12/21: removed 2 gels; 3/18/21 Remaining gel was at the surface and sutures had been disrupted
	12	DMSO	No	3/8/21			LX2	C57BL/6	G	3/22/21	Bouins	4 days; 2wks	6mm ø disk	2	6mm ø disk	1	3/12/21: removed 1 gel; 3/22/21: Remining gel was removed
Large Gel Pilot	13	DMSO	No	2/23/21			SLH11	NSG	B	3/23/21	Bouins	1 wk; 1 month	6mm ø disk	2	6mm ø disk	1	3/2/21: removed 1 gel; 3/23/21: removed 1 gel & 1 pc of control tissue
	13	DMSO	No	2/23/21			SLH12	NSG	B	3/23/21	Bouins	1wk; 1 month	6mm ø disk	2	6mm ø disk	1	3/2/21: removed 1 gel; 3/23/21: removed 1 gel & 1 pc of control tissue
	13	DMSO	No	2/23/21			SLH13	NSG	B	3/23/21	Bouins	1 wk; 1 month	6mm ø disk	2	6mm ø disk	1	3/2/21: removed 1 gel; 3/23/21: removed 1 gel & 1 pc of control tissue
	13	DMSO	No	2/23/21			SLH14	NSG	B	3/23/21	Bouins	1 wk; 1 month	6mm ø disk	2	6mm ø disk	1	3/2/21: removed 1 gel; 3/23/21: removed 1 gel & 1 pc of control tissue
	13	DMSO	No	2/23/21			SLH15	NSG	B	3/23/21	Bouins	1 wk; 1 month	6mm ø disk	2	6mm ø disk	1	3/2/21: removed 1 gel; 3/23/21: removed 1 gel & 1 pc of control tissue
Stimulation Study 2	13/14	DMSO	No	6/9/21	3.5	14	H31	NSG	T	9/9/21	PFA	13 wks	6mm ø disk	NA	6mm ø disk	3	G2 - 1IU FSH
	18/19	DMSO	No	7/7/21	2.8	11.2	H32	NSG	G	10/7/21	PFA	20 wks	6mm ø disk	3	6mm ø disk	NA	G5 - 1IU FSH + hCG
	13/14	DMSO	No	6/9/21	3.5	14	H33	NSG	G	9/9/21	PFA	20 wks	6mm ø disk	3	6mm ø disk	NA	G5 - 1IU FSH + hCG
	13/14	DMSO	No	6/9/21	3.5	14	H34	NSG	T	9/9/21	PFA	13 wks	6mm ø disk	NA	6mm ø disk	3	G4 - Saline
	14/17	DMSO	No	6/23/21	2.8	11.2	H35	NSG	T	9/23/21	PFA	13 wks	6mm ø disk	NA	6mm ø disk	3	G2 - 1IU FSH
	13/14	DMSO	No	6/9/21	3.5	14	H36	NSG	T	9/9/21	PFA	13 wks	6mm ø disk	NA	6mm ø disk	3	G2 - 1IU FSH
	13/14	DMSO	No	6/9/21	3.5	14	H37	NSG	G	9/9/21	PFA	13 wks	6mm ø disk	3	6mm ø disk	NA	G1 - 1IU FSH
	18/19	DMSO	No	7/7/21	2.8	11.2	H38	NSG	G	10/7/21	PFA	13 wks	6mm ø disk	3	6mm ø disk	NA	G4 - Saline
	14/17	DMSO	No	6/23/21	2.8	11.2	H39	NSG	G	6/23/21	PFA	13 wks	6mm ø disk	3	6mm ø disk	NA	G1 - 1IU FSH
	13/14	DMSO	No	6/9/21	2.6	10.4	H40	NSG	G	9/9/21	PFA	13 wks	6mm ø disk	3	6mm ø disk	NA	G3 - Saline
	14/17	DMSO	No	6/23/21	2.8	11.2	H41	NSG	G	6/23/21	PFA	13 wks	6mm ø disk	3	6mm ø disk	NA	G3 - Saline
	14/17	DMSO	No	6/23/21	2.8	11.2	H42	NSG	T	6/23/21	PFA	13 wks	6mm ø disk	NA	6mm ø disk	3	G2 - 1IU FSH
	18/19	DMSO	No	7/7/21	2.4	9.6	H43	NSG	G	10/7/21	PFA	20 wks	6mm ø disk	3	6mm ø disk	NA	G5 - 1IU FSH + hCG
	14/17	DMSO	No	6/23/21	2.8	11.2	H44	NSG	G	6/23/21	PFA	20 wks	6mm ø disk	3	6mm ø disk	NA	G5 - 1IU FSH + hCG
	18/19	DMSO	No	7/7/21	2.1	8.4	H45	NSG	T	10/7/21	PFA	13 wks	6mm ø disk	NA	6mm ø disk	3	G1 - 1IU FSH
	14/17	DMSO	No	6/23/21	2.8	11.2	H46	NSG	G	6/23/21	PFA	13 wks	6mm ø disk	3	6mm ø disk	NA	G3 - Saline
	13/14	DMSO	No	6/9/21	2.6	10.4	H47	NSG	G	9/9/21	PFA	13 wks	6mm ø disk	3	6mm ø disk	NA	G1 - 1IU FSH
	13/14	DMSO	No	6/9/21	2.6	10.4	H48	NSG	T	9/9/21	PFA	13 wks	6mm ø disk	NA	6mm ø disk	3	G4 - Saline
	14/17	DMSO	No	6/23/21	2.8	11.2	H49	NSG	T	6/23/21	PFA	13 wks	6mm ø disk	NA	6mm ø disk	3	G4 - Saline
	14/17	DMSO	No	6/23/21	2.8	11.2	H50	NSG	G	6/23/21	PFA	13 wks	6mm ø disk	3	6mm ø disk	NA	G3 - Saline

Appendix Table D1 Cot'd

	Lab Donor #	Thaw Media Components	OVX?	Implant Date	Mouse Age @ Implant [months]	Mouse Age @ Implant [weeks]	Mouse Identifier	Mouse Strain	Gels, Tissue, or Both?	Euthanasia Date	Fixative	Implantation Time	Gel Tissue Size	# of Gels	Control Tissue Size	# of pieces of control tissue	Notes
Balb/c Implant Study	19/22/24	DMSO	No	9/15/21	3.1	12.4	X1	Balb/c	G	10/27/21	PFA	6 wks	5mm ø disk	4	5mm ø disk	NA	GC
	19/22/24	DMSO	No	9/2/21	2.6	10.4	X2	Balb/c	T	9/16/21	PFA	2 wks	5mm ø disk	NA	5mm ø disk	4	GD
	19/22/24	DMSO	No	9/2/21	2.6	10.4	X3	Balb/c	T	9/30/21	PFA	4 wks	5mm ø disk	NA	5mm ø disk	4	GE
	19/22/24	DMSO	No	9/15/21	3.1	12.4	X4	Balb/c	T	10/27/21	PFA	6 wks	5mm ø disk	NA	5mm ø disk	4	GF
	19/22/24	DMSO	No	9/15/21	3.1	12.4	X5	Balb/c	G	10/13/21	PFA	4 wks	5mm ø disk	4	5mm ø disk	NA	GB
	19/22/24	DMSO	No	9/9/21	2.9	11.6	X6	Balb/c	T	9/23/21	PFA	2 wks	5mm ø disk	NA	5mm ø disk	4	GD
	19/22/24	DMSO	No	9/2/21	2.6	10.4	X7	Balb/c	T	9/30/21	PFA	4 wks	5mm ø disk	NA	5mm ø disk	4	GE
	19/22/24	DMSO	No	9/2/21	2.6	10.4	X8	Balb/c	G	9/16/21	PFA	2 wks	5mm ø disk	4	5mm ø disk	NA	GA
	19/22/24	DMSO	No	9/9/21	2.9	11.6	X9	Balb/c	G	10/21/21	PFA	6 wks	5mm ø disk	4	5mm ø disk	NA	GC
	19/22/24	DMSO	No	9/9/21	2.9	11.6	X10	Balb/c	G	10/7/21	PFA	4 wks	5mm ø disk	4	5mm ø disk	NA	GB
	19/22/24	DMSO	No	9/2/21	2.6	10.4	X11	Balb/c	G	9/30/21	PFA	4 wks	5mm ø disk	4	5mm ø disk	NA	GB
	19/22/24	DMSO	No	9/15/21	3.1	12.4	X12	Balb/c	G	10/27/21	PFA	6 wks	5mm ø disk	4	5mm ø disk	NA	GC
	19/22/24	DMSO	No	9/9/21	2.9	11.6	X13	Balb/c	T	9/23/21	PFA	2 wks	5mm ø disk	NA	5mm ø disk	4	GD
	19/22/24	DMSO	No	9/15/21	3.1	12.4	X14	Balb/c	G	9/29/21	PFA	2 wks	5mm ø disk	4	5mm ø disk	NA	GA
	19/22/24	DMSO	No	9/9/21	2.9	11.6	X15	Balb/c	T	10/7/21	PFA	4 wks	5mm ø disk	NA	5mm ø disk	4	GE
	19/22/24	DMSO	No	9/9/21	2.9	11.6	X16	Balb/c	T	10/21/21	PFA	6 wks	5mm ø disk	NA	5mm ø disk	4	GF
	19/22/24	DMSO	No	9/2/21	2.6	10.4	X17	Balb/c	G	9/16/21	PFA	2 wks	5mm ø disk	4	5mm ø disk	NA	GA
	19/22/24	DMSO	No	9/15/21	3.1	12.4	X18	Balb/c	T	10/27/21	PFA	6 wks	5mm ø disk	NA	5mm ø disk	4	GF
Large Disk Study	~~22/24~~	~~DMSO~~	~~No~~	~~2/4/22~~	~~3.6~~	14.4	~~A1~~	~~NSG~~	~~G~~	~~2/11/22~~	~~PFA~~	~~1 wk~~	~~5mm ø disk~~	~~3~~	~~5mm ø disk~~	~~NA~~	Early sac, replaced with A17
	18/26	DMSO	No	2/25/22	3.1	12.4	A2	NSG	G	3/25/22	PFA	4 wks	5mm ø disk	3	5mm ø disk	NA	
	19/24/26	DMSO	No	2/25/22	3.1	12.4	A3	NSG	G	3/4/22	PFA	1 wk	5mm ø disk	3	5mm ø disk	NA	
	19/22/26	DMSO	No	2/25/22	3.2	12.8	A4	NSG	T	3/4/22	PFA	1 wk	5mm ø disk	NA	5mm ø disk	3	
	26	DMSO	No	**5/10/22**	**4.8**	**19.2**	**A5**	**NSG**	**T**	**6/7/22**	**PFA**	**4 wk**	**5mm ø disk**	**NA**	**5mm ø disk**	**3**	
	19/24/26	DMSO	No	2/4/22	2.5	10	A6	NSG	G	3/4/22	PFA	4 wks	5mm ø disk	3	5mm ø disk	NA	
	19/24	DMSO	No	2/4/22	2.5	10	A7	NSG	T	3/4/22	PFA	4 wks	5mm ø disk	NA	5mm ø disk	3	
	18/22	DMSO	No	2/4/22	3.6	14.4	A8	NSG	G	3/4/22	PFA	4 wks	5mm ø disk	3	5mm ø disk	NA	
	18/22	DMSO	No	2/25/22	3.1	12.4	A9	NSG	**G**	3/25/22	PFA	**4 wks**	5mm ø disk	3	5mm ø disk	NA	
	19/24/26	DMSO	No	2/25/22	3.1	12.4	A10	NSG	G	3/25/22	PFA	4 wks	5mm ø disk	3	5mm ø disk	NA	
	19/26	DMSO	No	2/4/22	3.6	14.4	A11	NSG	G	2/11/22	PFA	1 wk	5mm ø disk	3	5mm ø disk	NA	
	19/24	DMSO	No	2/4/22	3.3	13.2	A12	NSG	T	2/12/22	PFA	1 wk	5mm ø disk	NA	5mm ø disk	3	
	19/24	DMSO	No	2/25/22	3.1	12.4	A13	NSG	T	3/4/22	PFA	1 wk	5mm ø disk	NA	5mm ø disk	3	
	18/19/26	DMSO	No	2/25/22	3.2	12.8	A14	NSG	T	3/25/22	PFA	4 wks	5mm ø disk	NA	5mm ø disk	3	
	19/24	DMSO	No	2/4/22	3.7	14.8	A15	NSG	T	2/11/22	PFA	1 wk	5mm ø disk	NA	5mm ø disk	3	
	22/24	DMSO	No	2/4/22	3.3	13.2	A16	NSG	G	3/4/22	PFA	4 wks	5mm ø disk	3	5mm ø disk	NA	
	22/24	DMSO	No	2/4/22	3.1	12.4	A17	NSG	G	3/4/22	PFA	1 wks	5mm ø disk	3	5mm ø disk	NA	

Appendix Table D1 Cot'd

	Lab Donor #	Thaw Media Components	OVX?	Implant Date	Mouse Age @ Implant [months]	Mouse Age @ Implant [weeks]	Mouse Identifier	Mouse Strain	Gels, Tissue, or Both?	Euthanasia Date	Fixative	Implantation Time	Gel Tissue Size	# of Gels	Control Tissue Size	# of pieces of control tissue	Notes
Stimulation Study 3	17/26	DMSO + EG	Yes	5/10/22	4.3	17.2	S1	NSG	T	8/3/22	PFA	6	5mm ø disk	NA	5mm ø disk	3	
	18/19/27	DMSO + EG	Yes	5/13/22	4.4	17.6	S2	NSG	T	9/21/22	PFA	20	5mm ø disk	NA	5mm ø disk	3	
	19/26	DMSO + EG	Yes	5/10/22	4.3	17.2	S3	NSG	G	8/3/22	PFA	6	5mm ø disk	3	5mm ø disk	NA	
	19/26	DMSO + EG	Yes	5/10/22	4.3	17.2	S4	NSG	T	8/3/22	PFA	15	5mm ø disk	NA	5mm ø disk	3	
	17/26	DMSO + EG	Yes	5/10/22	4.3	17.2	S5	NSG	G	9/21/22	PFA	20	5mm ø disk	3	5mm ø disk	NA	
	18/26	DMSO + EG	Yes	5/13/22	4.4	17.6	S6	NSG	T	8/3/22	PFA	15	5mm ø disk	NA	5mm ø disk	3	
	26/27	DMSO + EG	Yes	5/13/22	4.4	17.6	S7	NSG	T	9/21/22	PFA	20	5mm ø disk	NA	5mm ø disk	3	
	26/27	DMSO + EG	Yes	5/13/22	4.4	17.6	S8	NSG	G	9/21/22	PFA	20	5mm ø disk	3	5mm ø disk	NA	
	18/24/26	DMSO + EG	Yes	4/24/22	3.7	14.8	S9	NSG	T	9/22/22	PFA	20	5mm ø disk	NA	5mm ø disk	3	
	18/24/26	DMSO + EG	Yes	4/21/22	3.6	14.4	S10	NSG	G	8/4/22	PFA	6	5mm ø disk	3	5mm ø disk	NA	
	18/26	DMSO + EG	Yes	4/21/22	3.6	14.4	S11	NSG	G	8/4/22	PFA	15	5mm ø disk	3	5mm ø disk	NA	
	24/26	DMSO + EG	Yes	4/21/22	3.6	14.4	S12	NSG	G	9/22/22	PFA	20	5mm ø disk	3	5mm ø disk	NA	
	26	DMSO + EG	Yes	4/21/22	3.6	14.4	S13	NSG	G	9/22/22	PFA	20	5mm ø disk	3	5mm ø disk	NA	
	24/26	DMSO + EG	Yes	4/24/22	3.7	14.8	S14	NSG	T	8/4/22	PFA	6	5mm ø disk	NA	5mm ø disk	3	
	17/18/26	DMSO + EG	Yes	4/24/22	3.7	14.8	S15	NSG	G	8/4/22	PFA	15	5mm ø disk	3	5mm ø disk	NA	
	17/26	DMSO + EG	Yes	4/24/22	3.7	14.8	S16	NSG	T	9/22/22	PFA	20	5mm ø disk	NA	5mm ø disk	3	
	27	DMSO + EG	Yes	6/21/22	2	8	S17	NSG	G	11/22/22	PFA	20	5mm ø disk	3	5mm ø disk	NA	
	24/27/28	DMSO + EG	Yes	6/21/22	2	8	S18	NSG	T	8/2/22	PFA	6	5mm ø disk	NA	5mm ø disk	3	
	27/28	DMSO + EG	Yes	6/21/22	2	8	S19	NSG	T	10/4/22	PFA	15	5mm ø disk	NA	5mm ø disk	3	
	24/27	DMSO + EG	Yes	6/21/22	2	8	S20	NSG	G	8/2/22	PFA	6	5mm ø disk	NA	5mm ø disk	3	
	27/28	DMSO + EG	Yes	6/22/22	2	8	S21	NSG	G	10/5/22	PFA	15	5mm ø disk	3	5mm ø disk	NA	
	27	DMSO + EG	Yes	6/22/22	2	8	S22	NSG	G	10/5/22	PFA	20	5mm ø disk	NA	5mm ø disk	3	
	24/27/28	DMSO + EG	Yes	6/22/22	2	8	S23	NSG	T	11/23/22	PFA	15	5mm ø disk	3	5mm ø disk	NA	
	24/27/28	DMSO + EG	Yes	6/22/22	2	8	S24	NSG	T	8/3/22	PFA	6	5mm ø disk	NA	5mm ø disk	3	
	24/27	DMSO + EG	Yes	6/23/22	2.1	8.4	S25	NSG	G	11/24/22	PFA	20	5mm ø disk	3	5mm ø disk	NA	
	~~24/27~~	~~DMSO + EG~~	~~Yes~~	~~6/23/22~~	~~2.1~~	~~8.4~~	~~S26~~	~~NSG~~	~~G~~	~~11/24/22~~	~~PFA~~	~~20~~	~~5mm ø disk~~	~~3~~	~~5mm ø disk~~	~~NA~~	Early euthanasia
	27	DMSO + EG	Yes	6/23/22	2.1	8.4	S27	NSG	G	10/6/22	PFA	15	5mm ø disk	3	5mm ø disk	NA	
	24/27	DMSO + EG	Yes	6/23/22	2.1	8.4	S28	NSG	G	8/4/22	PFA	6	5mm ø disk	NA	5mm ø disk	3	

Appendix Table D1 Cot'd

	Lab Donor #	Thaw Media Components	OVX?	Implant Date	Mouse Age @ Implant [months]	Mouse Age @ Implant [weeks]	Mouse Identifier	Mouse Strain	Gels, Tissue, or Both?	Euthanasia Date	Fixative	Implantation Time	Gel Tissue Size	# of Gels	Control Tissue Size	# of pieces of control tissue	Notes
Balb/c + Stim Study	34/38	DMSO + EG	Yes	2/17/23	3.1	12.4	XS1	Balb/c	G	5/1/23	PFA	10.4 wks	5mm ø disk	4	N/A	NA	Pus - sac'd early
	34/38	DMSO + EG	Yes	2/17/23	3.1	12.4	XS2	Balb/c	G	7/21/23	PFA	22 wks	5mm ø disk	4	N/A	NA	
	34/38	DMSO + EG	Yes	2/17/23	3.1	12.4	XS3	Balb/c	G	7/21/23	PFA	22 wks	5mm ø disk	4	N/A	NA	*May have punctured when implanting
	34/38	DMSO + EG	Yes	2/17/23	3.1	12.4	XS4	Balb/c	G	7/21/23	PFA	22 wks	5mm ø disk	4	N/A	NA	*some bubbles from flipping
	34/38	DMSO + EG	Yes	2/17/23	3.1	12.4	XS5	Balb/c	G	7/21/23	PFA	22 wks	5mm ø disk	4	N/A	NA	
	31/38	DMSO + EG	Yes	2/10/23	3.6	14.4	XS6	Balb/c	G	7/9/23	PFA	21.3 wks	5mm ø disk	4	N/A	NA	*May have punctured when implanting Lesion appeared overnight 7/8, sac'd early
	31/38	DMSO + EG	Yes	2/10/23	3.6	14.4	XS7	Balb/c	G	6/21/23	PFA	18.7 wks	5mm ø disk	4	N/A	NA	Lesion + orbital tightening; CLN 00102708 TAO applied 5/15-5/19
	31/38	DMSO + EG	Yes	2/10/23	3.6	14.4	XS8	Balb/c	G	5/5/23	PFA	12 wks	5mm ø disk	4	N/A	NA	Scabs - sac'd early; CLN 00100370 Carprofen given 4/18-4/20, TAO given 4/19-4/23
	31/38	DMSO + EG	Yes	2/17/23	3.9	15.6	XS9	Balb/c	G	7/21/23	PFA	22 wks	5mm ø disk	4	N/A	NA	

Bibliography

1. American Cancer Society. Cancer Facts & Figures 2023. *American Cancer Society*. Published online 2022.
2. Akasha AM, Woodruff TK. *Oncofertility: Preservation of Ovarian Function After a Cancer Diagnosis*. 3rd ed. (Leung PCK, Adashi EY, eds.). Elsevier Inc.; 2019. doi:10.1016/B978-0-12-813209-8.00031-5
3. Jayasinghe YL, Wallace WHB, Anderson RA. Ovarian function, fertility and reproductive lifespan in cancer patients. *Expert Rev Endocrinol Metab*. 2018;13(3):125-136. doi:10.1080/17446651.2018.1455498
4. Van Dorp W, Haupt R, Anderson RA, et al. Reproductive Function and Outcomes in Female Survivors of Childhood, Adolescent, and Young Adult Cancer: A Review. *J Clin Oncol*. 2018;36:2169-2180. doi:10.1200/JCO.2017
5. Spears N, Lopes F, Stefansdottir A, et al. Ovarian damage from chemotherapy and current approaches to its protection. *Hum Reprod Update*. 2019;25(6):673-693. doi:10.1093/humupd/dmz027
6. Akasha AM, Woodruff TK. *Oncofertility: Preservation of Ovarian Function After a Cancer Diagnosis*. 3rd ed. (Leung PCK, Adashi EY, eds.). Elsevier Inc.; 2019. doi:10.1016/B978-0-12-813209-8.00031-5

7. Filippi F, Meazza C, Paffoni A, Raspagliesi F, Terenziani M, Somigliana E. Egg freezing in childhood and young adult cancer survivors. *Pediatrics*. 2016;138(4). doi:10.1542/peds.2016-0291

8. Barbieri RL. Female Infertility. In: *Yen & Jaffe's Reproductive Endocrinology: Physiology, Pathophysiology, and Clinical Management*. Eighth. Elsevier Inc.; 2019:556-581.e7. doi:10.1016/B978-0-323-47912-7.00022-6

9. Van Santen HM, Van Den Heuvel-Eibrink MM, Van De Wetering MD, Wallace WH. Hypogonadism in Children with a Previous History of Cancer: Endocrine Management and Follow-Up. *Horm Res Paediatr*. 2019;91(2):93-103. doi:10.1159/000495943

10. Knauff EAH, Eijkemans MJC, Lambalk CB, et al. Anti-Müllerian hormone, inhibin b, and antral follicle count in young women with ovarian failure. *Journal of Clinical Endocrinology and Metabolism*. 2009;94(3):786-792. doi:10.1210/jc.2008-1818

11. Duncan FE, Feinberg E, Brannigan RE, Edmonds M, Ataman L, Woodruff TK. Fertility Preservation. In: *Yen & Jaffe's Reproductive Endocrinology: Physiology, Pathophysiology, and Clinical Management*. Eighth. Elsevier Inc.; 2019:857-886.e6. doi:10.1016/B978-0-323-47912-7.00033-0

12. Findlay JK, Dunning KR, Gilchrist RB, Hutt KJ, Russell DL, Walters KA. Follicle Selection in Mammalian Ovaries. In: Leung PCK, Adashi EY, eds. *The Ovary*. 3rd ed. Elsevier Inc.; 2019:3-21. doi:10.1016/b978-0-12-813209-8.00001-7

13. Strauss JF, Williams CJ. Ovarian Life Cycle. In: *Yen & Jaffe's Reproductive Endocrinology: Physiology, Pathophysiology, and Clinical Management*. Eighth. Elsevier Inc.; 2018:167-205.e9. doi:10.1016/B978-0-323-47912-7.00008-1

14. Young JM, McNeilly AS. Theca: The forgotten cell of the ovarian follicle. *Reproduction*. 2010;140(4):489-504. doi:10.1530/REP-10-0094

15. Orisaka M, Tajima K, Tsang BK, Kotsuji F. Oocyte-granulosa-theca cell interactions during preantral follicular development. *J Ovarian Res*. 2009;2(1):1-7. doi:10.1186/1757-2215-2-9

16. Basuino L, Silveira CF. Human follicular fluid and effects on reproduction. *J Bras Reprod Assist*. 2016;20(1):38-40. doi:10.5935/1518-0557.20160009

17. Gougeon A. Dynamics of follicular growth in the human: a model from preliminary results. *Hum Reprod*. 1986;1(2):81-87. doi:10.1093/oxfordjournals.humrep.a136365

18. Hillier SG, Whitelaw PF, Smyth CD. Follicular oestrogen synthesis: the “two-cell, two-gonadotrophin” model revisited. *Mol Cell Endocrinol*. 1994;100(1-2):51-54. doi:10.1016/0303-7207(94)90278-X

19. Bliss SP, Navratil AM, Xie J, Roberson MS. GnRH signaling, the gonadotrope and endocrine control of fertility. *Front Neuroendocrinol*. 2010;31(3):322-340. doi:10.1016/j.yfrne.2010.04.002

20. Silverthorn DU. *Human Physiology: An Integrated Approach*. 4th ed. Benjamin Cummings; 2006.

21. Diller L. Adult Primary Care after Childhood Acute Lymphoblastic Leukemia. *New England Journal of Medicine*. 2011;365(15):1417-1424. doi:10.1056/nejmcp1103645

22. Olsen NJ, Kovacs WJ. Gonadal steroids and immunity. *Endocr Rev*. 1996;17(4):369-384. doi:10.1210/er.17.4.369

23. Fungfuang W, Terada M, Komatsu N, Moon C, Saito TR. Effects of estrogen on food intake, serum leptin levels and leptin mRNA expression in adipose tissue of female rats. *Lab Anim Res*. 2013;29(3):168. doi:10.5625/lar.2013.29.3.168

24. McEwen BS, Alves SE. Estrogen Actions in the Central Nervous System 1. *Endocr Rev*. 1999;20(3):279-307. doi:10.1210/edrv.20.3.0365

25. Lobo RA. Menopause and Aging. In: *Yen & Jaffe's Reproductive Endocrinology: Physiology, Pathophysiology, and Clinical Management*. Eighth. Elsevier Inc.; 2019:322-356.e9. doi:10.1016/B978-0-323-47912-7.00014-7

26. Weise M, De-Levi S, Barnes KM, Gafni RI, Abad V, Baron J. Effects of estrogen on growth plate senescence and epiphyseal fusion. *Proc Natl Acad Sci U S A*. 2001;98(12):6871-6876. doi:10.1073/pnas.121180498

27. Matthews D, Bath L, Högler W, Mason A, Smyth A, Skae M. Hormone supplementation for pubertal induction in girls. *Arch Dis Child*. 2017;102(10):975-980. doi:10.1136/archdischild-2016-311372

28. Langer RD. The evidence base for HRT: what can we believe? *Climacteric*. 2017;20(2):91-96. doi:10.1080/13697137.2017.1280251

29. Christin-Maitre S. Use of Hormone Replacement in Females with Endocrine Disorders. *Horm Res Paediatr*. 2017;87(4):215-223. doi:10.1159/000457125

30. Sullivan SD, Sarrel PM, Nelson LM. Hormone replacement therapy in young women with primary ovarian insufficiency and early menopause. *Fertil Steril*. 2016;106(7):1588-1599. doi:10.1016/j.fertnstert.2016.09.046

31. Matthews D, Bath L, Högler W, Mason A, Smyth A, Skae M. Hormone supplementation for pubertal induction in girls. *Arch Dis Child*. 2017;102(10):975-980. doi:10.1136/archdischild-2016-311372

32. Agarwal S, Alzahrani FA, Ahmed A. Hormone replacement therapy: Would it be possible to replicate a functional ovary? *Int J Mol Sci*. 2018;19(10). doi:10.3390/ijms19103160

33. ROSSMANITH WG, LAUGHLIN GA, MORTOLA JF, JOHNSON ML, VELDHUIS JD, YEN SSC. Pulsatile Cosecretion of Estradiol and Progesterone by the Midluteal Phase Corpus Luteum: Temporal Link to Luteinizing Hormone Pulses*. *J Clin Endocrinol Metab*. 1990;70(4):990-995. doi:10.1210/jcem-70-4-990

34. David A, Day J, Shikanov A. Immunoisolation to prevent tissue graft rejection: Current knowledge and future use. *Exp Biol Med*. 2016;241(9):955-961. doi:10.1177/1535370216647129

35. Bose S, Volpatti LR, Thiono D, et al. A retrievable implant for the long-term encapsulation and survival of therapeutic xenogeneic cells. *Nat Biomed Eng*. Published online March 30, 2020. doi:10.1038/s41551-020-0538-5

36. Hwa AJ, Weir GC. Transplantation of Macroencapsulated Insulin-Producing Cells. *Curr Diab Rep*. 2018;18(8). doi:10.1007/s11892-018-1028-y

37. Xu J, Lawson MS, Yeoman RR, et al. Fibrin promotes development and function of macaque primary follicles during encapsulated three-dimensional culture. *Human Reproduction*. 2013;28(8):2187-2200. doi:10.1093/humrep/det093

38. Pangas SA, Saudye H, Shea LD, Woodruff TK. Novel Approach for the Three-Dimensional Culture of Granulosa Cell-Oocyte Complexes. *Tissue Eng*. 2003;9(5):1013-1021. doi:10.1089/107632703322495655

39. Rios PD, Kniazeva E, Lee HC, et al. Retrievable hydrogels for ovarian follicle transplantation and oocyte collection. *Biotechnol Bioeng*. 2018;115(8):2075-2086. doi:10.1002/bit.26721

40. Vanacker J, Luyckx V, Dolmans MM, et al. Transplantation of an alginate-matrigel matrix containing isolated ovarian cells: First step in developing a biodegradable scaffold to transplant isolated preantral follicles and ovarian cells. *Biomaterials*. 2012;33(26):6079-6085. doi:10.1016/j.biomaterials.2012.05.015

41. Shikanov A, Zhang Z, Xu M, et al. Fibrin encapsulation and vascular endothelial growth factor delivery promotes ovarian graft survival in mice. *Tissue Eng Part A*. 2011;17(23-24):3095-3104. doi:10.1089/ten.tea.2011.0204

42. Kniazeva E, Hardy AN, Boukaidi SA, Woodruff TK, Jeruss JS, Shea LD. Primordial Follicle Transplantation within Designer Biomaterial Grafts Produce Live Births in a Mouse Infertility Model. *Sci Rep*. 2015;5(June):1-11. doi:10.1038/srep17709

43. Shikanov A, Xu M, Woodruff TK, Shea LD. Interpenetrating fibrin-alginate matrices for in vitro ovarian follicle development. *Biomaterials*. 2009;30(29):5476-5485. doi:10.1016/j.biomaterials.2009.06.054

44. Shikanov A, Smith RM, Xu M, Woodruff TK, Shea LD. Hydrogel network design using multifunctional macromers to coordinate tissue maturation in ovarian follicle culture. *Biomaterials*. 2011;32(10):2524-2531. doi:10.1016/j.biomaterials.2010.12.027

45. Tomaszewski CE, Constance E, Lemke MM, et al. Adipose-derived stem cell-secreted factors promote early stage follicle development in a biomimetic matrix. *Biomater Sci*. 2019;7(2):571-580. doi:10.1039/c8bm01253a

46. Kim J, Perez AS, Claflin J, David A, Zhou H, Shikanov A. Synthetic hydrogel supports the function and regeneration of artificial ovarian tissue in mice. *NPJ Regen Med*. 2016;1(1). doi:10.1038/npjregenmed.2016.10

47. Day JR, David A, Barbosa MG de M, Brunette MA, Cascalho M, Shikanov A. Encapsulation of ovarian allograft precludes immune rejection and promotes restoration of endocrine function in immune-competent ovariectomized mice. *Sci Rep*. 2019;9(1):16614. doi:10.1038/s41598-019-53075-8

48. Day JR, David A, Cichon AL, Kulkarni T, Cascalho M, Shikanov A. Immunoisolating poly(ethylene glycol) based capsules support ovarian tissue survival to restore endocrine function. *J Biomed Mater Res A*. 2018;106(5):1381-1389. doi:10.1002/jbm.a.36338

49. Day JR, David A, Hammersley M, Barbosa M, Cascalho M, Shikanov A. Dual phased poly(Ethylene glycol) immunoisolating capsule supports ovarian tissue development and precludes sensitization of the host immune response. In: *Transactions of the Annual Meeting of the Society for Biomaterials and the Annual International Biomaterials Symposium*. Vol 40. ; 2019.

50. Day JR, David A, Kim J, et al. The impact of functional groups of poly(ethylene glycol) macromers on the physical properties of photo-polymerized hydrogels and the local inflammatory response in the host. *Acta Biomater*. 2018;67:42-52. doi:10.1016/j.actbio.2017.12.007

51. Day JR, David A, Kim J, et al. The impact of functional groups of poly(ethylene glycol) macromers on the physical properties of photo-polymerized hydrogels and the local inflammatory response in the host. *Acta Biomater*. 2018;67:42-52. doi:10.1016/j.actbio.2017.12.007

52. Myers M, Britt KL, Wreford NGM, Ebling FJP, Kerr JB. Methods for quantifying follicular numbers within the mouse ovary. *Reproduction*. 2004;127(5):569-580. doi:10.1530/rep.1.00095

53. Griffin J, Emery BR, Huang I, Peterson CM, Carrell DT. Comparative analysis of follicle morphology and oocyte diameter in four mammalian species (mouse, hamster, pig, and human). *J Exp Clin Assist Reprod*. 2006;3(1):2. doi:10.1186/1743-1050-3-2

54. American Cancer Society. American Cancer Society: Cancer Facts and Figures 2021. *Atlanta, Ga: American Cancer Society*. Published online 2021:13-15.

55. Jones RM, Pattwell SS. Future considerations for pediatric cancer survivorship: Translational perspectives from developmental neuroscience. *Dev Cogn Neurosci*. 2019;38(May 2018):100657. doi:10.1016/j.dcn.2019.100657

56. International Programme on Chemical Safety. Endocrinology and Endocrine Toxicology. In: Damstra T, Barlow S, Bergman A, Kavlock R, Van Der Kraak G, eds. *Global Assessment of the State-of-the-Science of Endocrine Disruptors*. World Health Organization; 2002:11-32.

57. Pierson RA. Human Folliculogenesis Revisited: The Menstrual Cycle Visualized by Ultrasonography. In: Leung PCK, Adashi EY, eds. *The Ovary*. 3rd ed. Elsevier Inc.; 2019:51-69. doi:10.1016/b978-0-12-813209-8.00003-0

58. McCartney CR, Marshall JC. Neuroendocrinology of Reproduction. In: *Yen & Jaffe's Reproductive Endocrinology: Physiology, Pathophysiology, and Clinical Management*. Eighth. Elsevier Inc.; 2019:1-24.e8. doi:10.1016/B978-0-323-47912-7.00001-9

59. Shikanov A, Smith RM, Xu M, Woodruff TK, Shea LD. Hydrogel network design using multifunctional macromers to coordinate tissue maturation in ovarian follicle culture. *Biomaterials*. 2011;32(10):2524-2531. doi:10.1016/j.biomaterials.2010.12.027

60. Myers M, Britt KL, Wreford NGM, Ebling FJP, Kerr JB. Methods for quantifying follicular numbers within the mouse ovary. *Reproduction*. 2004;127(5):569-580. doi:10.1530/rep.1.00095

61. Schmidt KLT, Byskov AG, Andersen AN, Müller J, Andersen CY. Density and distribution of primordial follicles in single pieces of cortex from 21 patients and in individual pieces of cortex from three entire human ovaries. *Human Reproduction*. 2003;18(6):1158-1164. doi:10.1093/humrep/deg246

62. Griffin J, Emery BR, Huang I, Peterson CM, Carrell DT. Comparative analysis of follicle morphology and oocyte diameter in four mammalian species (mouse, hamster, pig, and human). *J Exp Clin Assist Reprod*. 2006;3(1):2. doi:10.1186/1743-1050-3-2

63. Xu M, Banc A, Woodruff TK, Shea LD. Secondary follicle growth and oocyte maturation by culture in alginate hydrogel following cryopreservation of the ovary or individual follicles. *Biotechnol Bioeng*. 2009;103(2):378-386. doi:10.1002/bit.22250

64. Kagawa N, Kuwayama M, Nakata K, et al. Production of the first offspring from oocytes derived from fresh and cryopreserved pre-antral follicles of adult mice. *Reprod Biomed Online*. 2007;14(6):693-699. doi:10.1016/S1472-6483(10)60670-0

65. Lee S, Ryu K jin, Kim B, Kang D, Kim YY, Kim T. Comparison between Slow Freezing and Vitrification for Human Ovarian Tissue Cryopreservation and Xenotransplantation. *Int J Mol Sci*. 2019;20(13):3346. doi:10.3390/ijms20133346

66. Duncan FE, Zelinski M, Gunn AH, et al. Ovarian tissue transport to expand access to fertility preservation: From animals to clinical practice. *Reproduction*. 2016;152(6):R201-R210. doi:10.1530/REP-15-0598

67. Donnez J, Dolmans MM. Transplantation of ovarian tissue. *Best Pract Res Clin Obstet Gynaecol*. 2014;28(8):1188-1197. doi:10.1016/j.bpobgyn.2014.09.003

68. Stoop D, Cobo A, Silber S. Fertility preservation for age-related fertility decline. *The Lancet*. 2014;384(9950):1311-1319. doi:10.1016/s0140-6736(14)61261-7

69. Gellert SE, Pors SE, Kristensen SG, Bay-Bjørn AM, Ernst E, Yding Andersen C. Transplantation of frozen-thawed ovarian tissue: an update on worldwide activity published in peer-reviewed papers and on the Danish cohort. *J Assist Reprod Genet*. 2018;35(4):561-570. doi:10.1007/s10815-018-1144-2

70. Nahata L, Woodruff TK, Quinn GP, et al. Ovarian tissue cryopreservation as standard of care: what does this mean for pediatric populations? *J Assist Reprod Genet*. 2020;37(6):1323-1326. doi:10.1007/s10815-020-01794-7

71. Huang H, Zhao G, Zhang Y, Xu J, Toth TL, He X. Predehydration and Ice Seeding in the Presence of Trehalose Enable Cell Cryopreservation. *ACS Biomater Sci Eng*. 2017;3(8):1758-1768. doi:10.1021/acsbiomaterials.7b00201

72. Isachenko V, Isachenko E, Reinsberg J, Montag M, Braun F, van der Ven H. Cryopreservation of human ovarian tissue: Effect of spontaneous and initiated ice formation. *Reprod Biomed Online*. 2008;16(3):336-345. doi:10.1016/S1472-6483(10)60593-7

73. The Practice Committees of the American Society for Reproductive Medicine and the Society for Assisted Reproductive Technology. Mature oocyte cryopreservation: a guideline. *Fertil Steril*. 2013;99(1):37-43. doi:10.1016/j.fertnstert.2012.09.028

74. Fan Y, Flanagan CL, Brunette MA, et al. Fresh and cryopreserved ovarian tissue from deceased young donors yields viable follicles. *F S Sci*. 2021;2(3):248-258. doi:10.1016/j.xfss.2021.06.003

75. Shi Q, Xie Y, Wang Y, Li S. Vitrification versus slow freezing for human ovarian tissue cryopreservation: A systematic review and meta-anlaysis. *Sci Rep*. 2017;7(1):1-9. doi:10.1038/s41598-017-09005-7

76. Leonel ECR, M. Lucci C, A. Amorim C. Cryopreservation of Preantral Follicles. In: *Cryopreservation Biotechnology in Biomedical and Biological Sciences*. IntechOpen; 2018:71-89. doi:10.5772/intechopen.79538

77. National Cancer Institute. NCCR*Explorer: An interactive website for NCCR cancer statistics. Published 2023. Accessed March 8, 2024. https://nccrexplorer.ccdi.cancer.gov.

78. American Cancer Society. American Cancer Society. Cancer Facts & Figures 2024. Published online 2024.

79. Duncan FE, Feinberg E, Brannigan RE, Edmonds M, Ataman L, Woodruff TK. Fertility Preservation. In: *Yen & Jaffe's Reproductive Endocrinology: Physiology, Pathophysiology, and Clinical Management*. Eighth. Elsevier Inc.; 2019:857-886.e6. doi:10.1016/B978-0-323-47912-7.00033-0

80. Diller L. Adult Primary Care after Childhood Acute Lymphoblastic Leukemia. *New England Journal of Medicine*. 2011;365(15):1417-1424. doi:10.1056/nejmcp1103645

81. Olsen NJ, Kovacs WJ. Gonadal steroids and immunity. *Endocr Rev*. 1996;17(4):369-384. doi:10.1210/er.17.4.369

82. Fungfuang W, Terada M, Komatsu N, Moon C, Saito TR. Effects of estrogen on food intake, serum leptin levels and leptin mRNA expression in adipose tissue of female rats. *Lab Anim Res*. 2013;29(3):168. doi:10.5625/lar.2013.29.3.168

83. McEwen BS, Alves SE. Estrogen Actions in the Central Nervous System 1. *Endocr Rev*. 1999;20(3):279-307. doi:10.1210/edrv.20.3.0365

84. Lobo RA. Menopause and Aging. In: *Yen & Jaffe's Reproductive Endocrinology: Physiology, Pathophysiology, and Clinical Management*. Eighth. Elsevier Inc.; 2019:322-356.e9. doi:10.1016/B978-0-323-47912-7.00014-7

85. Weise M, De-Levi S, Barnes KM, Gafni RI, Abad V, Baron J. Effects of estrogen on growth plate senescence and epiphyseal fusion. *Proc Natl Acad Sci U S A*. 2001;98(12):6871-6876. doi:10.1073/pnas.121180498

86. Christin-Maitre S. Use of Hormone Replacement in Females with Endocrine Disorders. *Horm Res Paediatr*. 2017;87(4):215-223. doi:10.1159/000457125

87. Vargiu V, Amar ID, Rosati A, et al. Hormone replacement therapy and cervical cancer: a systematic review of the literature. *Climacteric*. 2020;0(0):1-8. doi:10.1080/13697137.2020.1826426

88. Agarwal S, Alzahrani FA, Ahmed A. Hormone replacement therapy: Would it be possible to replicate a functional ovary? *Int J Mol Sci*. 2018;19(10). doi:10.3390/ijms19103160

89. DiVasta AD, Gordon CM. Hormone replacement therapy and the adolescent. *Curr Opin Obstet Gynecol*. 2010;22(5):363-368. doi:10.1097/GCO.0b013e32833e4a35

90. Bird D, Ravindra NM. Transdermal drug delivery and patches—An overview. *Med Devices Sens*. 2020;3(6):1-15. doi:10.1002/mds3.10069

91. Del Río JP, Alliende MI, Molina N, Serrano FG, Molina S, Vigil P. Steroid Hormones and Their Action in Women's Brains: The Importance of Hormonal Balance. *Front Public Health*. 2018;6. doi:10.3389/fpubh.2018.00141

92. Practice Committee of the American Society for Reproductive Medicine. Fertility preservation in patients undergoing gonadotoxic therapy or gonadectomy: a committee opinion. *Fertil Steril*. 2019;112(6):1022-1033. doi:10.1016/j.fertnstert.2019.09.013

93. Yding Andersen C, Mamsen LS, Kristensen SG. FERTILITY PRESERVATION: Freezing of ovarian tissue and clinical opportunities. *Reproduction*. 2019;158(5):F27-F34. doi:10.1530/REP-18-0635

94. Khattak H, Malhas R, Craciunas L, et al. Fresh and cryopreserved ovarian tissue transplantation for preserving reproductive and endocrine function: A systematic

review and individual patient data meta-analysis. *Hum Reprod Update*. 2022;28(3):400-416. doi:10.1093/humupd/dmac003

95. Wall MA, Padmanabhan V, Shikanov A. Hormonal Stimulation of Human Ovarian Xenografts in Mice: Studying Folliculogenesis, Activation, and Oocyte Maturation. *Endocrinology (United States)*. 2020;161(12):1-15. doi:10.1210/endocr/bqaa194
96. Day JR, David A, Cichon AL, Kulkarni T, Cascalho M, Shikanov A. Immunoisolating poly(ethylene glycol) based capsules support ovarian tissue survival to restore endocrine function. *J Biomed Mater Res A*. 2018;106(5):1381-1389. doi:10.1002/jbm.a.36338
97. Day JR, David A, Barbosa MG de M, Brunette MA, Cascalho M, Shikanov A. Encapsulation of ovarian allograft precludes immune rejection and promotes restoration of endocrine function in immune-competent ovariectomized mice. *Sci Rep*. 2019;9(1):16614. doi:10.1038/s41598-019-53075-8
98. Brunette MA, Kinnear HM, Hashim PH, et al. Human Ovarian Follicles Xenografted in Immunoisolating Capsules Survive Long Term Implantation in Mice. *Front Endocrinol (Lausanne)*. 2022;13(June):1-12. doi:10.3389/fendo.2022.886678
99. Ajayi AF, Akhigbe RE. Staging of the estrous cycle and induction of estrus in experimental rodents: an update. *Fertil Res Pract*. 2020;6(1). doi:10.1186/s40738-020-00074-3
100. Gougeon A. Dynamics of follicular growth in the human: a model from preliminary results. *Hum Reprod*. 1986;1(2):81-87. doi:10.1093/oxfordjournals.humrep.a136365

101. Zheng W, Zhang H, Liu K. The two classes of primordial follicles in the mouse ovary: Their development, physiological functions and implications for future research. *Mol Hum Reprod*. 2014;20(4):286-292. doi:10.1093/molehr/gau007

102. Man L, Lustgarten Guahmich N, Kallinos E, et al. Xenograft model of heterotopic transplantation of human ovarian cortical tissue and its clinical relevance. *Reproduction*. 2023;165(1):31-47. doi:10.1530/REP-22-0114

103. Man L, Park L, Bodine R, et al. Engineered endothelium provides angiogenic and paracrine stimulus to grafted human ovarian tissue. *Sci Rep*. 2017;7(1):1-11. doi:10.1038/s41598-017-08491-z

104. Strauss JF, FitzGerald GA. Steroid Hormones and Other Lipid Molecules Involved in Human Reproduction. In: *Yen & Jaffe's Reproductive Endocrinology: Physiology, Pathophysiology, and Clinical Management*. Eighth. Elsevier Inc.; 2019:75-114.e7. doi:10.1016/B978-0-323-47912-7.00004-4

105. Carvalho-Oliveira M, Valdivia E, Blasczyk R, Figueiredo C. Immunogenetics of xenotransplantation. *Int J Immunogenet*. 2021;48(2):120-134. doi:10.1111/iji.12526

106. Arabi TZ, Sabbah BN, Lerman A, Zhu XY, Lerman LO. Xenotransplantation: Current Challenges and Emerging Solutions. *Cell Transplant*. 2023;32. doi:10.1177/09636897221148771

107. Zhou Q, Li T, Wang K, et al. Current status of xenotransplantation research and the strategies for preventing xenograft rejection. *Front Immunol*. 2022;13. doi:10.3389/fimmu.2022.928173

108. Wang Z, Ye Q, Yu S, Akhavan B. Poly Ethylene Glycol (PEG)-Based Hydrogels for Drug Delivery in Cancer Therapy: A Comprehensive Review. *Adv Healthc Mater*. 2023;12(18). doi:10.1002/adhm.202300105

109. Gaballa SA, Naguib YW, Mady FM, Khaled KA. *Polyethylene Glycol: Properties, Applications, and Challenges*. Vol 7.; 2024. http://jabps.journals.ekb.eg

110. Isaac AH, Recalde Phillips SY, Ruben E, et al. Impact of PEG sensitization on the efficacy of PEG hydrogel-mediated tissue engineering. *Nat Commun*. 2024;15(1). doi:10.1038/s41467-024-46327-3

111. Fairbanks BD, Schwartz MP, Bowman CN, Anseth KS. Photoinitiated polymerization of PEG-diacrylate with lithium phenyl-2,4,6-trimethylbenzoylphosphinate: polymerization rate and cytocompatibility. *Biomaterials*. 2009;30(35):6702-6707. doi:10.1016/j.biomaterials.2009.08.055

112. Pierson RA. Human Folliculogenesis Revisited: The Menstrual Cycle Visualized by Ultrasonography. In: Leung PCK, Adashi EY, eds. *The Ovary*. 3rd ed. Elsevier Inc.; 2019:51-69. doi:10.1016/b978-0-12-813209-8.00003-0